

Studies of Quantum Chromodynamics at the LHC

Tancredi Carli[†], Klaus Rabbertz[‡], and Steffen Schumann[¶]

[†]CERN, 1211 Geneva 23, Switzerland

[‡]Institut für Experimentelle Kernphysik, KIT, Wolfgang-Gaede-Str. 1, 76131 Karlsruhe, Germany

[¶]II. Physikalisches Institut, Georg-August-Universität Göttingen, Friedrich-Hund-Platz 1, 37077 Göttingen, Germany

Abstract. A successful description of hadron-hadron collision data demands a profound understanding of quantum chromodynamics. Inevitably, the complexity of strong-interaction phenomena requires the use of a large variety of theoretical techniques—from perturbative cross-section calculations up to the modelling of exclusive hadronic final states. Together with the unprecedented precision of the data provided by the experiments in the first running period of the LHC, a solid foundation of hadron-hadron collision physics at the TeV scale could be established that allowed the discovery of the Higgs boson and that is vital for estimating the background in searches for new phenomena. This chapter on studies of quantum chromodynamics at the LHC is part of a recent book on the results of LHC Run 1 [1] and presents the advances in theoretical methods side-by-side with related key measurements in an integrated approach.

Contents

1	Introduction	1
2	Basic Elements of QCD	2
3	Perturbative QCD	4
4	Parton Showers: The Bulk of the Emissions	7
5	NLO: The New Standard	10
6	NNLO: The Quest for Precision	14
7	Multi-Jets: Precision Meets Multiplicity	22
8	Resummation: The Realm of Large Logarithms	26
9	Beyond Perturbative QCD	29
10	Summary and Outlook	36

1 Introduction

Quantum chromodynamics (QCD) is the well-established quantum field theory of the strong interaction [2, 3] and one cornerstone of the Standard Model (SM) of particle physics. Like the electromagnetic and the weak force, QCD belongs to the class of gauge field theories. The assumption that the corresponding gauge symmetry is an exact symmetry of nature results in truly massless force carriers of the strong force, the gluons. However, as a consequence of the non-Abelian character of the $SU(3)$ QCD gauge group, the gluons carry a strong or so-called “colour” charge and interact amongst themselves. This is a striking difference to the electromagnetic force, which is mediated by electrically uncharged photons, and it induces—amongst other effects—the confinement of strongly interacting particles at low energies. In the following, the colour-charged constituents of hadrons, i.e. quarks, antiquarks, and gluons, will generically be denoted as “partons”.

In hadronic collisions like at the LHC, QCD effects are omnipresent, and their detailed understanding is indispensable for the interpretation of collider data, whether to search for new phenomena or to perform

Originally published in “The Large Hadron Collider — Harvest of Run 1”, edited by T. Schörner-Sadenius, Springer, 2015, pp. 139–194 [1].

precision studies of model parameters. Despite complications through the gluon self-interactions, the perturbative expansion of QCD (pQCD) that describes interactions with large momentum exchanges (“hard interactions”) in terms of parton-parton scatterings remains the most powerful theoretical technique. This technique allows quantitative predictions at parton level for observables ranging from inclusive production rates to shape observables, which are sensitive to details of the QCD radiation pattern. Nevertheless the theory’s confining nature obliges us to address non-perturbative aspects. This includes a reliable understanding of the short-distance parton structure of the initial-state protons, the fragmentation of final-state partons into hadrons, or the modelling of soft proton interactions.

The unprecedented experimental precision achieved with the new detectors at the LHC requires equally accurate theoretical predictions and has sparked rapid progress in the field of perturbative calculations using both analytical methods and modern Monte Carlo (MC) event generators. The interplay between experiment and theory enforced the development of new observables and novel techniques to match the challenges arising on both sides. In summary, the improved theoretical understanding of the QCD dynamics including the ability to precisely predict even complicated high-multiplicity final states and the excellent performance and understanding of the LHC machine and detectors together with sophisticated analysis techniques reveal a more refined and detailed picture of QCD than ever before.

For the presentation of QCD-related experimental results obtained during LHC Run 1 and the underlying theoretical developments, an integrative approach is chosen—reflecting the productive and fruitful interplay of the two communities. As a consequence, compromises on the content had to be taken, and only a selection of the most important measurements is discussed—omissions in the presentation of theoretical methods were unavoidable.

The chapter at hands is structured as follows: After a brief reminder of the basics of the QCD theory and the central aspects of perturbative QCD, the discussion focuses on various approximations in the modelling of scattering processes, including parton-shower simulations and parton-level predictions at next-to-leading and next-to-next-to-leading order in the strong coupling. Then the discussion turns to the observation of multi-jet final states, the successful description of which requires the combination of both fixed-order calculations and all-order (i.e. parton-shower) techniques. This is followed by a section on analytical methods for the resummation of large logarithms; these are exemplified using gap-fraction and jet-substructure observables. The chapter closes with a presentation of various phenomena and measurements sensitive to non-perturbative aspects of QCD.

2 Basic Elements of QCD

The discussion shall begin with a brief reminder of the ingredients of the QCD Lagrangian that defines the Feynman rules required for a perturbative analysis of QCD. The classical QCD Lagrangian is composed out of the free Dirac Lagrangians for the six quark fields and the kinetic and self-interaction terms for the gluon fields A_μ^a , labelled by a colour index $a = 1, \dots, 8$. These two parts get minimally coupled through a gauge covariant derivative D_μ :

$$\mathcal{L}_{\text{QCD}} = \mathcal{L}_{\text{gauge}} + \mathcal{L}_{\text{quarks}},$$

where

$$\mathcal{L}_{\text{gauge}} = -\frac{1}{4} F_{\mu\nu}^a F_a^{\mu\nu}, \quad \text{with} \quad F_{\mu\nu}^a = \partial_\mu A_\nu^a - \partial_\nu A_\mu^a - g_s f_{abc} A_\mu^b A_\nu^c$$

the gluon field-strength tensor, and

$$\mathcal{L}_{\text{quarks}} = \sum_{q \in \{u, d, s, c, b, t\}} \bar{q} (i\gamma^\mu D_\mu - m_q) q, \quad \text{with} \quad D_\mu = \partial_\mu + ig_s t^a A_\mu^a$$

the QCD covariant derivative (see also the introduction to the SM Lagrangian in Chap. 4 of Ref. [1]). Quark masses are denoted by m_q . The SU(3) generator matrices introduced here obey the algebra

$$[t^a, t^b] = if_{abc} t^c,$$

defining the QCD structure constants f_{abc} . The classical QCD Lagrangian exhibits the property of local gauge invariance, i.e. invariance under a simultaneous redefinition of the quark and gluon fields. As a consequence of this internal symmetry, it is impossible to define the gluon field propagator without explicitly specifying a choice of gauge. A Lorentz-covariant way to fix the gauge is given by the class of R_ξ gauges, imposed by adding a term

$$\mathcal{L}_{\text{gauge-fixing}} = -\frac{1}{2\xi} (\partial^\mu A_\mu^a)^2$$

to the classical Lagrangian. Because of the non-Abelian character of the QCD gauge group, the full Lagrangian of the quantum field theory features a further contribution, the ghost Lagrangian

$$\mathcal{L}_{\text{ghost}} = \partial_\mu \eta^{a\dagger} (D_{ab}^\mu \eta^b),$$

that represents the field-dependent Faddeev–Popov determinant. The ghost fields η^a are represented by anti-commuting scalar fields. This completes the Lagrangian for a consistent version of a quantum field theory of the strong interaction. Accordingly one can read off the QCD Feynman rules, featuring three-point quark-quark-gluon and ghost-ghost-gluon interactions as well as triple and quartic gluon self-interactions. All of these interaction vertices are proportional to the strong charge g_s . This is also the relevant parameter when applying the method of perturbation theory to QCD. Defining the QCD counterpart of the QED fine-structure constant $\alpha_s = g_s^2/4\pi$, one can expect a truncation of the power-series expansion for a given observable \mathcal{O} , i.e.

$$\mathcal{O} = \mathcal{O}_0 + \mathcal{O}_1 \alpha_s + \mathcal{O}_2 \alpha_s^2 + \dots,$$

to yield meaningful estimates as long as $\alpha_s \ll 1$.

A prime example of a quantity evaluated in perturbation theory is the QCD β function. It determines the running of the coupling constant α_s through the renormalisation group equation

$$Q^2 \frac{\partial \alpha_s}{\partial Q^2} = \beta(\alpha_s), \quad \text{with} \quad \beta(\alpha_s) = -\alpha_s^2 (b_0 + b_1 \alpha_s + b_2 \alpha_s^2 + \mathcal{O}(\alpha_s^3)), \quad (1)$$

and

$$b_0 = \frac{33 - 2n_F}{12\pi}, \quad b_1 = \frac{153 - 19n_F}{24\pi^2}, \quad b_2 = \frac{77139 - 15099n_F + 325n_F^2}{3456\pi^3}. \quad (2)$$

n_F denotes the number of quark flavours with masses m_q smaller than the scale Q . Note that the higher coefficients b_2 and b_3 (see Ref. [4]) are renormalisation-scheme dependent. Here b_2 is quoted in the $\overline{\text{MS}}$ scheme. Retaining only the leading term b_0 , equation (1) is solved by

$$\alpha_s(Q^2) = \frac{\alpha_s(\mu^2)}{1 + b_0 \ln(Q^2/\mu^2) \alpha_s(\mu^2)}, \quad (3)$$

which relates the strength of the coupling at a scale Q to the one at scale μ , assuming both scales to be in the perturbative regime. The non-Abelian nature of QCD manifests itself in the negative sign of the β function. Thus, as long as $n_F < 17$, the coupling becomes weaker at higher scales Q , or, in other words, the QCD colour charge decreases when the distance decreases. For high scales Q , QCD becomes almost a free theory—a property known as “asymptotic freedom”. It is this weakly coupled regime where perturbative methods can successfully be applied and quantitative predictions for hard scattering processes can be made. The world average value of the strong coupling as of 2014, quoted at the scale of the Z -boson mass M_Z , is given by

$$\alpha_s(M_Z) = 0.1185 \pm 0.0006,$$

derived from hadronic τ -lepton decays, lattice QCD calculations, deep-inelastic scattering data, electron-positron annihilation processes, and electroweak precision fits [5]. Figure 1 shows a summary of measurements of the strong coupling at energy scales ranging from the mass of the τ -lepton of $M_\tau \approx 1.8$ GeV up to the TeV scale thanks to newly included LHC data. The historical development of α_s determinations is discussed in Chap. 12, Fig. 12.2, of Ref. [1].

The dynamical behaviour of $\alpha_s(Q^2)$ implies an increase of the QCD coupling at small momentum transfer, i.e. large distances. When the coupling approaches unity, perturbation theory is not valid anymore. The parameter Λ_{QCD} is defined as the scale, where $\alpha_s(Q^2)$ formally diverges. With this definition, equation (3) can be rewritten as $\alpha_s(Q^2) = (b_0 \ln(Q^2/\Lambda_{\text{QCD}}^2))^{-1}$. For $n_F = 5$ flavours in the $\overline{\text{MS}}$ scheme, Λ_{QCD} roughly amounts to 214 MeV and represents the dividing line below which one is in the manifestly non-perturbative regime of QCD. It is the growth of the coupling at small scales that makes QCD a theory of the strong interaction—the fundamental force that confines the quarks and gluons into ordinary hadronic matter, e.g. the protons and neutrons. For the purpose of LHC physics, one has to account for this phenomenon of “confinement” when modelling the transition from free quarks and gluons to the bound-state hadrons observed in the detectors. Lacking a first-principles understanding of this process, one mostly has to rely on MC models for this aspect. Even more fundamentally, the partonic content of the colliding protons needs to be parametrised in order to allow for a description of LHC collision events through partonic scattering processes.

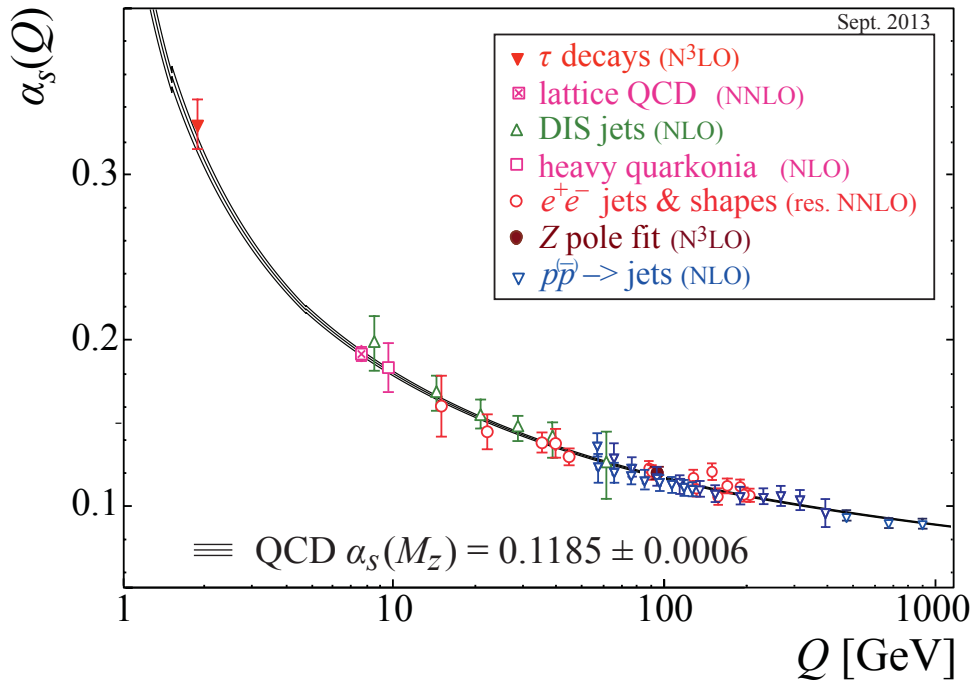


Fig. 1. Summary of measurements of the strong coupling α_s as a function of the respective energy scale Q . By including new LHC data, the range in Q could be extended to the TeV scale. (*Adapted from Ref. [5].*)

3 Perturbative QCD

Quantitative predictions based on the non-Abelian QCD Lagrangian can be obtained either with lattice methods employing a discretised space-time or using perturbation theory. Given the complexity of the final states produced in proton-proton collisions with high momentum transfer, lattice techniques are of no practical importance for the prediction of LHC events at present. Instead one has to rely on perturbative methods, which are possibly supplemented by models for the transition of partons to hadrons.

3.1 Cross-Section Predictions

In perturbative QCD, the cross section for a hard scattering process at a hadron-hadron collider can be written in the following factorised form

$$\begin{aligned} \sigma_{H_1 H_2 \rightarrow X} &= \sum_{i,j} \int dx_1 dx_2 f_{i/H_1}(x_1, \mu_F) f_{j/H_2}(x_2, \mu_F) \\ &\quad \times \hat{\sigma}_{ij \rightarrow X} \left(x_1 P_1, x_2 P_2, \alpha_s(\mu_R), \frac{Q}{\mu_F} \right), \end{aligned} \quad (4)$$

where the sum extends over all contributing initial-state partons $i, j \in \{q, \bar{q}, g\}$. It is assumed here that the scale associated with the hard process, Q , is much larger than Λ_{QCD} , the delimiting scale for the applicability of perturbative methods to QCD. In this high-energy limit, effects related to the binding of the partons in the initial-state protons can be neglected. As a consequence, the cross section simply factorises into a product of parton distribution functions (PDFs) $f_{i/H}(x, \mu_F)$ of non-perturbative origin and the perturbatively calculable partonic cross section. The parton distribution functions model the probability to find a parton of flavour i in the incoming hadron H (protons at the LHC) with a fraction x of the hadron's momentum P . The resulting squared partonic centre-of-mass energy is given by $\hat{s} = x_1 x_2 s$, with $s = (P_1 + P_2)^2$ the squared hadronic centre-of-mass energy.

The collinear factorisation ansatz underlying equation (4) is the key to quantitative predictions in the framework of QCD that can be compared to actual LHC collision data. Based on the property of asymptotic freedom of QCD, the desired cross section can be expanded as a power series of the coupling

constant α_s . The lowest-order coefficient is denoted as leading order (LO), the subsequent ones as next-to-leading order (NLO) and next-to-next-to-leading order (NNLO), respectively.

When calculating the LO, NLO or NNLO estimate for a partonic cross section, the appropriate QCD evolution of the parton distribution functions has to be used.

Leading-order cross-section calculations are fully automated by means of tree-level matrix-element generator programs such as ALPGEN [6], AMEGIC [7], COMIX [8], HELAC/PHEGAS [9], MADGRAPH [10] or WHIZARD [11]. These codes are capable of providing integrated cross sections and parton-level events for almost arbitrary Standard Model final states, with multiplicities ranging up to ten particles. In particular for high-multiplicity final states, implementations relying on recursive algorithms for the generation of the expressions for the amplitudes, e.g. Berends–Giele recursion [12], prove most efficient [13, 14].

Over the past years there has been enormous progress in the evaluation of processes at NLO and NNLO in the strong coupling. These developments and related precision measurements will be addressed in detail in later sections of this chapter.

3.2 Fragmentation and Hadronic Jets

One entity from equation (4) that has not yet been discussed is the final state X of a collision. The simplest reaction that can be considered is the Drell–Yan process [15], where a quark and an antiquark annihilate to produce a lepton pair: $\hat{\sigma}(q\bar{q} \rightarrow \ell^+\ell^-)$. In this case there are no strongly interacting particles in the final state, and the theory prediction can directly be compared to the measured leptons. Merely the proton remnants, which fragment into hadrons along the beam lines, have to be described by non-perturbative models in MC event generators. At high transverse momenta, the two leptons are well separated from any such proton debris and high-precision comparisons with theory even at NNLO become possible. This is discussed in more detail later in this chapter.

However, in the vast majority of reactions at least some colour-charged partons are produced so that a further step covering the transition from the partonic final state to measurable particles, the so-called “particle level”, is needed. Here, “measurable” refers to colour-neutral particles with mean decay lengths such that $c\tau > 10\text{ mm}$, where c is the speed of light and τ the lifetime of a particle. One possibility to account for this transition is to reuse the concept underlying the PDFs that describe the partonic content of a hadron, only in an inverted sense. The necessary functions $D_{k \rightarrow h}(z, \mu_F)$ are called fragmentation functions (FFs) and are the final-state analogues of the PDFs. They parametrise the probability of finding a hadron h within the fragmentation products of parton k , carrying the fraction z of the parton momentum. Like the PDFs, fragmentation functions depend on a non-physical resolution or fragmentation scale μ_F . Again, these functions can currently not be determined by first principles in QCD, but once they have been measured (for example under the experimentally more favourable conditions of e^+e^- collisions at the LEP collider), they are universally valid.

A second possibility to account for the transition to measurable particles makes use of the concept of hadronic jets. Instead of looking into the detailed production of identified particles—an experimentally very challenging endeavour—for the majority of processes it is sufficient to know how much energy and momentum is carried away by hadrons. QCD predicts that large-distance non-perturbative (NP) effects are mostly decoupled from the hard reaction so that highly energetic partons fragment into a collimated stream or “jet” of hadrons, which inherits energy and momentum from its parent parton. To define what “collimated” means, a prescription is required that, given some distance measure, unambiguously decides which objects belong to a jet. As one wants to compare predictions by pQCD with measured particles, tracks, or energy depositions as illustrated in figure 2, a jet algorithm is needed that is applicable to theoretical calculations as well as to measurements from different experiments.

Most importantly, to deal with the cancellation of collinear and soft singularities appearing in pQCD, a jet algorithm must be collinear- and infrared-safe. This means that the outcome of a jet-clustering procedure depends neither on the splitting or merging of collinear parton four-vectors nor on the addition of arbitrarily soft partons to the list of objects to be clustered. The first description of a collinear- and infrared-safe jet algorithm, which grouped partons or particles together that are inside an angular cone around a specific direction, was given by G. Sterman and S. Weinberg in 1977 [16].

The most important requirements for jet algorithms from the experimental side are i) independence of detector details, ii) maximal reconstruction efficiency, iii) minimal resolution smearing, iv) computational efficiency, and v) ease of calibration. The extension of the original jet definition, which was specialised to 2-jet events in e^+e^- collisions, to all kind of reactions and the partially conflicting requirements lead to various new propositions that were tried and discussed in several workshops [17–19]. Two classes of jet algorithms emerged:

1. cone algorithms that geometrically assign objects to the leading energy-flow objects in an event;

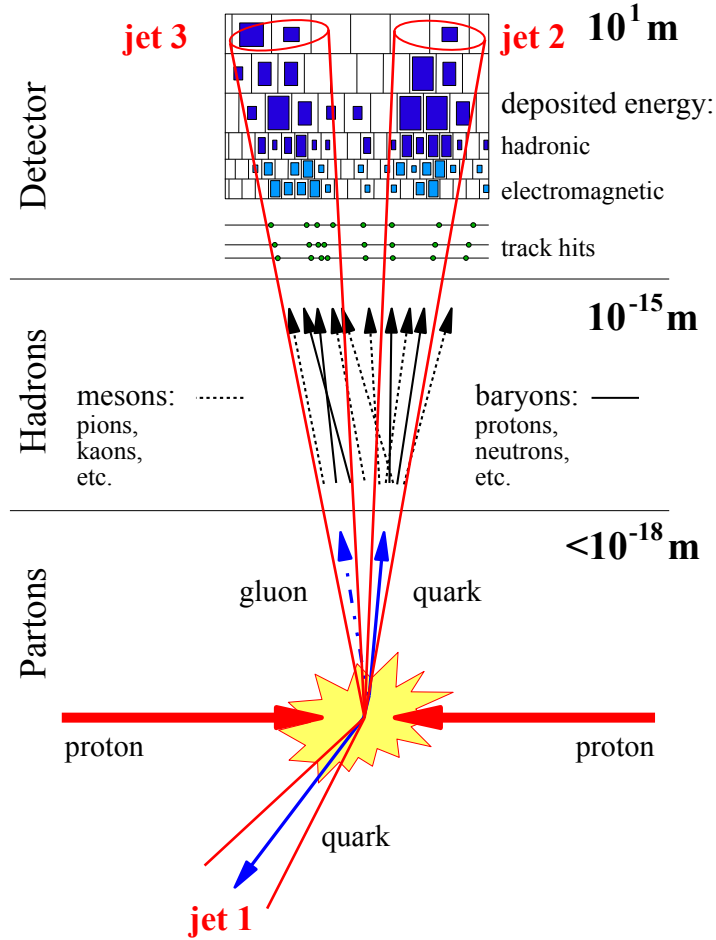


Fig. 2. Illustration of a jet to which bundles of partons, hadrons, or detector measurements are grouped together.

2. sequential-recombination algorithms that iteratively combine the closest pairs of objects [20].

Many cone algorithms need starting points with a minimum energy or momentum for the cone directions—so-called “seeds”. These spoil the condition of collinear safety. A seedless infrared-safe cone algorithm exists in the form of the SISCON algorithm [21], which avoids this problem. For reasons of computational efficiency, though, the method of choice employed at the LHC is the anti- k_t clustering algorithm [22] as implemented in the FASTJET package [23]. For the jet size parameter R (the equivalent to the cone size in cone algorithms) the LHC collaborations chose the values 0.4 and 0.6 for ATLAS respectively 0.5 and 0.7 for CMS. An extensive overview of jet definitions in QCD and their history is presented in Ref. [24].

The most fundamental quantity of jet production that can be investigated is the inclusive jet cross section as a function of the jet p_T and rapidity y , $d^2\sigma/dp_T^{\text{jet}}dy$, where every jet of an event contributes. Figure 3 presents a summary of inclusive jet cross section measurements, performed with various jet algorithms, from pp or $p\bar{p}$ collisions at centre-of-mass energies from 546 GeV up to 7 TeV at central rapidity. The measured cross sections stretch over eleven orders of magnitude and range up to 200 GeV at SPS, 600 GeV at the Tevatron, and 2 TeV at the LHC.

LO predictions (not shown) correctly describe the steep drop with increasing p_T^{jet} , but fail to predict the absolute values more precisely than in an order-of-magnitude estimation. More accurate calculations at NLO are able to improve this situation.

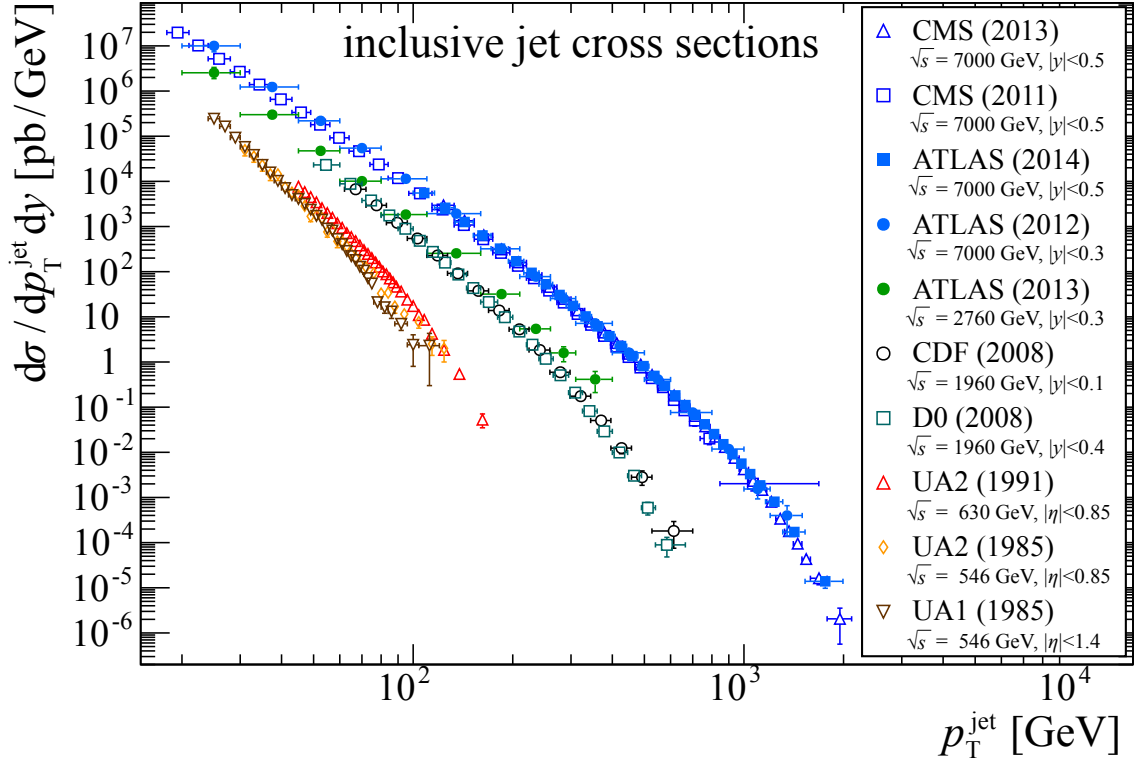


Fig. 3. Summary of inclusive jet cross-section measurements at pp or $p\bar{p}$ colliders. Data taken from Refs. [25–35].

4 Parton Showers: The Bulk of the Emissions

The strength of the collinear factorisation ansatz allowing us to define universal PDFs and FFs lies in its repeated applicability. It enables us to define evolution equations such as the DGLAP equations [36–39], which determine the variation of the PDFs and FFs when the factorisation scale μ_F is changed. For the case of the initial state PDFs one derives

$$\mu_F^2 \frac{\partial f_i(x, \mu_F)}{\partial \mu_F^2} = \sum_{j=\{q, \bar{q}, g\}} \int_x^1 \frac{dz}{z} \frac{\alpha_s}{2\pi} P_{ij}(z) f_{j/H}(x/z, \mu_F), \quad (5)$$

with P_{ij} the (plus-prescription) regularised Altarelli–Parisi splitting functions

$$\begin{aligned} P_{gq}(z) &= C_F \left(\frac{1 + (1-z)^2}{z} \right), & P_{qq}(z) &= C_F \left(\frac{1+z^2}{(1-z)_+} + \frac{3}{2} \delta(1-z) \right), \\ P_{qg}(z) &= T_R (z^2 + (1-z)^2), & & \\ P_{gg}(z) &= 2C_A \left(\frac{z}{(1-z)_+} + \frac{1-z}{z} + z(1-z) \right) + \delta(1-z) \frac{11C_A - 4n_F T_R}{6}. \end{aligned} \quad (6)$$

Furthermore, it should be noted that $P_{g\bar{q}} = P_{gq}$ and $P_{\bar{q}\bar{q}} = P_{qq}$. While the LO, i.e. one-loop, approximation is quoted here, the QCD splitting functions are known up-to NNLO, i.e. three-loop accuracy [40, 41]. The LO DGLAP evolution allows for an interpretation by means of simple branching processes. A parton i resolved at scale μ_F may have originated from a branching of parton j resolved at some higher scale. This transition of parton j to i is accompanied by the emission of an additional QCD parton. When applying the DGLAP equations to solve for the scale evolution of PDFs or FFs, these emitted particles get ignored, by considering inclusive processes only.

However, in parton-shower MC programs these emissions are made explicit, and the subsequent branching of initial-state and final-state partons results in a cascade-like picture, modelling the initial-

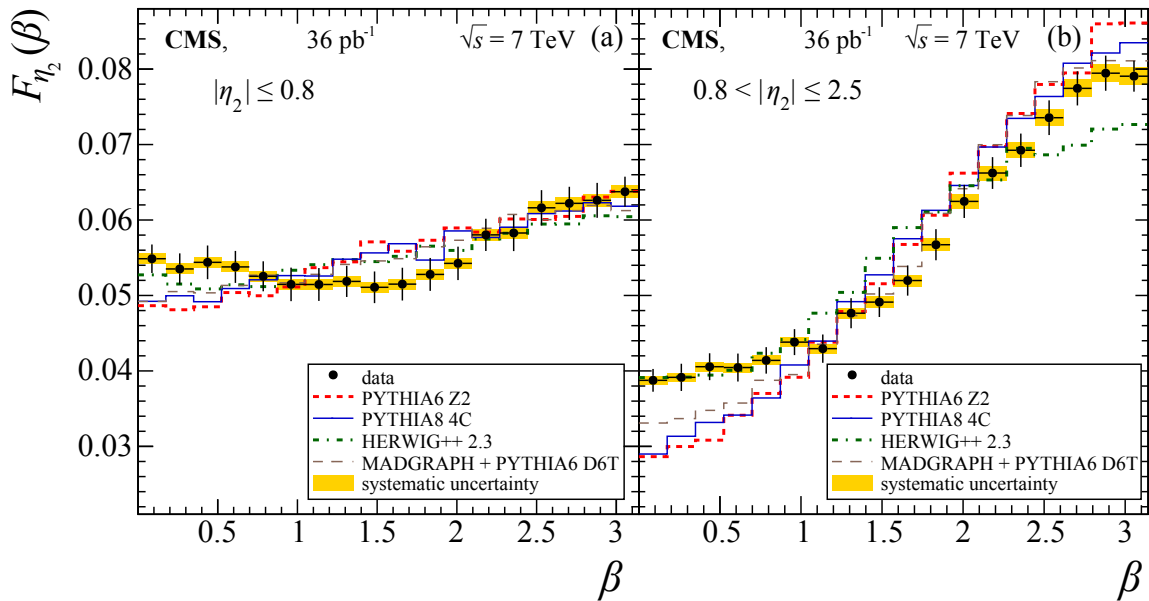


Fig. 4. Measured normalised β distribution, corrected for detector effects, in comparison to various MC predictions. The error bars indicate the statistical uncertainties, while the shaded bands correspond to the total systematic uncertainty. (Adapted from Ref. [50].)

and final-state evolution of the hard process' parton configuration into an ensemble of many QCD partons. In essence these parton-shower emissions approximate higher-order real-emission corrections to the hard scattering process. Shower simulations form an integral part of MC event generators—simulation tools to describe the fully exclusive hadronic final states of individual scattering events [42]. They link the hard scattering at some high scale Q^2 to an exclusive set of partons with typical separation scales of order $Q_0^2 \approx 1 \text{ GeV}^2$, the cut-off scale of the shower evolution. Through this parton-shower link it is possible to invoke universal models for the hadronisation of partons into hadrons, independent of the hard process scale Q^2 . Physically, parton showers account for the intra-jet evolution of jets by accounting for the emission of almost collinear partons, and they model the inter-jet QCD activity through the emission of soft, wide-angle partons.

4.1 Colour Coherence

In particular the correct incorporation of soft-gluon emissions needs special consideration. In contrast to collinear emissions, which factorise at the cross-section level, soft-gluon emissions factorise at the level of individual QCD amplitudes. One should therefore consider soft gluons to be emitted by the scattering process as a whole, given by the squared sum of all contributing amplitudes. At first glance this approach seems to spoil the parton-shower picture of independent subsequent emissions. However, soft colour-coherence effects originating from the interference of individual amplitudes can be incorporated into parton-shower simulations by suitable choices for the shower-evolution variable. Most prominently this can be achieved by using the emission's opening angle as ordering parameter, as employed in the HERWIG and HERWIG++ generators [43, 44].

However, angular ordering is not the only option to include colour-coherence effects. A lot of effort went into the construction of new parton-shower algorithms based on subtraction formalisms as they are used in NLO QCD calculations. These new shower schemes, either based on Catani–Seymour dipole factorisation [45–47] or antenna subtraction [48, 49], implement soft-gluon coherence through a partial fractioning of the QCD radiator antennas, thereby introducing the notion of an emitter, i.e. splitter, and an associated spectator parton that accompanies the splitting process.

In order to study QCD coherence effects one needs to devise observables sensitive to rather soft emissions. This can be achieved by selecting final states with at least three jets exhibiting a sizeable spread in transverse momentum between the hardest and the softest jet. One such analysis was presented by the CMS collaboration in Ref. [50], based on a data set with an integrated luminosity of 36 pb^{-1} collected in 2010. The analysis inspects events with at least three anti- k_t jets using a distance parameter

of $R = 0.5$, ordered in transverse momentum such that $p_{T,1} > p_{T,2} > p_{T,3}$. The event selection criteria are given by

$$\begin{aligned} p_{T,1} &> 100 \text{ GeV}, \quad p_{T,3} > 30 \text{ GeV}, \quad |\eta_{1,2}| < 2.5 \\ M_{12} &> 220 \text{ GeV}, \quad 0.5 < \Delta R_{23} < 1.5. \end{aligned}$$

The observable considered to probe colour-coherence effects, called β , is defined as the azimuthal angle of the third jet with respect to the second jet, i.e.

$$\tan \beta = \frac{|\Delta\phi_{23}|}{\Delta\eta_{23}}.$$

In the presence of QCD coherence, the emission of the parton initiating the third jet is expected to preferentially lie in the event plane defined by the emitting parton and the beam axis. Figure 4 shows the normalised β distributions measured for two regions of the second-jet pseudo-rapidity, i.e. central $|\eta_2| \leq 0.8$ and forward $0.8 < |\eta_2| \leq 2.5$. The observable is thereby defined as $F_{\eta_2,i}(\beta) = N_{\eta_2,i}/N_\eta$, with N_η the total number of events in the respective η_2 region and $N_{\eta_2,i}$ the number of events in the i th β bin. The data are compared to various particle-level MC predictions, i.e. specific tunes of PYTHIA6, PYTHIA8 [51] and HERWIG++, all based on LO $2 \rightarrow 2$ matrix elements plus parton showers, and a combination of MADGRAPH using exact $2 \rightarrow 2$ and $2 \rightarrow 3$ tree-level matrix elements supplemented by PYTHIA6 parton showers. It has been shown in Ref. [50] that the data clearly support the inclusion of coherence effects in the simulation; the regions of small β and $\beta \approx \pi/2$ are particularly sensitive. However, none of the generators used in the analysis describes the data satisfactorily over the entire phase space. HERWIG++ models the data best but the agreement is rather poor in the forward region around $\beta \approx \pi$. The inclusion of the exact $2 \rightarrow 3$ matrix element from MADGRAPH slightly improves the pure PYTHIA6 parton-shower prediction.

4.2 Azimuthal Decorrelation

Clearly, the inclusion of parton showers is indispensable when attempting to simulate event configurations sensitive to the emission of multiple partons. Exemplary quantities are event shapes [52–54], or sub- or intra-jet-related observables [55–58]. Here, the measurement of dijet azimuthal decorrelations as performed by ATLAS and CMS [59, 60] shall briefly be discussed. The analyses evaluate 36 pb^{-1} and 2.9 pb^{-1} of pp collision data at $\sqrt{s} = 7 \text{ TeV}$ by ATLAS and CMS, respectively. The observable considered is the azimuthal angle $\Delta\phi$ between the two jets leading in jet p_T . For events with exactly two high- p_T jets and nothing else, the azimuthal angle between the two jets is fully correlated through momentum conservation in the transverse plane and $\Delta\phi \approx \pi$. Multi-jet production disturbs this balance so that the two leading jets become decorrelated in azimuthal angle and $\Delta\phi < \pi$. Hence, the observable $\Delta\phi$ is indicative of multi-jet production, while at the same time only the azimuthal angles of the two leading jets are measured, avoiding the large uncertainties associated to the jet energy calibration.

With $\Delta\phi$ it is possible to probe complementary aspects of perturbative QCD. The region $\Delta\phi \approx \pi$ is sensitive to multiple soft and collinear emissions and thus requires a proper resummation of soft and collinear logarithms. The region of large azimuthal decorrelations, i.e. $\Delta\phi \ll \pi$, indirectly probes the production mechanism for additional hard jets and requires the inclusion of higher-order matrix elements. Figure 5(a) shows a comparison of the normalised distribution of $\Delta\phi$ for five slices in leading-jet p_T as measured by CMS [60] to perturbative predictions for three-parton production at LO and NLO, respectively, in the region $2\pi/3 < \Delta\phi < \pi$. The leading order has predictive power only in a very narrow range of $\Delta\phi$. The NLO calculation improves this substantially, but fails when approaching $\Delta\phi \approx \pi$, and below $2\pi/3$ matrix elements for 4-jet production are required.

In figure 5(b) the normalised $\Delta\phi$ distributions as measured by ATLAS [59] are compared for nine slices in leading-jet p_T to predictions from the MC event generators PYTHIA6, HERWIG, and SHERPA. PYTHIA6 and HERWIG are based on LO $2 \rightarrow 2$ QCD matrix elements matched with parton showers. SHERPA additionally includes tree-level matrix elements for $2 \rightarrow 3$ –6 jet production properly matched to its parton-shower algorithm [45, 61]. All three generators describe the data well over the measured range of $\pi/2 < \Delta\phi < \pi$ and all p_T^{max} slices. This includes both the region $\pi/2 < \Delta\phi < 2\pi/3$ where multi-jet contributions are significant and $\Delta\phi \approx \pi$ that cannot be described by a fixed-order calculation.

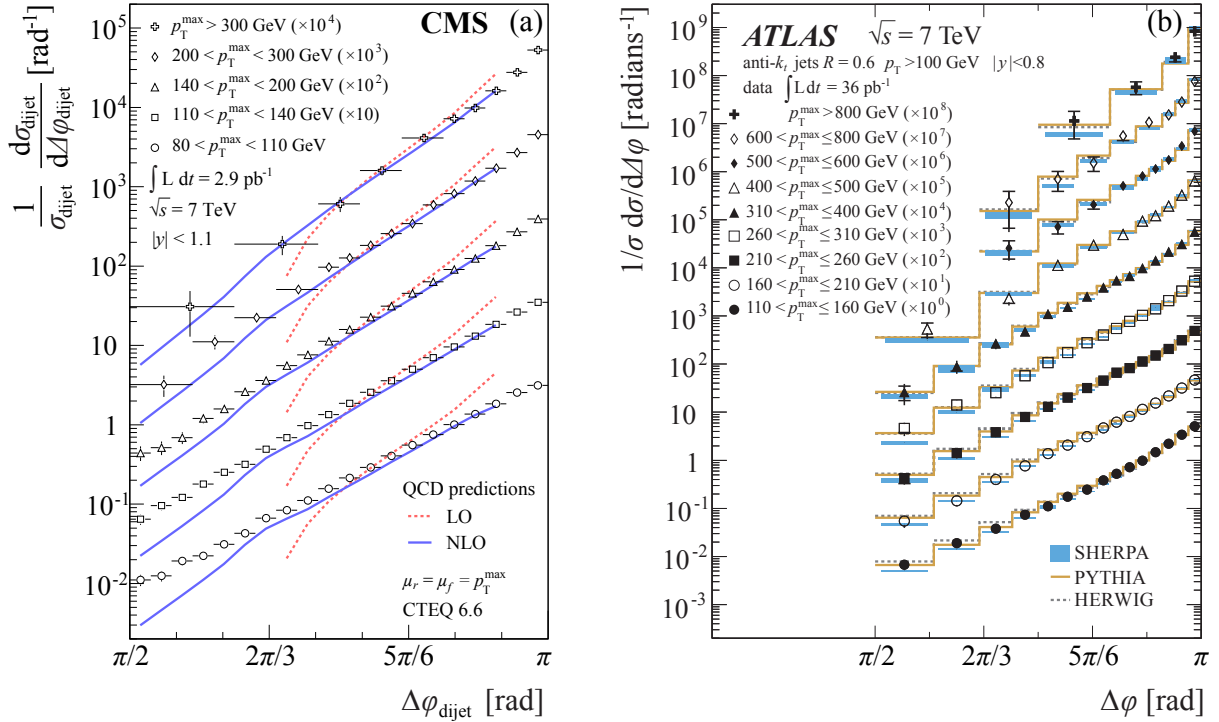


Fig. 5. Normalised differential cross section $(1/\sigma)(d\sigma/d\Delta\phi)$ for multiple slices in leading-jet p_T : (a) CMS data compared to fixed-order predictions in pQCD; (b) ATLAS data compared to predictions by the MC event generators PYTHIA6, HERWIG, and SHERPA. (Adapted from auxiliary material provided with Refs. [59, 60].)

5 NLO: The New Standard

For most observables, NLO predictions in the strong coupling represent the first accurate theoretical estimate that allows an assessment of associated theoretical uncertainties. The evaluation of NLO cross sections, however, is more involved and requires to consider real-emission and virtual one-loop corrections that are individually singular in the infrared region. While these divergences cancel in the sum of both contributions for sufficiently inclusive observables, they render the numerical evaluation of such cross sections difficult. Several state-of-the-art techniques exist that allow the exact cancellation of the divergences separately for the real and virtual contributions through the introduction of suitable subtraction terms. Most widely used is the dipole-factorisation method by Catani and Seymour [62]; alternatives are provided by the Frixione–Kunszt–Signer (FKS) method [63], antenna subtraction [64], or the recently developed Nagy–Soper formalism [65, 66].

The enormous progress recently experienced in the field of NLO QCD calculations was sparked by two important developments: i) the introduction of fast and efficient methods for the calculation of virtual amplitudes, see for instance Refs. [67–72]; ii) the organisation and implementation of complete NLO calculations in the framework of parton-level Monte Carlo event generators such as HELAC/PHEGAS [73], MADGRAPH5_AMC@NLO [74], or SHERPA [75, 76]. All these approaches employ automated subtraction-term generators, see Refs. [66, 77–80], that implement the Catani–Seymour or FKS subtraction formalism. The real-emission corrections as well as the phase-space integration are handled by tree-level matrix-element generators such as AMEGIC [7], COMIX [8], MADGRAPH [10], MADGRAPH5_AMC@NLO [74, 81], or HELAC [9]. Virtual amplitudes, typically provided by specialised one-loop generators such as BLACKHAT [72], GOSAM [82], HELAC-1LOOP [83], MADLOOP [84], NJET [85], OPENLOOPS+COLLIER [86] or RECOLA [87] can be incorporated via the universal BLHA interface [88, 89] or dedicated solutions. Examples of recent NLO calculations that have been performed using a combination of the tools listed above include: $W + 4, 5$ jets [90, 91], $Z + 4$ jets [92], 4-jet and 5-jet production [93–95], $t\bar{t} + 2$ jets [96] and $\gamma\gamma + 3$ jets [97]. Most of these new tools are readily available to perform NLO QCD event generation for use in LHC data analyses.

5.1 Jet Counting

With NLO predictions at hand, more precise comparisons of data and theory become possible. The production of single inclusive jets and of dijets constitute the most basic QCD processes at hadron colliders. Figure 6 shows a comparison between data and theory at NLO, i.e. $\mathcal{O}(c_1\alpha_s^2 + c_2\alpha_s^3)$, for (a) inclusive jets from CMS [32] and (b) dijets from ATLAS [98], both at 7 TeV centre-of-mass energy. Recently, also trijet cross sections were measured [99, 100]. The inclusive jet cross section has been measured as a function of p_T^{jet} and y in ranges of $0.1 \leq p_T < 2.0$ TeV and $|y| < 2.5$ (see Refs. [32, 33]). The dijet cross section is presented as a function of the dijet mass, m_{12} , and rapidity separation, $y^* = |y_1 - y_2|/2$, of the two highest- p_T jets in regions of $0.3 \leq m_{12} < 5.0$ TeV and $y^* < 3.0$, respectively. In both cases the NLO theory has been corrected for non-perturbative effects, and for the more recent ATLAS publication also electroweak (EW) corrections have been considered. While EW effects start being sizeable at high p_T^{jet} and $|y|$ or large m_{12} [101], non-perturbative effects, estimated via their modelling in MC event generators, become negligible. The data are well described by theory over many orders of magnitude in cross section and in wide kinematic ranges so that fits of parameters entering the pQCD calculations become feasible.

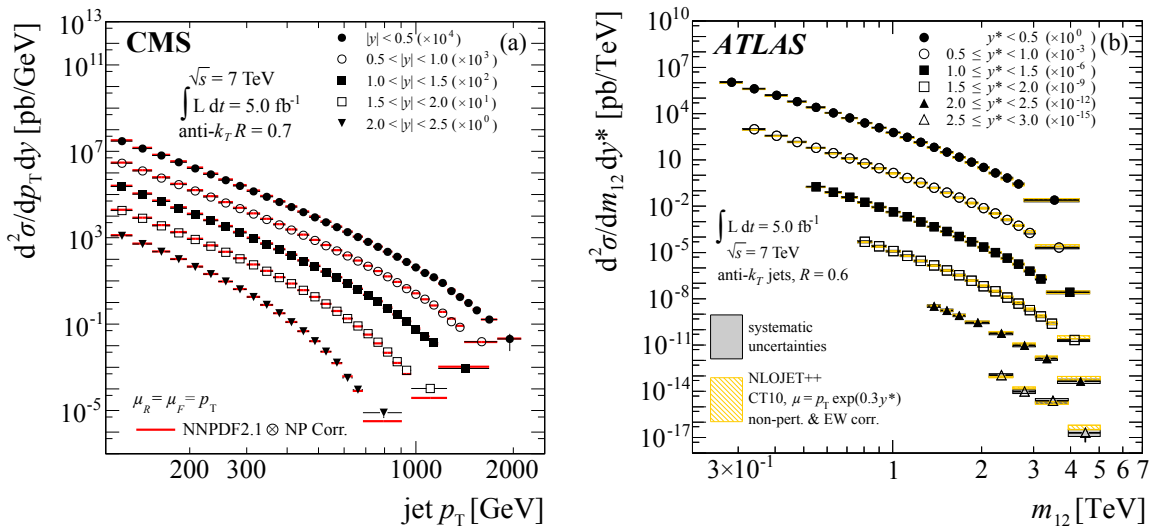


Fig. 6. (a) Inclusive jet cross section from CMS and (b) dijet cross section from ATLAS, both at 7 TeV centre-of-mass energy, in comparison to theory at NLO including non-perturbative (CMS) or non-perturbative and electroweak corrections (ATLAS). The anti- k_t algorithm has been applied with the jet-size parameter R being 0.7 for CMS and 0.6 for ATLAS. (*Adapted from Refs. [32, 98].*)

5.2 Jets and the Gluon PDF

In the following, PDF fits are considered as a first example of determining parameters entering pQCD calculations. Many choices are possible in terms of data set selection, theoretical ingredients and approximations, parameterisation, or fitting techniques and criteria. There is no unique approach to PDF fits. The PDF sets in use at the LHC are produced by six PDF fitting groups: ABM, CTEQ, (G)JR, HERAPDF, MSTW, and NNPDF [102–107], where the quoted publications refer to pre-LHC determinations. The fundamental experimental input central to all PDF determinations are deep-inelastic scattering (DIS) data collected by the H1 and ZEUS collaborations at the ep collider HERA. The HERA collaborations' own PDF fits based solely on their data are presented as HERAPDF sets. The ABM group extends the choice of data to other DIS measurements and fixed-target Drell–Yan data, while the (G)JR group also considers high- p_T jet production, which cannot yet be described at NNLO, to better fix the gluon PDF. The trio of CTEQ, MSTW, and NNPDF finally try to incorporate as many data sets as possible and to provide truly global fits. New PDF sets including LHC data became available recently or are in preparation for the next start-up of the LHC with 13 TeV center-of-mass energy.

It is possible to judge the potential impact of new data, e.g. from the LHC, on a given PDF set without a complete refit. The technique of “Bayesian reweighting” was first implemented in the context of the NNPDF approach [108]. The NNPDF collaboration [109] provides PDF sets in the form of an ensemble of replicas, which sample variations in the PDF parameter space within allowed uncertainties. Their method fits a PDF to smeared data points, where each data point is sampled from a multi-Gaussian distribution. The central value of the distribution is equal to the measurement point and the covariance is taken from the experimental uncertainties. This procedure is repeated N times and provides an ensemble of N PDFs representing the uncertainty of the PDF fit. Hence, the NNPDF prediction for an observable is given by the mean and standard deviation as estimators for the true value and its uncertainty. Via the Bayesian reweighting, the impact of new data can be approximately taken into account by giving according weights different from unity to each replica. If this leads to many replicas with zero or very small weights, this technique cannot be applied and refits must be performed. Otherwise the re-evaluation of an observable while using the re-weighted set of replicas approximately accounts for changes in the PDFs due to the additional data.

In a similar way to the mean and standard deviation as estimators for the main prediction and uncertainty of an observable, the NNPDF ensemble of replicas can be used to investigate the correlation between an observable and the PDFs as a function of energy scale Q and momentum fraction x . As an example, figure 7(a) shows the correlation coefficient ρ between the inclusive jet cross section as measured by CMS [110] and the gluon PDF. For $x > 0.01$ a large positive correlation is exhibited between the two.

In case of the other five PDF sets, the method of diagonalisation of the Hessian matrix [111] (also called “eigenvector method”) is employed to express uncertainty estimates for their respective choices of PDF parameterisation. Their prediction for an observable in pQCD can thus be evaluated from one central PDF set with an uncertainty given by quadratic addition of all deviations obtained while using additional PDFs that correspond to variations along the directions of the eigenvectors. A Bayesian reweighting was shown to be feasible here as well [112], and an alternative approach is studied in Ref. [113].

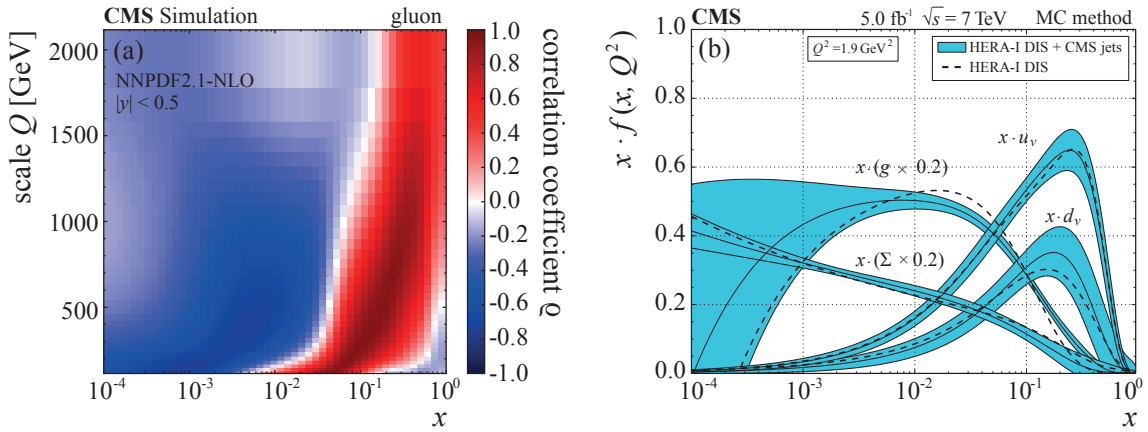


Fig. 7. (a) Correlation coefficient ρ between the inclusive jet cross section and the gluon PDF as a function of energy scale Q and momentum fraction x . (b) PDFs as determined from fits to HERA DIS data alone or in combination with CMS jet data. The uncertainties on the gluon PDF at high x are reduced compared to a fit with DIS data alone (uncertainties not shown). (*Adapted from Ref. [110] and auxiliary material.*)

Employing an open-source tool like the HERAFITTER project [105, 114, 115], which provides fitting code, data sets, and theory predictions in a common framework, it is even possible to perform complete PDF fits. The CMS collaboration used this tool to study the impact of their inclusive jet measurements on the gluon PDF [110] following the fitting setup and using the same DIS data as described in Ref. [105]. The shape of the PDFs at a starting scale Q_0 is assumed to be:

$$\begin{aligned}
xg(x) &= A_g x^{B_g} (1-x)^{C_g} - A'_g x^{B'_g} (1-x)^{C'_g}, \\
xu_v(x) &= A_{u_v} x^{B_{u_v}} (1-x)^{C_{u_v}} (1 + E_{u_v} x^2), \\
xd_v(x) &= A_{d_v} x^{B_{d_v}} (1-x)^{C_{d_v}}, \\
x\bar{U}(x) &= A_{\bar{U}} x^{B_{\bar{U}}} (1-x)^{C_{\bar{U}}}, \\
x\bar{D}(x) &= A_{\bar{D}} x^{B_{\bar{D}}} (1-x)^{C_{\bar{D}}}.
\end{aligned}$$

Here, $xg(x)$ is the gluon distribution, $xu_v(x)$ and $xd_v(x)$ represent the valence quarks with $u_v(x) = u(x) - \bar{u}(x)$, $d_v(x) = d(x) - \bar{d}(x)$, and $\bar{U}(x)$, $\bar{D}(x)$ are the up- and down-type antiquark distributions $\bar{U}(x) = \bar{u}(x)$, $\bar{D}(x) = \bar{d}(x) + \bar{s}(x)$. The indexed symbols A_i , B_i , C_i with $i \in \{g, u_v, d_v, \bar{U}, \bar{D}\}$, A'_g , B'_g , C'_g , and E_{u_v} stand for 19 parameters in the definition of the PDFs. Note that there are no heavy quarks at a starting scale that is chosen to be $Q_0^2 = 1.9 \text{ GeV}^2$. The evolution of PDFs in Q^2 follows from QCD according to equation (5), where in the HERAFITTER setup a generalised-mass variable flavour number scheme [116, 117] is used.

A_g , A_{u_v} , and A_{d_v} are normalisation parameters that are constrained by QCD sum rules. The B and C parameters describe the limiting behaviour when very small, $x \rightarrow 0$, or very large, $x \rightarrow 1$, proton momentum fractions are approached. Additional terms with parameters for the gluon and u -valence distribution allow for some more flexibility in shape, while constraints of $B_{\bar{U}} = B_{\bar{D}}$ and $A_{\bar{U}} = A_{\bar{D}}(1 - f_s)$ are applied to ensure the same normalisation for the \bar{u} and \bar{d} densities at high x . The strangeness fraction is set to $f_s = 0.31$, as obtained from neutrino-induced dimuon production [118]. The parameter C'_g is fixed to 25 [106, 117] and the strong coupling constant to $\alpha_s(M_Z) = 0.1176$ so that in total 13 free parameters remain to be determined.

The PDF fit result using HERA DIS data alone or in combination with CMS jet data is presented in figure 7(b). As expected, a clear impact on the gluon PDF for momentum fractions $x > 0.01$ and a reduction of uncertainties (not shown) is exhibited.

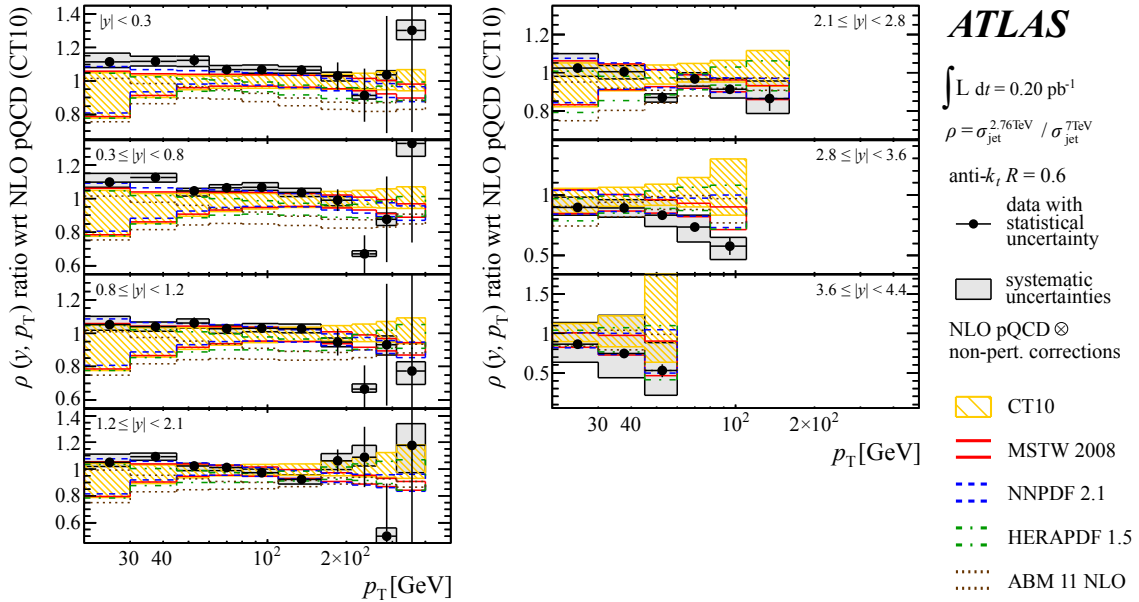


Fig. 8. The ratio of the inclusive jet cross sections at $\sqrt{s} = 2.76$ and 7 TeV as measured by ATLAS divided by a pQCD prediction at NLO (with CT10 PDFs) of the same ratio. Experimental uncertainties are indicated by error bars (statistical) and gray boxes (systematic). The uncertainties inherent to the PDFs are represented by bands. (Adapted from Ref. [35].)

5.3 Jets, Cross-Section Ratios, and the Strong Coupling

Absolute jet cross sections as used in the above CMS example are subject to many experimental sources of uncertainty, and in particular to details of the jet energy calibration. Since the jet- p_T spectrum is steeply falling (see figure 6), an uncertainty in the jet energy scale (JES) of 5% would translate into an uncertainty on the measured cross section of about 25–30%. A means to at least partially cancel such experimental uncertainties was investigated by ATLAS in the form of the ratio of inclusive jet cross sections measured for two different center-of-mass energies (2.76 and 7 TeV) [35]. Figure 8 shows the considerably reduced experimental uncertainties of this ratio compared to the cross sections themselves, thus demonstrating the possibility to provide stronger constraints on PDFs. For comparison, the PDF uncertainties for various PDF sets are indicated as well.

Finally, the possibility to extract the strong coupling constant $\alpha_s(M_Z)$ from inclusive jet production data is studied. As can be seen from figure 7 and the DGLAP equations (5), the appearance of gluons and the strength of $\alpha_s(Q)$ are coupled. Therefore, a simultaneous fit of PDFs and $\alpha_s(M_Z)$ with DIS data alone is not possible, which is also the reason why the value of $\alpha_s(M_Z)$ is fixed in the above-mentioned PDF fit of Ref. [105]. The inclusion of jet data facilitates such a simultaneous fit of PDFs and the strong coupling as demonstrated by CMS [110]. In the following, the focus shall be, however, on the running behaviour of $\alpha_s(Q)$ according to equation (3). To eliminate or reduce numerous experimental sources of uncertainty—such as those related to the luminosity measurement or the jet energy scale—again a ratio is used: that of the inclusive 3-jet over the inclusive 2-jet production cross section, R_{32} . In this quantity, also theoretical uncertainties like those stemming from the PDFs are reduced. Since 3-jet production requires one real emission more than the usual dijets, the numerator is approximately proportional to α_s^3 , while the denominator is $\propto \alpha_s^2$. R_{32} is therefore a direct measure for the strength of the strong coupling. The CMS collaboration has investigated this ratio with the result $\alpha_s(M_Z) = 0.1148 \pm 0.0014(\text{exp}) \pm 0.0018(\text{PDF}) \pm 0.0050(\text{theo})$ [119]. By performing the analysis separately for different regions of the average p_T of the two leading jets, the running could be tested up to scales of 1.39 TeV. Figure 9(a) shows the ratio R_{32} measured by CMS in comparison to predictions at NLO obtained with the CT10 PDF set for a series of assumptions on $\alpha_s(M_Z)$. Figure 9(b) presents a summary of extractions of $\alpha_s(Q)$ including the latest results achieved at the LHC with scales Q reaching beyond 1 TeV.

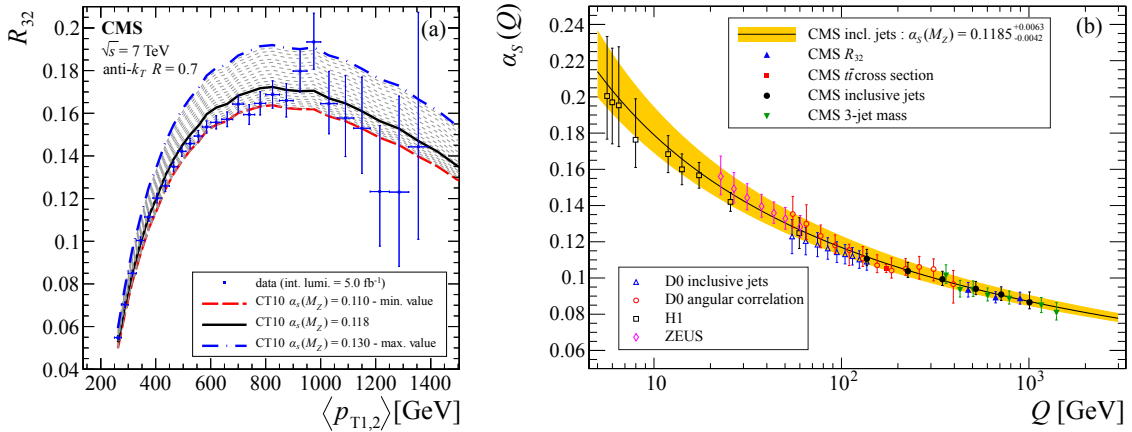


Fig. 9. (a) R_{32} as measured by CMS in comparison to predictions at NLO with the CT10 PDF for a series of assumptions on $\alpha_s(M_Z)$. (b) Summary of extractions of $\alpha_s(Q)$ from low to very high scales Q from various experiments including the latest results achieved at the LHC up to $Q \approx 1$ TeV. (Adapted from Refs. [100, 119] and auxiliary material.)

6 NNLO: The Quest for Precision

For a few benchmark processes and observables, the experimental accuracy of QCD measurements at the LHC is aiming for the few-percent level or even better. Examples are inclusive single-jet or dijet

production, vector boson (pair) production, and top-quark or Higgs-boson production. Clearly, for these channels theoretical predictions at NNLO in the strong coupling are needed, as otherwise the extraction of Standard Model parameters will be limited by theoretical uncertainties.

The evaluation of NNLO corrections for a given process requires the calculation of three contributions: i) generic two-loop graphs; ii) one-loop graphs with one extra final-state parton; iii) real-emission tree diagrams with two additional partons. All of these contributions exhibit infrared singularities, and only their sum yields finite results. In explicit calculations, the divergences are typically treated in dimensional regularisation. Similar to what was discussed for the treatment of infrared singularities appearing in NLO corrections before, there exist now several subtraction schemes to handle these divergences consistently [120–123].

Concerning the above-mentioned processes in need of precision calculations, full NNLO results exist for inclusive W/Z -boson production [124–126], for diboson [127–129] and diphoton production [130], for top-quark pair production [131] and for various Higgs-boson production channels [132–139]. For the NNLO evaluation of dijet production, results have been achieved for two-gluon final states, initiated by gluon annihilation [140], and for quark-antiquark initial states [141]. For the inclusive jet cross section at $\sqrt{s} = 8$ TeV, considering anti- k_t jets with $R = 0.7$, transverse jet momenta of $p_T > 80$ GeV and jet rapidities $|y| < 4.4$, the authors find an increase of the NNLO prediction with respect to the NLO estimate of about 27–16%. The corrections are largest for small jet transverse momenta and decrease for larger values of jet p_T . The given calculation relies on the MSTW08-NNLO PDF set [106] and uses a dynamical scale choice of $\mu = \mu_R = \mu_F$ equal to the transverse momentum of the leading jet. The size of these corrections highlights the importance of higher-order calculations for LHC precision observables. In what follows, two standard “candles” (i.e. well-measured processes or processes with theoretically well-understood cross sections) at the LHC—the Drell–Yan processes and diphoton production—shall be discussed in some more detail.

6.1 Inclusive Vector-Boson Production

Due to the relatively simple colour-singlet production mechanism and an experimental signature based on leptons that can be measured very accurately, the production of W and Z bosons is well suited for precision tests of QCD and electroweak interactions.

At hadron colliders, massive electroweak bosons are dominantly produced via quark-antiquark annihilation. The production of Z bosons is commonly referred to as Drell–Yan process, since in 1970 S. Drell and T.M. Yan applied the developing parton model to predict the scaling of the $pp \rightarrow \gamma/Z \rightarrow \mu^+\mu^-$ cross sections $d\sigma/dM^2 \propto K L(M^2/s)$, with M the invariant boson mass, L the parton luminosity and K a constant that depends on the parton spin and coupling [142]. In modern QCD, the cross section can be expressed as $d\sigma/dM^2 = (4\pi\alpha_{\text{EM}}^2)/(3n_c M^2 s) L_{q\bar{q}}(M^2/s)$, where $L_{q\bar{q}}$ is the quark-antiquark luminosity, α_{EM} the electromagnetic coupling, and n_c the number of colours.

Vector-boson processes are relatively simple to calculate, since there is no QCD interaction involving the final-state particles. In fact, the Drell–Yan process was the first hadron-collider channel known to NNLO accuracy [124–126]. The NNLO Drell–Yan production cross sections can be calculated with a precision of 1% for the renormalisation-scale and factorisation-scale uncertainty. The calculations also include the decay of W and Z bosons to leptons. For inclusive Z -boson production at the LHC, the NLO-to-LO correction is sizeable (about 20%), while the NNLO-to-NLO correction amounts to 2% only. Two public codes implement the NNLO QCD calculations for inclusive Z -boson and W -boson production: DYNNLO [126] and FEWZ [143, 144]. Furthermore, the dominant electroweak corrections have been determined [145–150].

The precise measurement of the inclusive W -boson and Z -boson production cross sections at LHC and their successful comparison to precise QCD calculations was one of the first and very important confirmations of pQCD at very high energies and momentum transfers. Measurements at $\sqrt{s} = 7$ TeV have been performed with the 2010 data set corresponding to an integrated luminosity of 36 pb^{-1} by ATLAS [151] and CMS [152]. CMS also measured the cross sections at $\sqrt{s} = 8$ TeV using a data set of 18.2 fb^{-1} [153].

The cross sections are measured by counting the number of events in the detector acceptance and subtracting the estimated background contributions. The efficiency ϵ is estimated from Monte Carlo simulations and corrected for differences between these simulations and the data. To better separate experimental and modelling uncertainties (in particular from the extrapolation of the detector acceptance to the total phase space), the efficiency is decomposed in a fiducial acceptance, A , and a correction for detector effects, C , i.e. $\epsilon = A \cdot C$.

	$W^+ \rightarrow l^+ \nu$	$W^- \rightarrow l^- \nu$	$Z \rightarrow \ell^+ \ell^-$
7 TeV			
ATLAS	$6.05 \pm 0.12 \pm 0.21$ nb	$4.16 \pm 0.10 \pm 0.14$ nb	$0.937 \pm 0.02 \pm 0.03$ nb
CMS	$6.04 \pm 0.10 \pm 0.24$ nb	$4.26 \pm 0.08 \pm 0.17$ nb	$0.974 \pm 0.02 \pm 0.04$ nb
NNLO QCD	5.98 ± 0.3 nb	4.2 ± 0.2 nb	0.991 ± 0.05 nb
8 TeV			
CMS	$7.11 \pm 0.14 \pm 0.18$ nb	$5.09 \pm 0.12 \pm 0.13$ nb	$1.15 \pm 0.02 \pm 0.03$ nb
NNLO QCD	7.12 ± 0.2 nb	5.06 ± 0.13 nb	1.13 ± 0.04 nb

Table 1. Summary of the cross-section results of the inclusive W -boson and Z -boson analyses of ATLAS and CMS. The total uncertainty (statistical, experimental and acceptance modelling added in quadrature) and the luminosity uncertainties are also given. The theory cross sections are calculated with FEWZ [143, 144] with the MSTW2008-NNLO PDF set [106] and contain renormalisation-scale and factorisation-scale uncertainties and PDF uncertainties.

The fiducial acceptance A is given by the ratio of the number of events passing the kinematic cuts applied on particle-level (i.e. without detector simulation) over the total number of generated events. The kinematic selection cuts are set close to the requirements on the reconstructed objects typically for leptons: $p_T > 20$ GeV and $|\eta| < 2.5$. The detector correction factor C is defined as the number of selected events in the sample including the detector simulation over the number of events passing the fiducial acceptance A . Typically A is 0.45–0.50 and C is 0.7–0.8, depending on the analysis.

A summary of the inclusive Drell–Yan cross-section measurements is shown in table 1. The statistical uncertainty amounts to about 0.3% for W -boson production and 0.7% for Z -boson production. The systematic uncertainty is dominated by the knowledge of the integrated luminosity, which at $\sqrt{s} = 7$ TeV results in an uncertainty of 3.4% (ATLAS) and 4.0% (CMS) and in 2.5% at $\sqrt{s} = 8$ TeV. The measurements of ATLAS and CMS agree within their uncertainties, and both agree with the NNLO prediction that has an uncertainty of about 5% (dominated by the PDF uncertainty).

6.2 Differential Vector-Boson Cross Sections

Apart from the total W and Z production cross sections, also some differential cross sections are known to order $\mathcal{O}(\alpha_s^2)$; this includes the dilepton invariant-mass spectrum, the vector-boson’s transverse momentum and its rapidity distribution.

As an example, figure 10 presents a CMS measurement of the Z -boson production cross section as a function of the invariant mass M of the two leptons from the Z decay at $\sqrt{s} = 7$ TeV [154]. The cross section falls over eight orders of magnitudes in the mass range of $15 < M < 1500$ GeV and clearly shows the Z -boson resonance at 90 GeV. The NNLO calculation using the CT10 PDF set describes the data well. Similar measurements were performed by ATLAS [155].

The boson’s transverse momentum is an interesting observable to test various regimes in the strong-interaction dynamics. The high- p_T part of the spectrum can be modelled by perturbative QCD calculations considering processes with additional jets ($W/Z + n$ -jet processes). Presently calculations can be performed with up to $n = 5$ additional partons. When the transverse momentum of the vector boson is much smaller than its invariant mass reconstructed from the two leptons, soft QCD radiation is enhanced and fixed-order perturbation theory has to be supplemented by the resummation of large logarithmic corrections of the form $\alpha_s^n \ln^m(p_T/M)$ to all orders of α_s . The resummed cross sections also include a non-perturbative component at momentum scales below 1 GeV. This region can also be modelled using Monte Carlo generators implementing parton showers and models for hadronisation.

To lowest order, W and Z bosons are produced via quark-antiquark annihilation, i.e. $q\bar{q} \rightarrow Z$. Indeed, this process dominates for inclusive Z production within a rapidity range of $|y| < 2.1$. However, already for Z transverse momenta around 25 GeV quark-gluon scattering $qg \rightarrow Zq$ is of similar size, and around $p_T = 100$ GeV the latter process constitutes 80% of the total cross section [157]. For Z -boson transverse momenta of 180 GeV, parton-momentum fractions $x_{1/2} = (M/\sqrt{s}) \exp(\pm y)$ of about $x = 0.05$ are probed.

The program RESBOS [158] implements soft-gluon resummation at low p_T at next-to-next-to-leading-logarithm (NNLL) accuracy and matches to a matrix-element calculation of order $\mathcal{O}(\alpha_s^2)$ at high p_T . It provides fully differential cross sections as a function of the rapidity, the invariant mass and the transverse momentum of the vector boson. It also attempts to estimate non-perturbative corrections [159]. Recently, first calculations for Drell–Yan lepton-pair production at NNLO accuracy including parton-shower effects have been presented [160, 161].

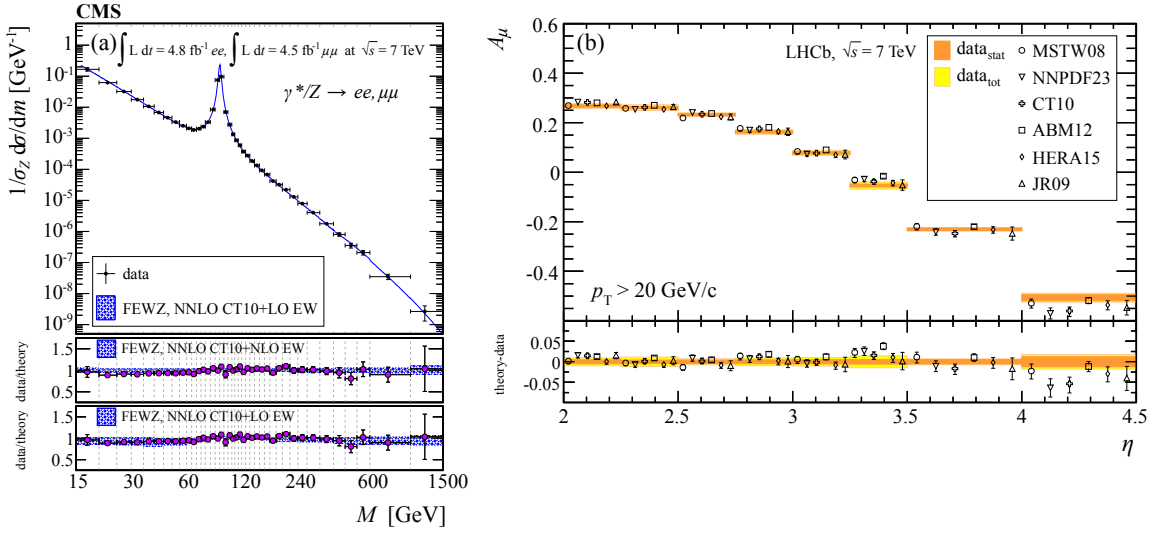


Fig. 10. (a) Drell–Yan cross sections at $\sqrt{s} = 7 \text{ TeV}$ as a function of the dilepton invariant mass M . (b) W -boson charge asymmetry as a function of the lepton pseudo-rapidity. Data are compared to NNLO QCD predictions using various PDF sets. (Adapted from Refs. [154, 156].)

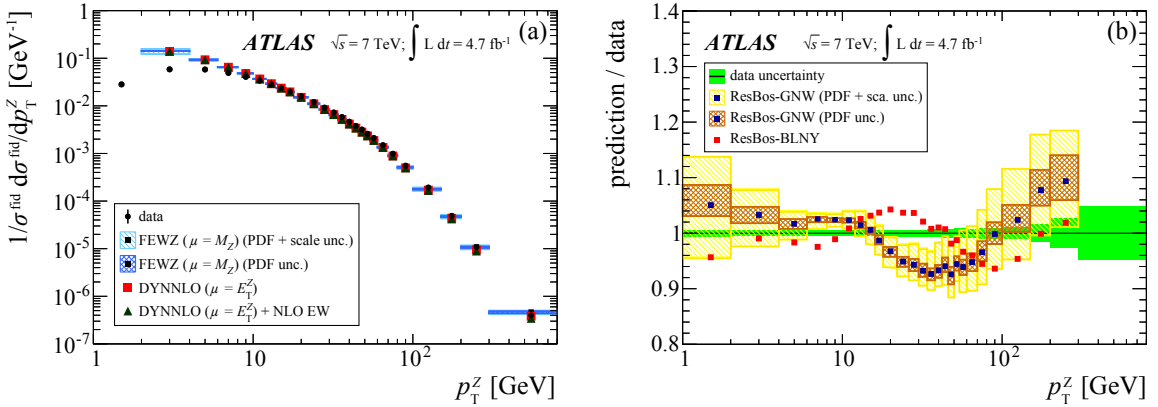


Fig. 11. Normalised transverse momentum of the Z boson measured within the detector acceptance at $\sqrt{s} = 7 \text{ TeV}$. (a) ATLAS data compared to NNLO QCD calculations based on DYNLNLO [126] and FEWZ [143, 144]) with different renormalisation-scale and factorisation-scale settings. (b) Ratio of an NNLO QCD prediction including NNLL resummation to the data. Shown are calculations that differ in the parametrisation of non-perturbative effects. The bands indicate the respective theory uncertainty estimate. The band around 1 denotes the data measurement uncertainty. (Adapted from Ref. [162].)

Early measurements of differential cross sections at $\sqrt{s} = 7 \text{ TeV}$ for Z [163] and W [164, 165] bosons were based on an integrated luminosity of 35-40 pb^{-1} . Recently, the ATLAS experiment updated this measurement to a larger data set corresponding to an integrated luminosity of 4.7 fb^{-1} . This measurement reaches Z -boson transverse momenta of 800 GeV for rapidities up to 2.4 [162]. The measurement uncertainty amounts to 1% for $p_T < 150 \text{ GeV}$ and rises to about 5% for the highest p_T . The leptonic decays of the Z boson to electrons or muons are used in the analysis, and electrons or muons with $p_T > 20 \text{ GeV}$ and rapidity $|y| < 2.4$ are required. The invariant mass of the dilepton pair must lie between $66 < M < 116 \text{ GeV}$. Figure 11 shows the comparison of the data to the NNLO QCD predictions based on DYNLNLO [126] and FEWZ [143, 144] using the CT10 PDF set. Shown as a band are theory uncertainties that are due to the renormalisation-scale and factorisation-scale variations and associated with the choice of PDFs for both calculations. The measurement uncertainties are below a percent in most bins and are smaller than the theory uncertainties that reach 10% around 50 GeV . The two calculations are in excellent agreement with each other for $p_T < 100 \text{ GeV}$, but differ at large p_T by about 10%. In the

region $10 < p_T < 100$ GeV the predictions are 10% lower than the data. For $p_T < 10$ GeV the fixed-order calculations diverge and clearly disagree with the data.

The resummed calculation based on RESBOS using the CTEQ6M PDF [166] describes the data within 10%. The observed deviations are covered by the theory uncertainties of the standard non-perturbative parametrisation (denoted “BLNY”). A recent new parameterisation denoted “GNW” [159] predicts a somewhat different shape.

An NLO QCD calculation based on POWHEG interfaced with PYTHIA for parton showers and hadronisation describes the data within 5% for $p_T < 60$ GeV, but deviates by up to 20% over the full p_T range. An NLO QCD calculation based on MC@NLO interfaced with HERWIG for parton shower and hadronisation deviates by up to 40% at high p_T . Leading order Monte Carlo generators based on multi-leg matrix elements, like SHERPA or ALPGEN, agree with data within 5% except for the highest p_T bin. A dedicated tuning of parton-shower parameters in PYTHIA8 interfaced to POWHEG [162] achieves agreement within 2% for $p_T < 50$ GeV. Since the dominant W^\pm production mechanisms at the LHC are $d\bar{u} \rightarrow W^-$ and $u\bar{d} \rightarrow W^+$, measurements of W^\pm -boson production cross sections provide a powerful tool to study the parton density functions of d and u quarks in the proton. In particular, the measurement of the lepton charge asymmetry $A_\ell = (\sigma_{W^+ \rightarrow \ell^+ \nu} - \sigma_{W^- \rightarrow \ell^- \bar{\nu}}) / (\sigma_{W^+ \rightarrow \ell^+ \nu} + \sigma_{W^- \rightarrow \ell^- \bar{\nu}})$ gives valuable information on the d -to- u ratio and also on the sea-quark and sea-antiquark distributions, in particular of the strange quark. By measuring differential cross sections, for instance as a function of the lepton rapidity, different parton-momentum fraction values x can be probed, since the parton-momentum fraction depends on the vector-boson mass and on the rapidity y : $x_{1/2} = (M_{W,Z}/\sqrt{s}) \exp(\pm y)$.

ATLAS published such differential cross-section measurements $d\sigma_{W^\pm/Z}/dy_\ell$ for electrons and muons up to lepton rapidities of $y_\ell = 4.9$ based on the 2010 data set at $\sqrt{s} = 7$ TeV [151]. Leptons with a $p_T > 20$ -25 GeV are selected. For Z bosons, the accuracy reaches about 2% in the central region of the Z -boson rapidity and 10% at $y_Z = 3.2$. A precision of about 2% is obtained for W -boson cross sections measured within $|y_\ell| < 2.5$. For the A_ℓ measurement the accuracy ranges between 4 and 8%. The data can be described by an NNLO calculation using the HERAPDF1.5 and the MSTW08-NNLO PDF sets. Further measurements by ATLAS and CMS can be found in Refs. [152, 165, 167–170].

The LHCb experiment measured W -boson production in the forward region covering lepton rapidities in the range $2 < |y_\ell| < 4.5$. A measurement was performed with the 2011 data set at $\sqrt{s} = 7$ TeV using an integrated luminosity of 1 fb^{-1} . Figure 10(b) shows the measured lepton charge asymmetry for muons with $p_T > 20$ GeV as a function of the muon rapidity compared to NNLO calculations using various PDF sets. The band shows the statistical (inner, dark) and total uncertainty (light) on the data. The experimental accuracy is similar to the theoretical uncertainty estimate, and the predictions are in good agreement with the measurement.

6.3 Production of Photon Pairs with Large Invariant Mass

At leading order in pQCD, the production of photon pairs can rather easily be described by quark-antiquark annihilation, ($q\bar{q} \rightarrow \gamma\gamma$), as for the Drell–Yan process before. However, in contrast to the massive vector bosons W and Z , which are predominantly produced in hard scattering processes and can easily be identified via their leptonic decay modes, massless photons can also be radiated off initial-state or final-state partons or may be created in decays. In particular the π^0 and η mesons, and to some extent also the ω , all of which are copiously produced within jets, have neutral decay modes. Since these particles are boosted within the jets, their decay photons are collimated and difficult to distinguish from a single highly energetic photon. Without applying further selection criteria, the mode of “photon” pair production at large invariant mass via meson decays within two (different) jets is even dominating by several orders of magnitude.

To distinguish the “non-prompt” decay photons within jets from “prompt” photons stemming from the hard scattering, isolation criteria are applied. Typically, isolation demands that the transverse energy not associated to a photon candidate but deposited within a cone of $\Delta R = \sqrt{(\Delta\eta)^2 + (\Delta\phi)^2} = 0.4$ around it may not exceed a few GeV. In addition, a minimal separation of the two photons is required to avoid overlap: $\Delta R_{\gamma\gamma} > 0.40, 0.45$ for ATLAS and CMS, respectively. In practice, the experimental selections are more complicated (see e.g. Refs. [171–174]), and great care has to be taken to ensure that they can be matched properly to selection criteria applicable in theory (see Ref. [175] for a recent discussion on photon isolation).

Finely segmented electromagnetic calorimeters are of great advantage in such photon studies. Investigating the shower shape of energy deposits in these calorimeters helps to differentiate between electromagnetic showers that are caused by a single high-energetic signal photon and those from multiple photons like in $\pi^0 \rightarrow \gamma\gamma$ decays. Photon candidates are separated from electron (or positron) candidates

by using reconstructed tracks. Depending on the amount of material to be traversed (e.g. the beampipe or the silicon-pixel and silicon-strip detectors), however, highly energetic photons may convert into e^+e^- pairs before reaching the electromagnetic calorimeter. Dedicated reconstruction methods are applied to avoid losing these converted photons, which can make up to 50% [174] of the total photon yield.

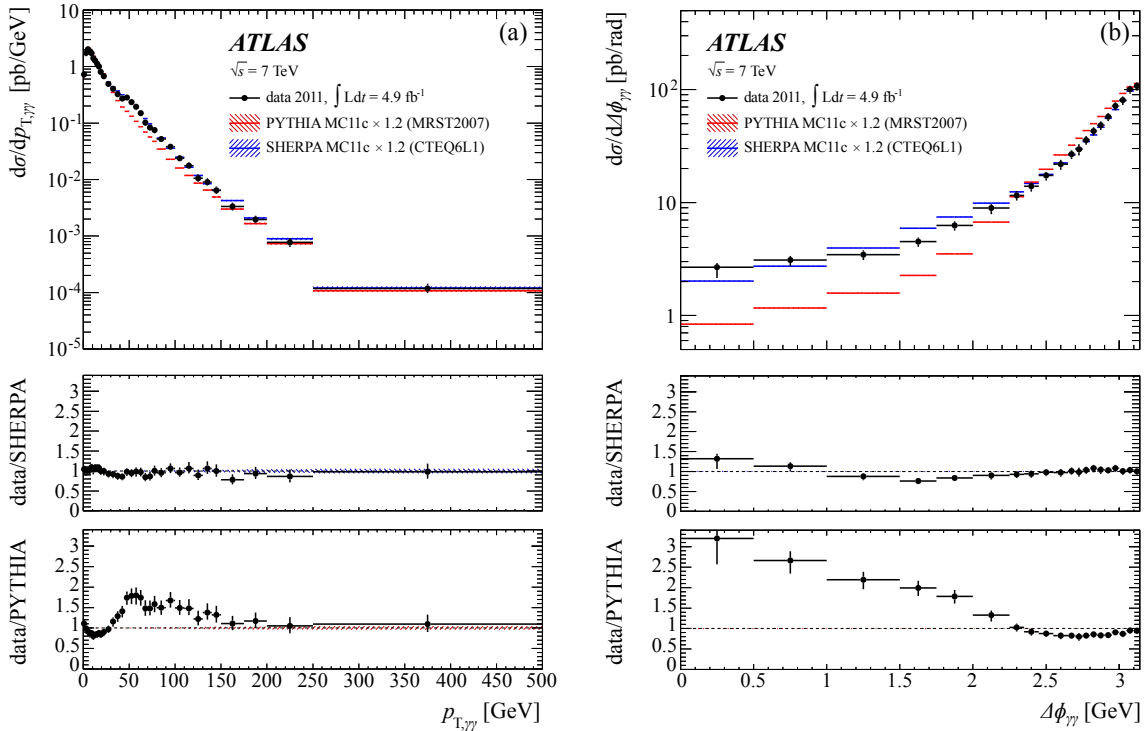


Fig. 12. Photon-pair production cross section at 7 TeV centre-of-mass energy as a function of (a) the diphoton transverse momentum $p_{T,\gamma\gamma}$ and (b) the azimuthal angular separation $\Delta\phi_{\gamma\gamma}$ as measured by ATLAS [172]. The data are compared to parton-shower-improved LO predictions by PYTHIA6 and SHERPA. The MC predictions are rescaled by a factor of 1.2 to match the total cross section observed in data. (*Adapted from Ref. [172].*)

For background subtraction, techniques relying on data are preferred. Detailed studies, necessary to further quantify detector effects on the photon reconstruction and isolation and to unfold the signal yields, are performed with simulated events provided by the LO event generator PYTHIA [51, 176] or by multi-jet-improved event generators that include additional real emissions (extra jets) like SHERPA [76, 177] or MADGRAPH [10]. The latter is combined with PYTHIA for parton showering, hadronisation, and for the modelling of the underlying event, see section 9.

At next-to-leading order, the gluon-initiated processes ($gq(\bar{q}) \rightarrow \gamma\gamma q(\bar{q})$) join the annihilation process ($q\bar{q} \rightarrow \gamma\gamma g$) together with corresponding virtual corrections. Here, a further complication arises from the collinear fragmentation of a hard outgoing parton into a photon. Theoretically, this process is described using fragmentation functions $D_{q \rightarrow \gamma}(z, \mu_F)$ and $D_{g \rightarrow \gamma}(z, \mu_F)$. In the limit of $\mu_F \approx Q$, where Q is the scale of the hard scattering, this fragmentation process results in a contribution to the cross section that is similar in size to the one of the LO annihilation process [178].

Prompt photons not emerging via fragmentation from the hard process are also called “direct”. The effect of the above-mentioned isolation conditions, which aim to suppress fragmentation photons in favour of direct ones, have to be properly estimated not only experimentally for mesons decaying within jets, but also theoretically, e.g. via FFs in the perturbative calculations. The NLO parton-level program RESBOS [179, 180] effectively includes the fragmentation of one quark/gluon to a single photon at leading order and additionally features soft and collinear gluon resummation (see section 8). DIPHOX [178] provides parton-level results at NLO taking fully into account up to two fragmentation photons. Although formally an NNLO box graph, the process ($gg \rightarrow \gamma\gamma$) is drastically enhanced at the LHC through the large gluon luminosity. It is comparable in size to the LO terms, and therefore DIPHOX includes this contribution at NLO precision, i.e. up to N^3 LO corrections in the strong coupling α_s , via GAMMA2MC [181].

Finally, a full NNLO calculation is available in the form of the 2γ NNLO [130] program, however without consideration of fragmentation photons.

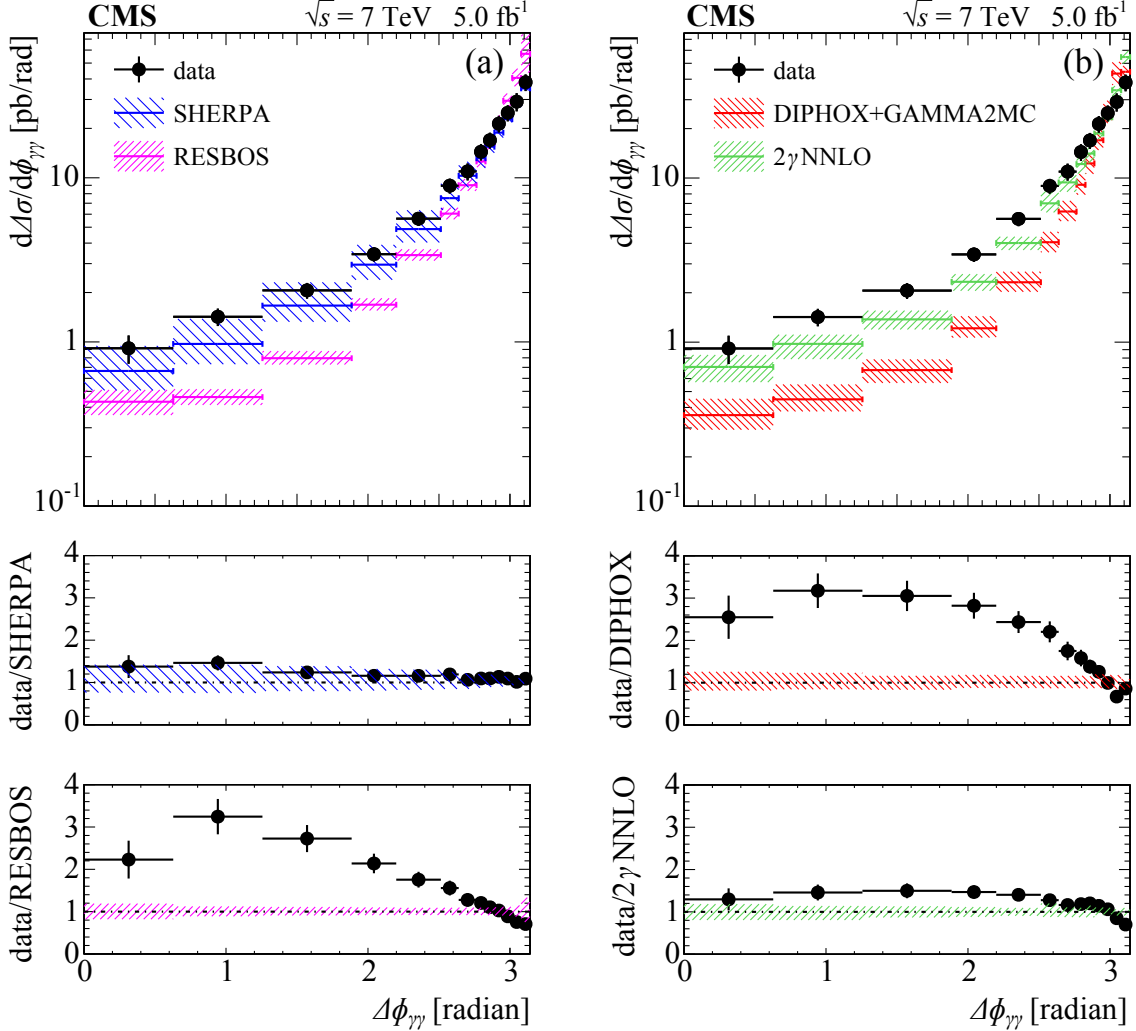


Fig. 13. Photon-pair production cross section at 7 TeV centre-of-mass energy as a function of the diphoton azimuthal angular separation $\Delta\phi_{\gamma\gamma}$ as measured by CMS [174]. (a) Comparison of the data to SHERPA using tree-level matrix elements matched to the parton shower and to NLO results from RESBOS that also include soft-gluon resummation. (b) Comparison to full NLO calculations including contributions of photons produced in jet fragmentation from DIPHOX + GAMMA2MC as well as to NNLO results from 2γ NNLO. (*Adapted from Ref. [174].*)

Four kinematic variables are usually chosen to investigate the differential photon-pair production cross section: the invariant mass $m_{\gamma\gamma}$, the transverse momentum of the photon pair $p_{T,\gamma\gamma}$, the azimuthal angular separation $\Delta\phi_{\gamma\gamma}$, and the cosine of the polar angle in the Collins–Soper reference frame [182] of the diphoton system, $\cos\theta_{\gamma\gamma}^*$. The invariant mass is of obvious interest for resonance searches, where $\cos\theta_{\gamma\gamma}^*$ is useful to examine the spin of diphoton resonances. The transverse momentum $p_{T,\gamma\gamma}$ and the quantity $\Delta\phi_{\gamma\gamma}$ are well-suited for the comparison of specific aspects of the theoretically very challenging description of photon-pair production. In particular, at low $p_{T,\gamma\gamma}$ or for well-balanced photons at $\Delta\phi_{\gamma\gamma} \approx \pi$, where multiple soft-gluon emission becomes important, fixed-order calculations are not expected to work. As an example, figure 12 shows a comparison between data and parton-shower improved LO predictions by PYTHIA6 and SHERPA for $p_{T,\gamma\gamma}$ and $\Delta\phi_{\gamma\gamma}$ from ATLAS [172]. Since both MC event generators fail to accurately predict the total cross section, the distributions have been rescaled by a factor of 1.2 to

match the total cross section in data. In both cases SHERPA provides a good description of the whole distribution, while PYTHIA6 exhibits some discrepancy at low $p_{T,\gamma\gamma}$.

Figure 13(a) furthermore presents comparisons for the cross section differential in $\Delta\phi_{\gamma\gamma}$ for SHERPA and to NLO from RESBOS including soft-gluon resummation. Again SHERPA gives a good overall description, while RESBOS predictions are too low by factors of 2–3 at small separation angles. A similar behaviour can be seen in the comparison to NLO from DIPHOX + GAMMA2MC in figure 13(b), although due to resummation RESBOS performs somewhat better around $\Delta\phi_{\gamma\gamma} \approx \pi$. The best description of the data is given by the NNLO result from 2γ NNLO (figure 13(b)), even though the fragmentation contribution is not included. ATLAS observes similar results when comparing their data to the predictions from DIPHOX + GAMMA2MC and 2γ NNLO [172].

7 Multi-Jets: Precision Meets Multiplicity

Understanding the QCD dynamics governing the emergence of multi-jet final states is of utmost importance at the LHC. Given that typically jet objects with minimal values of their transverse momentum of order 30 GeV are considered, the phase space for producing multiple jets is huge. Accordingly, these jet-production processes need to be described as well as possible, as they constitute severe backgrounds to almost every search for new physics and furthermore have an impact on the appearance of the signals themselves. The modelling of inclusive processes that receive contributions from final states with potentially many jets is the realm of so-called “matching and merging” techniques that combine (multi-parton) fixed-order calculations with parton-shower simulations.

On the one hand, fixed-order calculations provide a well-defined estimate for inclusive production cross sections and reliably account for hard, well-separated parton configurations. On the other hand, parton-shower simulations capture the dominant terms driving the emission of additional soft and/or collinear partons and thus provide the means to perturbatively account for the internal structure of jets and inter-jet energy flows. When combining fixed-order matrix elements with parton-shower resummation beyond leading-order 2-to-2 scattering processes, the obstacle of double-counting configurations that appear in both approaches needs to be resolved. Furthermore, any consistent scheme should neither spoil the logarithmic accuracy of the inherent parton-shower resummation nor destroy the formal precision of the fixed-order part.

There are two basic strategies to distinguish. Tree-level merging techniques correct the hardest emissions of the parton shower off a given core process through exact leading-order QCD matrix elements [183–185]. This is achieved through a slicing of the real-emission phase space in terms of a hardness-measure that regulates any infrared singularities and allows to consistently combine matrix elements of varying parton multiplicity dressed with parton showers into an inclusive sample. Several variants of such leading-order merging techniques exist and are widely used in LHC analyses, see Refs. [61, 186–189].

The second ansatz relies on the exact matching of an NLO QCD calculation with a parton-shower cascade off the underlying Born process. Accordingly, the real-emission correction as part of the fixed-order calculation has to be properly synchronised with the first, i.e. hardest, shower splitting. Furthermore, the NLO accuracy with respect to the inclusive production process considered needs to be preserved. Two basic solutions exist to this problem, which are known as MC@NLO [190] and POWHEG [191]. Over the last years there has been tremendous development in implementing these techniques for a wide range of processes and ultimately their automation, see Refs. [74, 192–195].

Most recently hybrid solutions emerged that combine NLO plus parton-shower calculations with higher-order tree-level QCD corrections [196, 197] or that even combine parton-shower-matched NLO calculations of varying jet multiplicity [198–202].

In the following section, the main focus shall be on a class of processes that constitutes a prototypical Standard Model background and serves as a test bed for the various types of advanced QCD calculations outlined above: W/Z +jets production.

7.1 Weak Bosons and Jets

In the production of W and Z bosons in association with jets (W +jets), very high jet multiplicities can be reached at the LHC. Cross sections for the associated production with up to seven jets with transverse momentum p_T larger than 30 GeV have been measured by ATLAS and CMS. Already the leading-order prediction for this process is of order α_s^7 . However, this class of processes is extremely important as it constitutes a major background to many other processes with complex final states such as top-quark pair or diboson production or rare signatures from the Standard Model or beyond.

The W +jets processes allow an assessment of the validity of Monte Carlo generators like ALPGEN [6], SHERPA [75, 76], or MADGRAPH [10] (together with recent progress in MADGRAPH5_AMC@NLO [74]) that merge tree-level matrix-element calculations with up to five additional partons interfaced with parton showers and hadronisation. Presently, many experimental analyses are in a transition phase adopting NLO matrix-element calculations plus parton showers as baseline for MC event generation instead of the former LO based ones (see Section 5).

Figure 14 shows the W +jets cross section as a function of the leading-jet p_T as measured by CMS [203] and ATLAS [204] using proton-proton collision data recorded at $\sqrt{s} = 7$ TeV. In the ATLAS measurement, jets are defined by the anti- k_t jet algorithm using a radius parameter of $R = 0.4$ and measured within $30 \leq p_T < 300$ GeV and $|y| < 4.4$. The results for up to four additional jets are superimposed and are compared to the predictions of SHERPA and ALPGEN. The measured shape of the jet p_T distribution is described by the Monte Carlo simulation within the uncertainties.

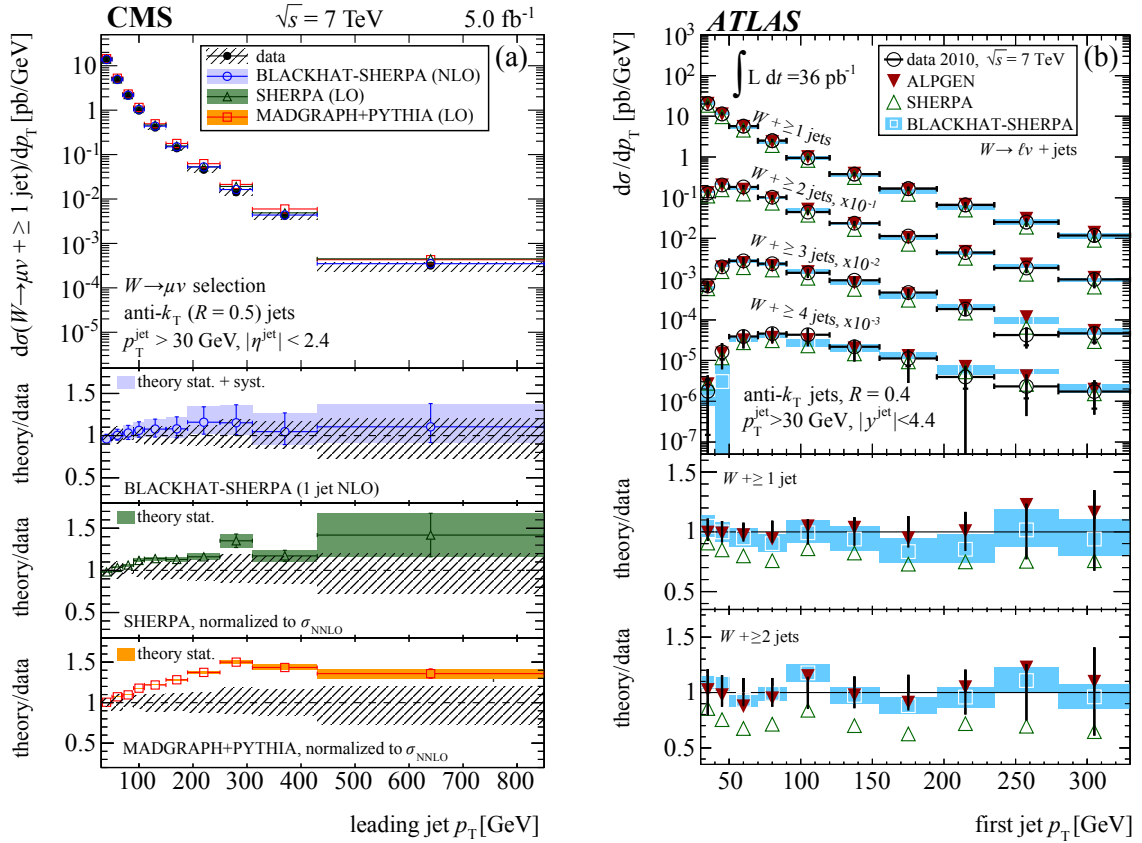


Fig. 14. The W +jet cross section as a function of the transverse momentum of the leading jet as measured by CMS (a) and ATLAS (b). The data are compared to various QCD calculations. For the ATLAS measurement, jet multiplicities up to four jets are shown. The results for higher jet multiplicities are scaled by the factors given in the figure. The leading-order multi-leg calculations are normalised to the inclusive NNLO cross section. (*Adapted from Refs. [203, 204].*)

In the CMS measurement, jets defined by the anti- k_t jet algorithm with $R = 0.5$ are selected with $p_T > 30$ GeV and $|y| < 2.4$. The jet spectrum reaches up to p_T values of 800 GeV. The data fall below the leading-order QCD predictions towards high p_T . The MADGRAPH (SHERPA) estimate using up to four additional partons is almost 50% (20%) higher than the data for $p_T > 200$ GeV.

At the time of the LHC start-up in 2008, NLO QCD calculations with maximally two associated jets were available [205]. Since then, in particular, with the BLACKHAT-SHERPA [90, 206] program significant progress was made in NLO QCD calculations for W or Z production in association with up to five additional partons [91]. Fixed-order calculations, by nature, are not matched to parton showers and hadronisation, so that corrections to account for these effects are derived from generators like PYTHIA or HERWIG are needed. The resulting predictions from BLACKHAT-SHERPA are in good agreement with the measured distributions within the systematic uncertainties as shown in figure 14.

Recently, automated computations of NLO QCD cross sections matched to parton-shower simulations for a large variety of processes (with up to four partons) have been developed. The programs SHERPA (in the MEPS@NLO option [8, 198]) and MADGRAPH5_AMC@NLO [74] presently provide the most accurate predictions for multi-jet final states at particle level.

Similar measurements [207] for the Z +jets processes using the full data set at $\sqrt{s} = 7$ TeV are presented in figure 15 as a function of the leading-jet p_T and the fourth-leading jet p_T . Jets are defined using the anti- k_t jet algorithm with $R = 0.4$ and are selected if $p_T > 30$ GeV and $|y| < 4.4$. The cross sections are normalised to the inclusive Z cross section. Again, the BLACKHAT-SHERPA predictions are in good agreement with both measured distributions.

An NLO QCD calculation for the inclusive Z cross section merged with parton showers and hadronisation as incorporated in MC@NLO is capable of describing the data for events with one or two low- p_T jets, but falls far below the data towards high values of the leading-jet p_T . This indicates that the fraction

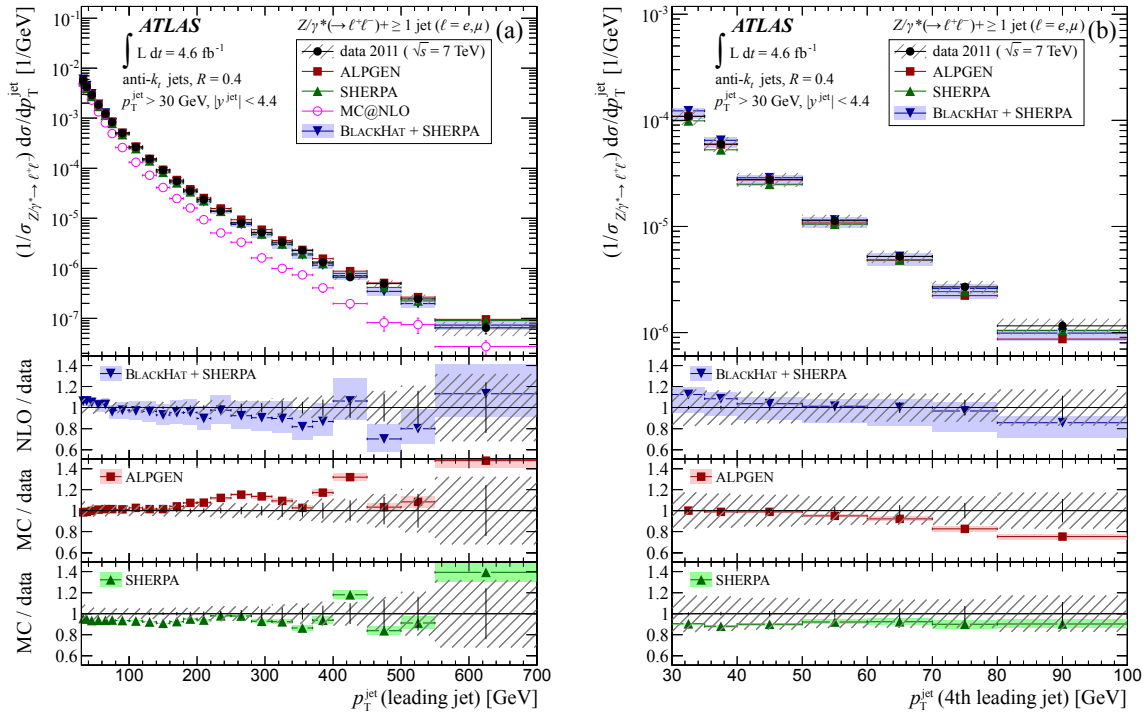


Fig. 15. Z +jets production cross section as a function of the leading and fourth-leading jet transverse momentum as measured by ATLAS. The data are compared to various QCD calculations. (Adapted from Ref. [207].)

of events exhibiting a second jet increases considerably with the p_T of the leading jet and that the parton shower approximation, which is used by MC@NLO for the second jet, fails to describe the data.

The results are also compared to two multi-leg Monte Carlo simulations produced with up to five additional partons. The ALPGEN simulation overestimates the data at high p_T for the leading jets and underestimates the data for the fourth-leading jets. SHERPA is in good agreement with the data considering the experimental uncertainties. The measurements of the Z +jets cross section are limited by the experimental uncertainty on the jet energy measurements. By considering jet-multiplicity ratios, many experimental and theoretical uncertainties cancel, allowing for an even more precise data-to-theory comparison.

The ratio of the Z +jet cross sections for $N_{\text{jet}} + 1$ over N_{jet} ($R_{(N+1)/N} = \sigma(Z + N_{\text{jet}} + 1)/\sigma(Z + N_{\text{jet}})$) was measured by ATLAS [207]. An earlier measurement was performed by the CMS experiment on a smaller data set [208]. Figure 16 shows the ratio $R_{(N+1)/N}$ for successive exclusive jet multiplicities for all events (“inclusive”) and for events with at least one jet with $p_T > 150$ GeV. For the inclusive case, the ratio shows a rather flat, approximately linear dependence on the jet multiplicity with a small slope only, while for events with $p_T > 150$ GeV the measured distribution steeply rises towards low jet multiplicities. These measurements illustrate two limiting cases of scaling patterns, the “staircase scaling” [209] with $R_{(N+1)/N}$ constant and the “Poisson scaling” [210] with $R_{(N+1)/N} = \langle N \rangle / N$, where $\langle N \rangle$ is the average number of jets. These scaling patterns can be qualitatively understood from the expected Poisson-distributed jet multiplicity. For large jet- p_T differences, the Poisson-scaling is directly observed (see figure 16(b)). However, for low p_T and small N_{jet} , the emission of additional partons is suppressed by the PDFs, and for high N_{jet} the emission of additional partons no longer follows a Poisson distribution due to the non-Abelian nature of QCD, leading to a proliferation of the number of jets originating from gluon splitting (see figure 16(a)).

The scaling patterns observed in data are described by the Monte Carlo simulations BLACKHAT-SHERPA, ALPGEN and SHERPA. The scale uncertainty is only shown for the NLO QCD calculation based on BLACKHAT-SHERPA. The different grey shades indicate the scale uncertainty when it is considered uncorrelated (as proposed in Ref. [211]) or correlated across the various jet multiplicities. Assuming the predicted and now observed scaling patterns to be valid, it becomes possible to give estimates for even higher jet multiplicities where there exists no complete NLO prediction yet [212].

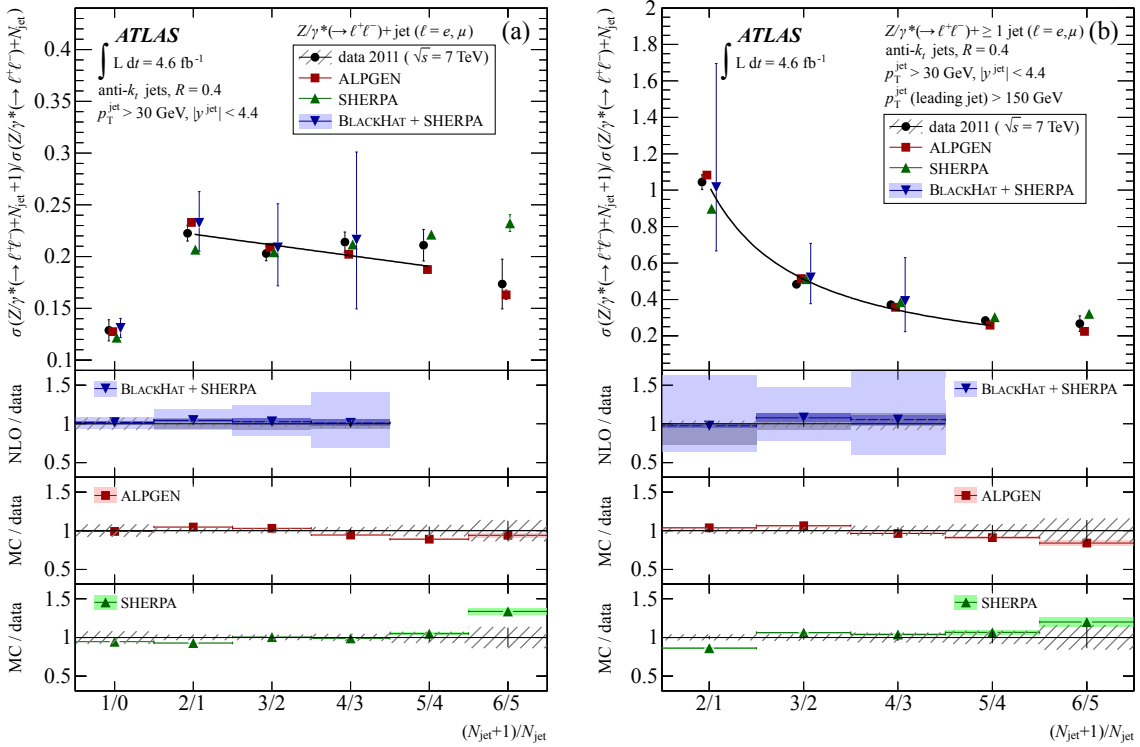


Fig. 16. Ratios of Z +jets cross sections for successive exclusive jet multiplicities for (a) inclusive events and (b) for events with at least one jet with $p_T > 150$ GeV and $|y_{\text{jet}}| < 4.4$. The data are compared to various QCD calculations. (Adapted from Ref. [207].)

7.2 Weak Bosons and Jets with Flavour

Several key processes in the Standard Model and beyond—such as the production of single top quarks, top-quark pairs or Higgs bosons—involve heavy quarks. The understanding of their production mechanisms is therefore an important part of the LHC physics programme. For a detailed discussion of flavour physics at the LHC see Chap. 8 of Ref. [1].

The predictions of processes with heavy-flavour content are more difficult to accomplish than those for the inclusive case. Bottom (b) quarks are significantly heavier than the proton, and in strong interactions at high scales they can only be created in pairs. The calculations can be classified in two types: In the 4-flavour (4F) scheme heavy quarks appear only in the final state and are typically considered massive, while 5-flavour (5F) scheme calculations include heavy quarks in the initial state, i.e. as present in the proton. For this purpose, c -quark and b -quark PDFs are used.

The production of W and Z bosons in association with heavy flavour is an important background for many processes. Several NLO QCD calculations are available [214–224]. Recently, the $W + b\bar{b}$ and $Z + b\bar{b}$ processes (with and without additional jets) have been included in automated NLO calculations matched with parton showers and hadronisation [74].

Z bosons provide a particularly clean experimental signature that allows for precise measurements. Figure 17 presents a recent ATLAS measurement of the cross section of Z bosons produced in association with b jets as a function of the p_T of the leading jet containing a B hadron. The measurements uses the full 2011 data set. Transverse jet momenta up to 500 GeV are reached. The data are compared to various QCD calculations.

The MCFM prediction is based on a 5F NLO QCD calculation of $Z + 1b$ jet [217, 219], corrected for hadronisation and effects of multi-parton interactions (see section 9.4). Full particle-level predictions with NLO QCD matrix element calculations are also obtained using MADGRAPH5_AMC@NLO [74] in both the 4F and 5F schemes. For these calculations, the renormalisation and factorisation scales are set to the transverse Z -boson mass and varied up and down independently by a factor of two to assess the residual dependence on this scale choice. The data are described within the experimental and theoretical uncertainties.

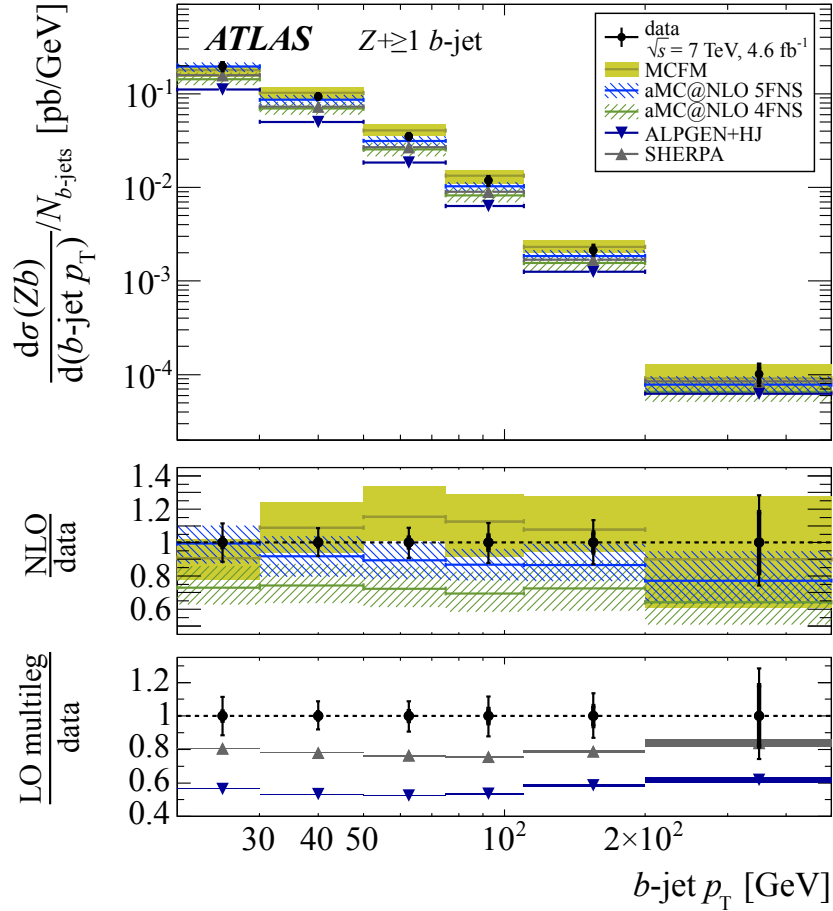


Fig. 17. Production cross sections for Z bosons produced in association with jets with heavy-flavour content as a function of the jet p_T . Superimposed are various QCD calculations. (*Adapted from Ref. [213].*)

Also shown are the predictions for multi-leg LO QCD calculations based on ALPGEN using the 4F scheme with up to five partons in the matrix element and SHERPA using the 5F scheme with up to four partons. The shape of these predictions is in good agreement with the data. However, the LO normalisation of these predictions undershoots the measurement, SHERPA reproducing the normalisation better than ALPGEN.

Further measurements by ATLAS and CMS of vector-boson production in association with heavy-flavour jets can be found in Refs. [225–227].

8 Resummation: The Realm of Large Logarithms

When discussing the process of vector-boson production before, the necessity to incorporate effects of multiple emissions of initial-state and final-state partons to appropriately model certain observables has been touched upon already. In fact, phase-space regions sensitive to the emission of soft and/or collinear QCD quanta often resist a satisfactory description in terms of fixed-order perturbation theory. Rather, one is forced to identify the relevant enhanced contributions, namely large logarithmic terms, and to reorganise the perturbative expansion for the observable at hand. The aim is to account for the enhanced terms to all orders in perturbation theory. This procedure is referred to as “resummation” and allows an appropriate treatment in a wide range of perturbative QCD phenomena.

Examples for hadron-hadron collider observables sensitive to multiple-emission effects include the transverse-momentum distribution of lepton pairs or gauge bosons at low p_T [158, 228, 229], event-shape variables [230–232], or certain jet-substructure observables [233–235]. Furthermore, resummation techniques become important when the real-emission phase space is constrained, leaving behind finite

but possibly large uncanceled QCD corrections. Examples thereof are observables that exhibit thresholds [236–239] or that rely on an explicit veto on QCD activity [240–244]. Resummed expressions for this type of observables might enable us to extract QCD parameters such as the strong coupling, quark masses and the parton distribution functions much more accurately than when having to rely on fixed-order perturbation theory alone. In the following, two concrete examples shall be considered: the application of a veto on additional jet activity and the jet-mass distribution in Z +jet production.

8.1 Jet Vetos and Gap Fractions

At first, so called “gap fractions” will be discussed. For this class of observables, used also to select the weak-boson-fusion production channel of Higgs bosons (see Chap. 6 of Ref. [1]), one considers a specific kinematic structure of two hard and widely separated jets. Analysing the QCD activity in-between these hard jets, events are vetoed in case there are additional jets with transverse momentum above a certain veto scale Q_0 , filtering out those events that exhibit a gap between the two boundary jets. On the one hand, the presence of the potentially soft jet-veto scale Q_0 induces large logarithms with argument Q/Q_0 , where Q denotes the typical hard process scale, e.g. the boundary jets’ transverse momenta. This demands for the all-orders treatment of wide-angle soft-gluon radiation [240, 241]. On the other hand, when considering large rapidity separations Δy between the boundary jets, manifestations of BFKL-like dynamics [245, 246] are expected, requiring to sum terms proportional to $\alpha_s^n (\Delta y)^n$ to all orders n [247, 248]. In Refs. [249, 250] ATLAS presented measurements of dijet production with a veto on additional jets. In order to gain further insight into the QCD dynamics determining the gap-fraction and gap-jet measurements, Ref. [250] considers additional azimuthal-decorrelation observables. In this latter analysis, the data are compared to predictions from POWHEG [193, 251], interfaced to the PYTHIA8 and HERWIG event generators, as well as to the program HEJ [252] with and without invoking the ARIADNE shower model [253]. The two POWHEG simulations provide NLO accuracy for the inclusive dijet production process invoking leading-logarithmic DGLAP resummation through the parton showers attached. The HEJ approach provides a resummation of small- x , BFKL-type logarithmic terms that can be supplemented with DGLAP resummation through, in this case, the ARIADNE parton cascade.

In figure 18 the gap fraction as a function of the veto scale Q_0 is presented for various slices of the boundary jets’ rapidity separation Δy . The fraction of events exhibiting a rapidity gap decreases as the veto scale is lowered or when increasing Δy . This corresponds to the expectation of an increase of the jet activity when considering lower jet transverse-momentum thresholds together with the rise in jet multiplicity when considering larger rapidity intervals. The POWHEG +PYTHIA8 prediction yields a reasonable description of the data. Employing the HERWIG parton shower the agreement worsens, an effect that originates from a prediction of too many jets above the veto scale. For the two predictions from HEJ the agreement with data improves when considering large rapidity separations. Given the high precision of the measured data, no single theoretical prediction is capable of describing the data in all phase-space regions. Considering more observables, including angular variables, Ref. [250] establishes the DGLAP-based POWHEG +PYTHIA8 and BFKL-like HEJ +ARIADNE simulations to yield the best overall description of the data. So far no clear-cut statements about the evidence for BFKL effects can be established. However, the small experimental uncertainties allow theoretical models for QCD radiation between widely separated and high-transverse momentum jets to be further constrained and improved [210, 254–257].

8.2 The Jet-Mass Distribution

Many phenomenological studies over the past years have investigated and highlighted the potential of jet-substructure techniques to identify the hadronic decays of boosted heavy objects or to discriminate scenarios of new physics from Standard Model (i.e. QCD) backgrounds [258–260]. The successful application of jet-substructure methods requires a more detailed and even finer understanding and modelling of the inner structure of QCD jets. The new experimental challenges to address include the consideration of various jet algorithms and radii that need to be calibrated, the quantification and possible removal of non-perturbative contributions from underlying event or pile-up activity, or the application of tracking and flavour-tagging methods in busy environments. On the theoretical side, precise and reliable predictions for the new observables at hand are required. This, in particular, asks for resummed calculations, in the form of Monte Carlo parton-shower simulations or as dedicated analytical results.

ATLAS and CMS have presented several analyses that address these questions and compare their data to theoretical models [55–58, 262–265]. One particular and rather simple observable shall be considered as an example here: the invariant mass of jets—the jet-mass distribution. The jet-mass variable

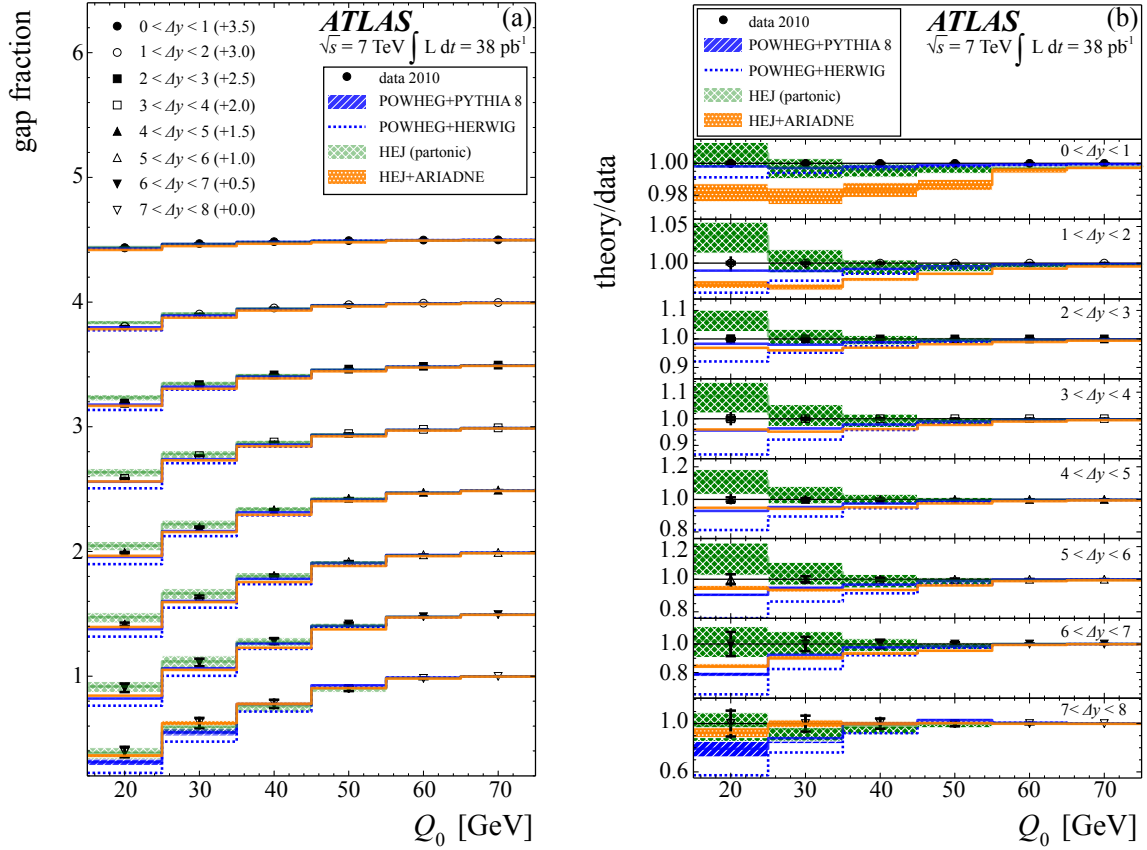


Fig. 18. Gap fraction for dijet events as a function of the jet-veto scale Q_0 for various Δy ranges. The data are compared to predictions from POWHEG +PYTHIA8, POWHEG +HERWIG and from the generator HEJ with and without inclusion of the ARIADNE shower algorithm. (a) Direct comparison with the unfolded data (for illustrative purposes the various results are shifted by arbitrary constants); (b) ratio of theory over data. (*Adapted from auxiliary material provided with Ref. [250].*)

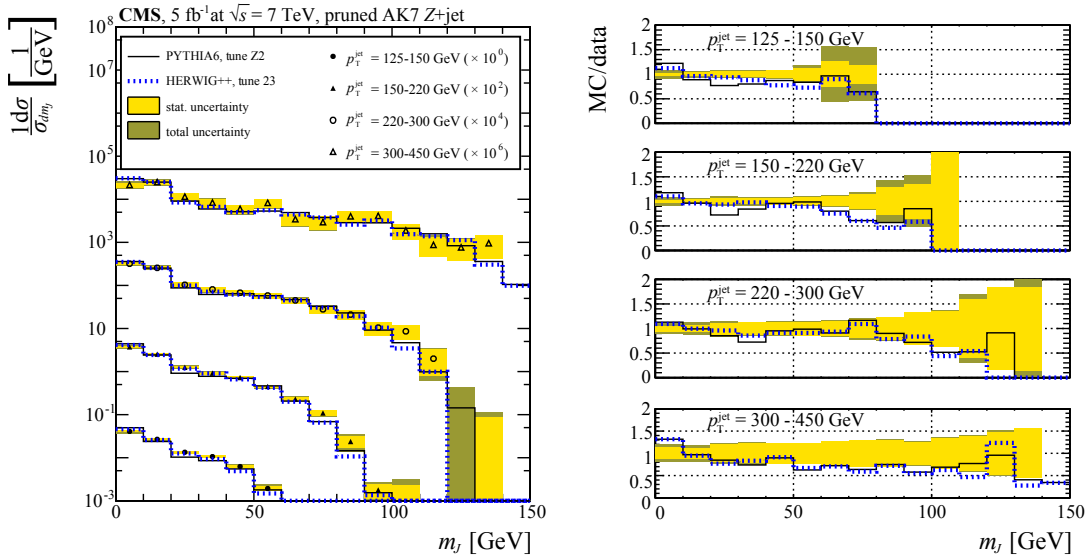


Fig. 19. Unfolded jet-mass distribution in $Z(\ell\ell)+\text{jet}$ events. Jets are reconstructed using the anti- k_t jet algorithm with distance parameter $R = 0.7$ and are groomed using the pruning technique [261]. The data from CMS are compared to Monte Carlo predictions from MADGRAPH +PYTHIA6 (solid) and HERWIG++ (dotted). The right panel shows the ratio of Monte Carlo over data. (*Adapted from Ref. [262].*)

probes the composition of jet objects and thus depends on the production process, the jet algorithm and its parameters used to cluster the jets, and on additional selection or filtering steps applied to the final states. The aim of “jet grooming” procedures is to reduce the impact of underlying-event and pile-up contributions on the jet properties and sometimes also to remove certain types of intra-jet parton splittings, all that in order to maximise the sensitivity to the desired signal. Examples of jet-grooming procedures include trimming [266], pruning [261], mass-drop [267, 268] or soft-drop [269] filtering. Dedicated theoretical predictions for the jet-mass distribution exist for a variety of production processes, including dijet final states, vector-boson plus jet production and Higgs-boson plus jet production [270–273]. The mass distribution of QCD jets after the application of grooming techniques has recently been discussed in Refs. [274, 275].

In Ref. [262] the CMS collaboration has presented an analysis of the jet-mass observable in dijet and W/Z +jet events, focusing on the effects of various grooming techniques and comparing data to parton-shower Monte Carlo predictions. For an integrated luminosity of 5 fb^{-1} of 7 TeV collision data they considered both the anti- k_t and Cambridge–Aachen [276–278] jet algorithms using various distance parameters, namely $R = 0.7$ for anti- k_t and $R = 0.8$ and $R = 1.2$ for Cambridge–Aachen. The groomed and ungroomed data are compared to Monte Carlo predictions from PYTHIA6 and HERWIG++. As an example, the unfolded jet-mass distribution of $Z(\ell\ell)$ +jet events is shown in figure 19. Depicted there is the jet-mass variable for anti- k_t jets after a pruning procedure, analysed for four slices in jet transverse momentum (note the arbitrary scaling factors). For all the jet- p_T slices both generators describe the data well. A similar level of congruence is observed for the alternative grooming techniques and combinations of jet algorithm and distance parameter. Somewhat larger deviations between data and Monte Carlo estimates are observed for regions of small jet mass. However, it is in particular this region of phase space that is most affected by non-perturbative corrections from pile-up, underlying event and hadronisation. Attempts to analytically estimate the effects of the underlying event and parton-to-hadron fragmentation on the jet-mass distribution have been presented in Ref. [279].

From the analysis presented by CMS and a similar one presented by ATLAS [56], agreement of jet-mass and substructure observables with modern parton-shower Monte Carlo tools is established. This paves the way to successfully use these techniques in future analyses and particularly in searches for new phenomena.

9 Beyond Perturbative QCD

So far the focus has been mainly on measurements that can reliably be addressed using QCD perturbative techniques. Experimentally, however, hadrons are observed in the detectors, and accordingly the transition of partons into hadrons needs to be accounted for. Furthermore, there is a wealth of effects that require the use of non-perturbative methods and models—most prominently the so-called “underlying event” that accompanies a hard scattering. As an example, the underlying event includes contributions from multiple interactions of the colliding protons’ constituents (“multi-parton interactions”) that give rise to the production of many additional final-state particles.

In this section these aspects shall be exemplified by presenting LHC measurements of jet-shape variables, of jet-radius ratios and of observables sensitive to soft-particle production and double and multi-parton scattering.

9.1 Jet Shapes

Focusing on the internal structure of jets, the profile of the distribution of transverse momentum within a jet can be examined. For this type of observable the term “jet shape” has been coined [280, 281]. The differential jet shape $\rho(r)$ as a function of the distance $r_i = \sqrt{(\Delta_{i,\text{jet}y})^2 + (\Delta_{i,\text{jet}\phi})^2}$ to the jet axis is defined as the average fraction of jet p_T contained inside an annulus of inner radius $r_a = r - \Delta r/2$ and outer radius $r_b = r + \Delta r/2$ for an ensemble of N jets:

$$\rho(r) = \frac{1}{N} \sum_{\text{jets}} \frac{1}{\Delta r} \frac{\sum_{r_a \leq r_i < r_b} p_{T,i}}{\sum_{r_i \leq R} p_{T,i}},$$

where the second sum runs over all jet constituents i . The integrated jet shape $\Psi(r)$ is then given by the integral of the differential jet shape up to a radius r (see the illustrations in figure 20(b)). Conventionally, measurements are presented in terms of $1 - \Psi(r = r_{\text{core}})$, where r_{core} is usually taken to be 0.3 [282].

Perturbatively, the internal structure of jets is determined by multiple emissions of gluons and depends on the type of initiating parton, i.e. a quark or gluon. Perturbative QCD predicts that gluon-initiated jets are broader in shape with a higher particle multiplicity on average [283]. To some extent it is therefore possible to differentiate statistically between gluon and quark jets by looking into the jet substructure. Jet shapes, however, are also sensitive to non-perturbative effects of the parton fragmentation and the underlying event. Corresponding measurements are valuable inputs to improve the modelling of such soft contributions in MC event generators like PYTHIA, HERWIG++, or SHERPA.

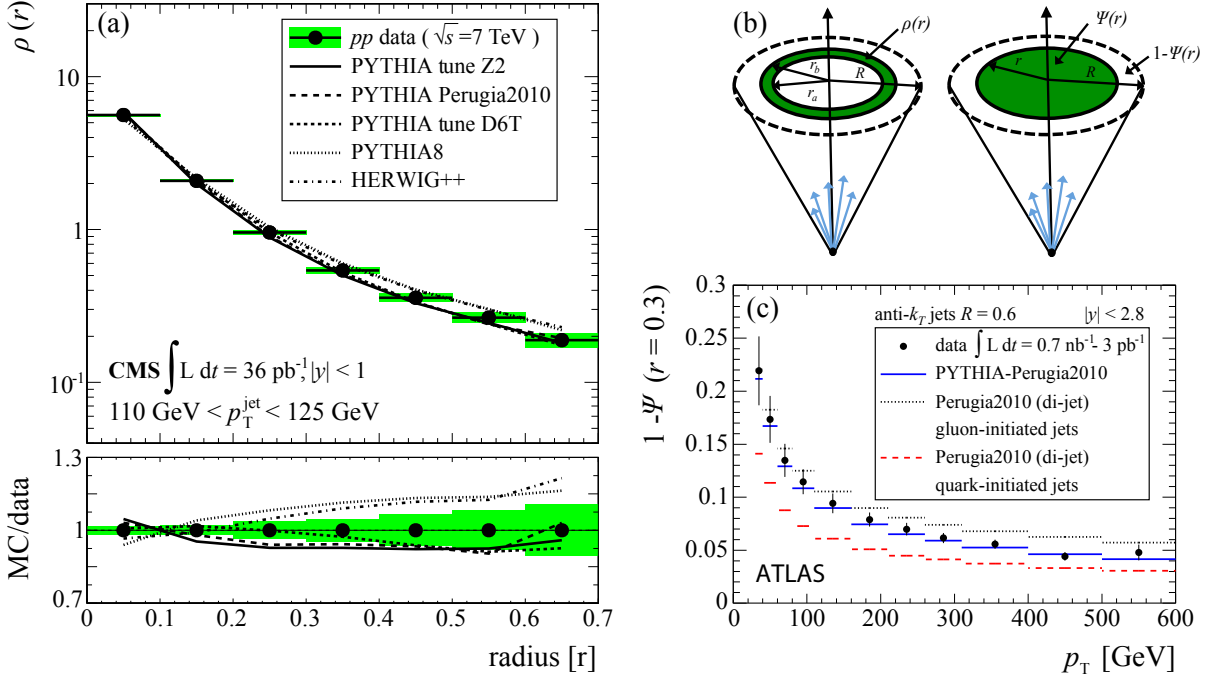


Fig. 20. (a) Differential jet shape $\rho(r)$ as a function of the distance r from the jet axis for jets with $110 < p_T < 125$ GeV from CMS. The data are compared to various tunes of the PYTHIA6 and to the PYTHIA8 and HERWIG++ event generators. (b) Illustration of the jet shape observables. (c) Integrated jet shape $1 - \Psi(r = 0.3)$ as a function of the jet p_T from ATLAS [284]. The data are compared to the prediction for gluon-initiated and quark-initiated jets using the PYTHIA6 MC event generator with tune Perugia2010. (Adapted from Refs. [284, 285].)

Figure 20(a) shows a CMS measurement [285] of the differential jet shape, for the example of the jet p_T interval $110 < p_T < 125$ GeV, in comparison to several LO MC event generators at particle level. While HERWIG++ and PYTHIA8 predict somewhat broader jet shapes than measured, the PYTHIA6 tunes D6T and Z2 deviate in the opposite direction. The best description of the data is given by PYTHIA6 with the tune Perugia2010, something, which is also observed in a similar investigation by the ATLAS collaboration [284]. By employing this tune for the integrated jet shape, shown in the form of $1 - \Psi(r = 0.3)$ as a function of the jet p_T in figure 20(c), ATLAS demonstrates the sensitivity of this observable with respect to the jet-initiating parton. At small jet p_T the examined inclusive jet sample is predominantly composed of gluon jets, while with increasing jet p_T the quark-initiated component grows. In the figure, the change in the fraction of quark-initiated to gluon-initiated jets is averaged over the jet rapidity up to $|y| < 2.8$. If studied double-differentially, a mild dependence on $|y|$ of this fraction is observed as expected. The sensitivity of jet shapes to non-perturbative effects and modelling uncertainties, however, prevents an extraction of the quark-gluon jet fraction. Instead, they provide valuable input to the tuning of these effects in MC event generators.

In the context of jets initiated by heavy boosted objects, the investigation of jet substructure has attracted much attention lately. Potential new particles like Z' bosons or heavy t' quarks that decay hadronically may be at the origin of jets with two or three, respectively, high-energetic partons fragmenting into only one jet. The required boosts for these hypothetical particles are attainable at the LHC, in particular at 13 TeV centre-of-mass energy as foreseen for the restart in 2015. Searches for these particles profit from a better understanding of the QCD background in the form of quark-initiated or

gluon-initiated jets. For some of the investigated observables, e.g. jet mass, resummed predictions are available (see section 8).

9.2 Jet-Radius Ratio

As described in section 5, the inclusive jet cross section can precisely be compared to NLO predictions, and the strong coupling constant can be extracted. A small correction for non-perturbative effects, which is p_T -dependent and increases at small p_T values, has to be taken into account. Looking more closely into the results presented by ATLAS for anti- k_t jet sizes of $R = 0.4$ and 0.6 [30] or by CMS for anti- k_t jet sizes of $R = 0.5$ and 0.7 [31, 32], it is observed that the relative normalisation of the measured cross sections to the theoretical predictions exhibits a dependence on R . Theoretically, this R dependence has been examined in Refs. [279, 286], where in a collinear approximation it was found that the impact of perturbative radiation and of the non-perturbative effects of hadronisation and the underlying event on jet transverse momenta scales roughly with $\ln R$, $-1/R$, and R^2 for small R , respectively. By choosing the jet size parameter R , one can therefore steer which aspects of jet formation are emphasised in a jet analysis. In Ref. [279] it is suggested, in order to gain insight into the interplay of these effects, to study the relative difference between inclusive jet cross sections that emerge from two different jet definitions:

$$\left(\frac{d\sigma^{\text{alt}}}{dp_T} - \frac{d\sigma^{\text{ref}}}{dp_T} \right) / \left(\frac{d\sigma^{\text{ref}}}{dp_T} \right) = \mathcal{R}(\text{alt, ref}) - 1.$$

Provided that partons in opposite hemispheres are not clustered together (a condition that is usually fulfilled), the LO two-parton cross sections are identical for arbitrary jet algorithms. Therefore, only partonic final states with three or more partons lead to a numerator different from zero. Hence, equation (9.2) defines a three-jet observable, \mathcal{R} , for which it was shown in Ref. [287] that it is calculable to NLO with terms up to α_s^4 with NLOJET++ [288, 289].

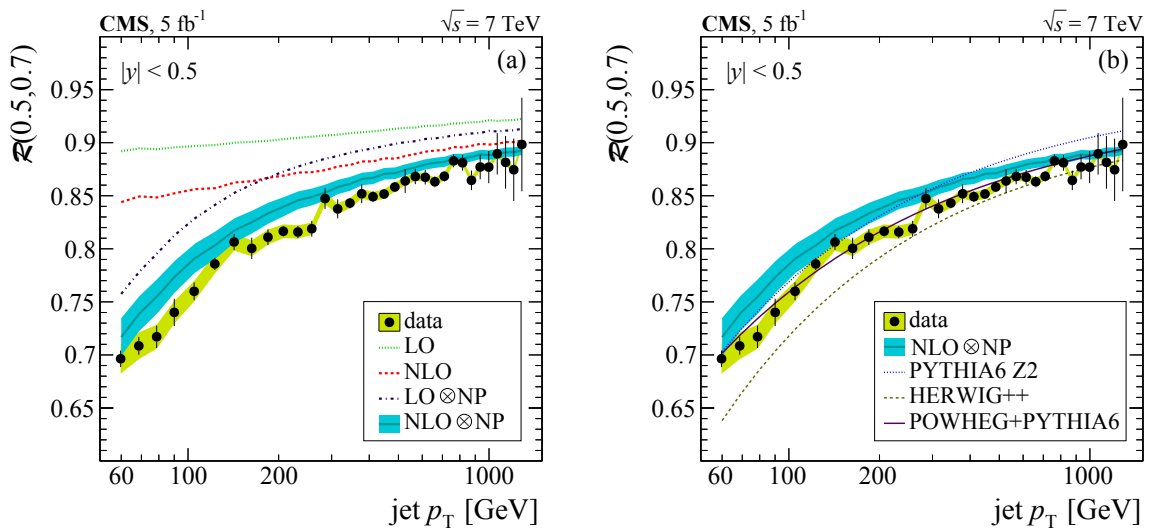


Fig. 21. Jet-radius ratio \mathcal{R} as measured by CMS in comparison to (a) fixed-order predictions with and without non-perturbative corrections and to (b) particle-level predictions of LO and NLO event generators with matched parton showers and modelling of hadronisation and the underlying event at central rapidity $|y| < 0.5$. (Adapted from auxiliary material provided with Ref. [34].)

Studies in that direction have been performed at the HERA collider by the ZEUS collaboration for two different jet algorithms [290] and by the ALICE experiment for the two different anti- k_t jet sizes of $R = 0.2$ and 0.4 [291]. The results of a CMS analysis for their two jet sizes of 0.5 and 0.7 is presented in Ref. [34] as a function of jet p_T and rapidity y . It is expected that QCD radiation reduces this jet-radius ratio \mathcal{R} below unity and that this effect disappears with increasing collimation of jets at high p_T . Figure 21 confirms this assumption with a comparison of the measured ratio \mathcal{R} as a function of the jet p_T up to the TeV scale to theoretical predictions at central rapidity $|y| < 0.5$. Figure 21(a) clearly demonstrates

that fixed-order calculations up to NLO, even when combined with non-perturbative corrections, are systematically above the data. The LO event generators PYTHIA6 and HERWIG++ lie systematically on either side of the data, as can be seen in figure 21(b). Presumably, this can be improved by including this observable into the tuning of these generators. The best description is given by POWHEG that matches the dijet production process evaluated at NLO with the parton showers and non-perturbative models of PYTHIA6, emphasising the importance of parton showers for the given choice of jet sizes.

9.3 Soft Hadron-Hadron Collisions

When two hadrons collide at high energy, their entire volumes or at least a significant part of them participates in the collision. Most of these collisions are caused by so-called “soft” hadronic interactions.

In a simple geometrical model, the total hadron-hadron collision cross section is related to the transverse extension of the scattering system. Therefore, it is expected to be of the order of $\sigma_{\text{tot}} \approx \mathcal{O}(2 \text{ fm}^2) \approx \mathcal{O}(40 \text{ mb}^{-1})$. Since the effective range of soft hadron interactions does not change much with energy, only a weak energy dependence is expected. Moreover, if the collision is soft, the scattering cross section at high energy should not depend on the quark structure of the colliding hadrons.

In 1952 Heisenberg used a geometrical model where hadrons are modelled as Lorentz-contracted disks with a given energy density. The interaction takes place in the disk-overlap region, and only if there is sufficient energy to create two mesons. In this model the total cross section increases like $\ln^2 s$. A consequence of this model is that the interaction cross sections of all hadrons are similar at high energy. For a recent review on the model giving a $\ln^2 s$ high-energy behaviour see Ref. [292].

General arguments based on unitarity, analyticity and factorisation imply a bound on the high-energy behaviour of total hadronic cross sections. This bound is independent of the details of the strong-interaction dynamics and states that the total cross section can not rise faster than $\ln^2 s$ [293].

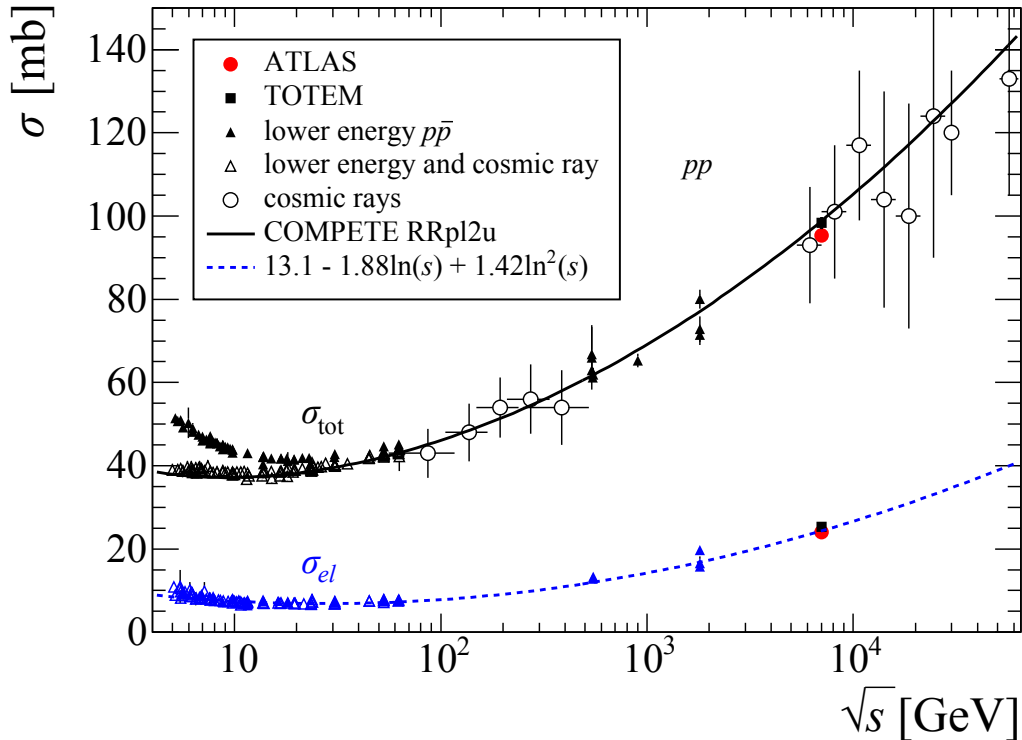


Fig. 22. Comparison of total and elastic cross-section measurements in proton-proton and antiproton-proton collisions and in cosmic-ray interactions as a function of the centre-of-mass energy. (Adapted from Ref. [294].)

Soft hadron collisions can not be calculated in perturbative QCD. Instead, they are usually described by phenomenological models where the force between hadrons is assumed to be mediated by mesons, for instance by pions [295]. The basic idea is that the exchanged meson interacts with the colour charges

confined in the scattered hadrons. Since many mesons exist, the strong force between hadrons can be quite complicated in such models. The typical range of the strong force is anti-proportional to the mass of the exchanged meson. Consequently, the largest range is provided by the lightest meson which has the appropriate quantum numbers. Such models are usually called “Regge theory”. For reviews see Refs. [296, 297]. Regge theory aimed at explaining the spectrum of the various hadrons, the forces between them, and the high-energy behaviour of the hadron-hadron scattering cross section. It is based on simple assumptions like that the scattering matrix is analytic and unitary. Mesons are understood as composite quark-antiquark states bound by an effective strong potential that depends on the distance between the quark-antiquark pair r and the orbital angular momentum J . Elastic hadron-hadron scattering is viewed as the exchange of a meson in the s -channel or t -channel. In 1961, Chew and Frautschi [298] made the observation that for $\pi^- p \rightarrow \pi^0 n$ scattering there is a linear relation between the mass of the exchanged hadron (m) and its angular momentum J . Each integer value of the slope α —called “Regge trajectory”—corresponds to one particle that can be experimentally identified (“Regge-pole”). In the time-like region where $t > 0$ (s -channel meson exchange) the momentum transfer t corresponds to the hadron mass m . If one continues the linear relation between m and J using the slope α for $t < 0$, i.e. the space-like regime, a good description of the experimental measurements for α is obtained. In this case, however, t can take any value. This trajectory is called “Pomeron trajectory”. The exchanged object carrying the quantum numbers of the vacuum ($C = P = 1$) is called “Pomeron”.

The meson exchange leads to a simple power behaviour $s^{\alpha-1}$ of total hadron-hadron scattering cross sections. In 1992 Donnachie and Landshoff [299] made the observation that hadron-hadron total cross sections can be described by two powers, one $\alpha \approx 1.1$ corresponding to Pomeron exchange and one $\alpha = 0.5$ corresponding to the exchange of mesons like ρ , ω , f_2 and a_2 . Therefore at low-energies, where the Reggeon exchange dominates, a behaviour $\sigma \sim s^{-0.5}$ is expected, while at high energies $\sigma \sim s^{0.1}$ should prevail.

Such a behaviour was indeed experimentally observed. Figure 22 shows the total inclusive proton-proton cross section as a function of the centre-of-mass energy \sqrt{s} for various experiments. In the range 2-20 GeV the proton-proton cross section decreases as measured by fixed-target experiments, while at higher energies it increases towards larger \sqrt{s} . The difference between proton-proton and proton-antiproton cross section decreases towards high energy; at about $\sqrt{s} \approx 30$ GeV, the two cross sections are very similar. The rise of the proton-antiproton cross section for $\sqrt{s} \gtrsim 30$ GeV was first observed at the SPS, confirmed by Tevatron and LHC, where the ATLAS [300], CMS [301] and TOTEM [302] experiments measured at $\sqrt{s} = 7$ TeV (TOTEM measured also at $\sqrt{s} = 8$ TeV [303]). Data from cosmic-ray experiments [304–306] are able to provide useful measurements at energies up to 60 TeV that are not covered by colliders. Overlaid in figure 22 as curve is a parameterisation [307] based on the $\ln^2 s$ behaviour that describes the data well at high energy. The power-law behaviour can also describe the present data [308]. Also shown in figure 22 are recent measurements of the elastic proton-proton cross section [294, 302].

9.4 The Underlying Event and Multi-Parton Interactions

An important aspect of hadron-hadron collisions, neglected in our discussion so far, is the observation that additional mostly low-energetic (soft) particles are produced. The simple picture of a hard scattering between one parton from each hadron with subsequent showering and hadronisation at least needs to be complemented by a treatment of the beam-beam remnants, which is beyond the capabilities of pQCD. In addition, the primary interaction may be accompanied by the production of further particles, a circumstance which is usually modelled in the form of multi-parton interactions (MPI). The concepts employed for MPI by PYTHIA and HERWIG++, for example, are described in Refs. [309–311] and [312], respectively. A very useful overview of general-purpose MC event generators including all aspects of event generation for the LHC is given in Ref. [42].

An unambiguous association of a specific particle to the reaction from which it originates is impossible. Therefore, the extra activity in a hadron-hadron collision cannot be uniquely separated from effects like initial-state or final-state radiation. One thus conventionally defines the “underlying event” (UE) as everything except for the hard process of interest. Two strategies are applied to measure the UE: The first evaluates events that are collected requiring only minimalistic trigger conditions such that even very soft collisions are registered. These so-called “minimum bias” (MB) measurements are supposed to be dominated by underlying-event physics.

In the second approach, reactions are considered that have a high rate for the production of a leading particle or jet with reasonably high p_T (for triggering purposes). The event is then separated into hard and soft contributions through a physically motivated definition of phase-space regions that are dominated by either the hard or soft component of a collision. Traditionally, this is achieved by geometrically subdividing

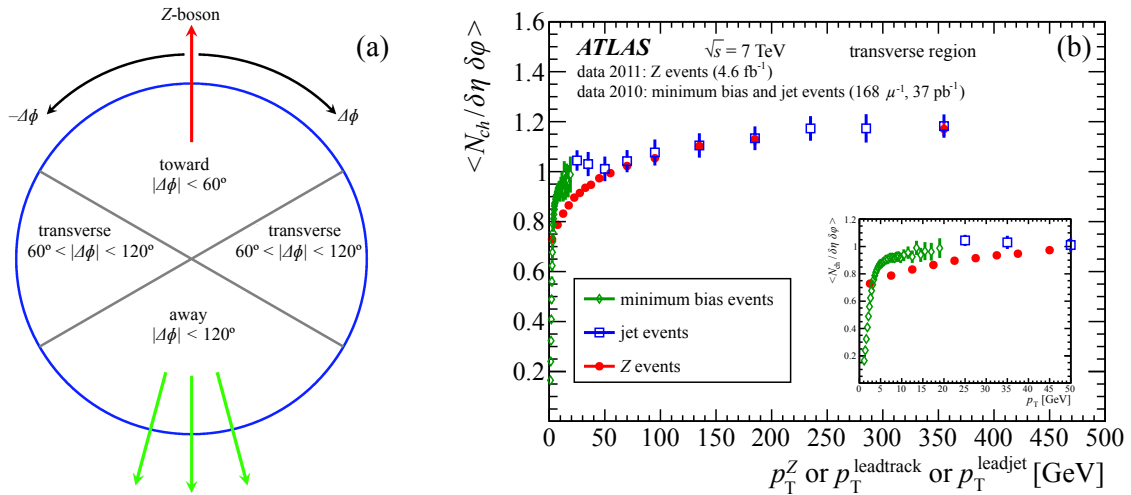


Fig. 23. (a) Sketch of the geometrical subdivision of events in azimuthal angle for UE measurements. (b) Average density of charged particles in the transverse region as a function of the leading-jet or leading-track p_T , or the p_T of the reconstructed Z boson. (Adapted from Ref. [313].)

the event into different regions (“towards”, “away”, and “transverse”) with respect to the direction of the triggering particle or jet (figure 23(a)). Reactions that are typically chosen for this second approach are dijet or Drell–Yan lepton-pair production. Implicitly, it is assumed that the soft particle production is uncorrelated to details of the hard process—an assumption that can be tested experimentally.

As an example for such a strategy figure 23(b) shows a measurement by ATLAS [313] of the charged-particle density in the transverse region as a function of the transverse momentum that is chosen as scale of the event hardness. Three event types are compared: minimum bias, dijet production, and inclusive Z production, with event scales chosen to be the p_T of the leading track, the leading jet, and the Z boson, respectively. An approximately continuous transition from MB to jet events is visible in the inset plot. In the comparison between jet and Z events of the soft-particle density in the transverse region, which is attributed to the UE, differences are exhibited, which are even more pronounced in the average summed p_T density of all tracks (not shown). These can be explained in terms of a bias between the definitions of the event scale. In the case of the jet events further jets with transverse momenta larger than the p_T of the leading jet are forbidden by definition, while for the inclusive Z events additional jet activity with $p_T^{\text{jet}} > p_T^Z$ is possible. Taking this bias into account, the conjecture that the UE activity is independent of the hard process is supported by the ATLAS measurement and by similar measurements from CMS [314].

Another quantity that is not predictable by perturbative methods is the average density of charged particles produced in MB events for example at central rapidity. Corresponding measurements usually must be performed early on at the beginning of a data-taking period, when the instantaneous luminosity is small and the probability of multiple hadron-hadron collisions in the same or adjacent bunch crossings, the so-called pile-up, is negligible. It should be emphasised that such measurements are of utmost importance for a precise understanding of LHC data as they are used to model individual pile-up collisions. At later stages of the data-taking and with high instantaneous luminosity, the occurrence of up to 10–100 of such pile-up collisions simultaneously to the hard reaction of interest demands that these MB-like collisions are very well understood and modelled in simulations. Otherwise it becomes very difficult to precisely calibrate jet energies (see Chap. 3 of Ref. [1]) or to estimate the background to searches for new physics. The charged-particle density is also of much interest for heavy-ion physics, and its dependence on the centre-of-mass energy is shown in Chap. 9, Fig. 9.1, of Ref. [1] for various combinations of colliding hadron-hadron beams.

9.5 Double-Parton Scattering

The basis for all perturbative results in the previous sections (see in particular section 3) is the assumption that collinear factorisation holds and that the cross section of interest can be calculated following equation (4). To some extent it is a great fortune that such a simple picture with only one interacting parton from each colliding hadron and only longitudinal degrees of freedom describes such a huge amount

of measurements. Partially this is due to the fact that one is mostly interested in inclusive processes at large p_T . Looking into the regime of small transverse momenta, however, it becomes apparent that this picture must fail, since otherwise the relevant cross sections would grow beyond all limits for $p_T \rightarrow 0$. They would thus violate unitarity, i.e. become even larger than the measured total cross sections. So, somehow, the cross sections have to be regularised. Realising that at p_T values of the order of a few GeV, protons are probed at fractional momenta of 10^{-3} or below, one can interpret the consequently large parton densities in such a way that more than one parton per hadron participates in a scattering process. In terms of the MPI, as explained above, this concept has already been successfully applied to model the part of the soft-particle production that manifests itself in the form of the underlying event. The possibility of two hard or semi-hard reactions with two partons from each of the colliding hadrons participating in their own parton-parton scatter has not yet been considered, though.

This type of process is called “double-parton scattering” (DPS), in contrast to the single parton scattering (SPS) discussed previously. Double-parton scattering is one possibility to dampen the rise of the low- p_T SPS cross sections. In a simplified form, the impact of double-parton scattering on the production rate for a final state $A + B$ can be parametrised by one effective cross section that can be written as

$$\sigma_{\text{eff}} = \frac{m}{2} \frac{\sigma_A \cdot \sigma_B}{\sigma_{A+B}^{\text{DPS}}}, \quad (7)$$

where σ_A and σ_B are the cross sections for the independent processes A and B , $\sigma_{A+B}^{\text{DPS}}$ is the cross section for processes A and B to occur simultaneously, and m is a symmetry factor that is equal to unity for indistinguishable final states and two otherwise. In this simple picture, σ_{eff} is a measure of the overlap in transverse size of the parton distributions in the colliding hadrons. A naive geometrical interpretation leads to an estimate of $\sigma_{\text{eff}} \approx \pi R_p^2 \approx 50$ mb, where R_p is the proton radius.

Measurements have been performed for a number of processes A and B : 4-jet [315, 316], γ +3-jet [317–319], and W +2-jet [320, 321] production. In each case, the second independent scattering reaction is chosen to have a dijet final state, because dijet production occurs at by far the highest rates. To differentiate double-parton scattering from normal high-multiplicity single parton scattering events, the particular properties of DPS events are exploited: the p_T of the jet pair (both jet pairs in 4-jet production) should be balanced and the azimuthal angle between the vectors of the final-state objects of the leading scattering and the lower- p_T jet pair should be uncorrelated, i.e. randomly oriented. Specialising to W +2-jet events, observables sensitive to DPS can then be defined as

$$\Delta^{\text{rel}} p_T = \frac{|\mathbf{p}_T(j_1) + \mathbf{p}_T(j_2)|}{|\mathbf{p}_T(j_1)| + |\mathbf{p}_T(j_2)|},$$

$$\Delta S = \arccos \left(\frac{|\mathbf{p}_T(\mu, E_T^{\text{miss}}) + \mathbf{p}_T(j_1, j_2)|}{|\mathbf{p}_T(\mu, E_T^{\text{miss}})| + |\mathbf{p}_T(j_1, j_2)|} \right),$$

where \mathbf{p}_T are the transverse momentum vectors of the jets j_1 , j_2 , or of the jet pair (j_1, j_2) and the decay products of the W boson, one muon and missing transverse energy E_T^{miss} representing the undetected neutrino. Figure 24(a) shows, as an example, the measurement of $\Delta^{\text{rel}} p_T$ by CMS [321] together with the composition of single parton scattering background and double-parton scattering signal, which peaks at small p_T differences, as determined in a template fit. Figure 24(b) summarises determinations of σ_{eff} from various experiments as a function of the centre-of-mass energy. The “Corrected CDF” point includes an improved estimate [322, 323] for the fact that equation (7) implies processes A and B to be inclusive such that also higher terms than double scatterings are parametrised by σ_{eff} . The bias of exclusive event selections, when applying equation (8) in the W +2-jet case,

$$\sigma_{\text{eff}} = \frac{\sigma_{W+0\text{-jet}}}{\sigma_{W+2\text{-jet}}^{\text{DPS}}} \cdot \sigma_{2\text{-jet}}, \quad (8)$$

has been considered in the presented analysis from CMS [321] and a similar measurement by ATLAS [320]. Otherwise, σ_{eff} would not be independent any more of the choice of scattering processes A and B .

The validity of the presented simplified theoretical approach anyway relies on a couple of additional assumptions. For a recent critical overview see Ref. [324].

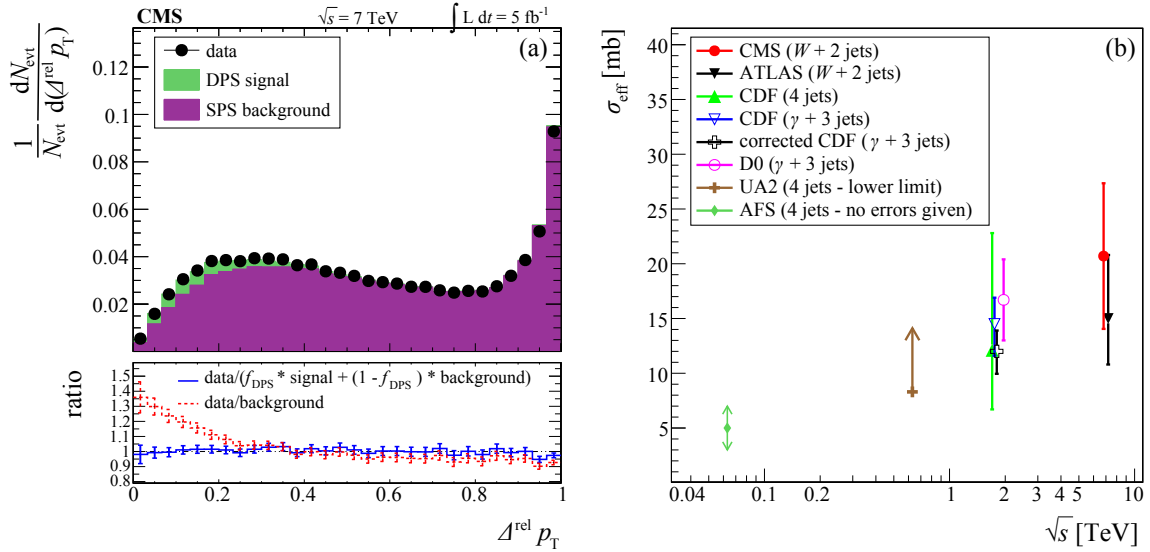


Fig. 24. (a) Template fit of SPS background and DPS signal to data for the $\Delta^{\text{rel}} p_{\text{T}}$ distribution in $W+2$ -jet events as measured by CMS. (b) Extracted effective cross section σ_{eff} as a function of the centre-of-mass energy as measured by various experiments. (*Adapted from Ref. [321].*)

10 Summary and Outlook

The excellent performance of the LHC machine and of the four major detectors around the ring made it possible to carry out precise measurements at very high particle, i.e. jet transverse momenta, high invariant masses, and for very complex event topologies with large particle multiplicities. The high luminosities and the centre-of-mass energies of 7 and 8 TeV reached for proton-proton collisions are unprecedented. These conditions allowed to assess the validity of the QCD theory in the TeV regime and to stress-test our current understanding of particle-production processes at such high energies. Many measurements in particular of vector-boson and jet-production processes reached an experimental accuracy of a few percent uncertainty only—true QCD precision tests.

To meet the experimental challenges, theoretical predictions are needed that match the precision and complexity requirements. Accordingly, enormous efforts have been undertaken to provide better and better theoretical predictions accompanied and driven by exciting new theoretical developments and insights. This includes largely automated NLO and many new NNLO calculations, improved analytical and parton-shower resummation techniques, the merging (i.e. matching) of parton showers and exact matrix elements, and attempts to gain a better understanding of the low-energy (i.e. non-perturbative) regime of the strong interaction. A major role is played by the Monte Carlo event generators that have been developed and optimised for the analysis and interpretation of LHC measurements.

Calculations at NNLO in the strong coupling provide predictions for inclusive production cross sections with an estimated uncertainty, e.g. due to missing higher orders, of a few percent only. Such precision predictions were successfully tested against the LHC data. Often the dominant theoretical uncertainty originates from the knowledge of the proton PDFs. Also in this field LHC measurements have already contributed to a refined understanding of the proton structure.

Around the year 2002, two theoretical break-throughs have revolutionised the field of Monte Carlo generators: first, the exact matching of $2 \rightarrow 2$ production processes evaluated at NLO accuracy with parton showers, and second, the consistent merging of tree-level matrix elements with varying final-state parton multiplicity with parton showers. These two innovative concepts enable fully exclusive predictions at particle-level with an inclusive production rate accurate to NLO or the first few hardest emissions being modelled through exact real-emission matrix elements. Consequently, Monte-Carlo simulations based on matching or merging of matrix elements and parton showers have become the standard tools in any LHC analysis. Driven by the enormous progress in the evaluation of NLO cross sections (which are largely automated by now), there appeared many multi-leg NLO calculations that can directly be matched with parton showers.

The currently emerging new standard are simulations based on exact NLO calculations with increasing parton multiplicity all matched with parton showers and combined into an inclusive description of the

considered production process. However, this is not the end of the development: first prototypes of exact NNLO calculations matched with parton showers have recently been presented. These exciting theoretical developments pave the way to a further scrutiny of our understanding of QCD in the upcoming high-energy and high-luminosity LHC runs. In consequence, they will significantly boost the sensitivity and prospects to find potential new physics at the LHC.

References

1. T. Schörner-Sadenius, ed., “The Large Hadron Collider — Harvest of Run 1”. Springer, Heidelberg, Germany, 2015.
2. D. J. Gross and F. Wilczek, “Ultraviolet Behavior of Nonabelian Gauge Theories”, *Phys. Rev. Lett.* **30** (1973) 1343, doi:10.1103/PhysRevLett.30.1343.
3. H. D. Politzer, “Reliable Perturbative Results for Strong Interactions?”, *Phys. Rev. Lett.* **30** (1973) 1346, doi:10.1103/PhysRevLett.30.1346.
4. T. van Ritbergen, J. A. M. Vermaseren, and S. A. Larin, “The four-loop β -function in quantum chromodynamics”, *Phys. Lett. B* **400** (1997) 379, doi:10.1016/S0370-2693(97)00370-5, arXiv:hep-ph/9701390.
5. Particle Data Group, K. Olive et al., “Review of Particle Physics”, *Chin. Phys. C* **38** (2014) 090001, doi:10.1088/1674-1137/38/9/090001.
6. M. L. Mangano et al., “ALPGEN, a generator for hard multiparton processes in hadronic collisions”, *JHEP* **07** (2003) 001, doi:10.1088/1126-6708/2003/07/001, arXiv:hep-ph/0206293.
7. F. Krauss, R. Kuhn, and G. Soff, “AMEGIC++ 1.0: A Matrix element generator in C++”, *JHEP* **02** (2002) 044, doi:10.1088/1126-6708/2002/02/044, arXiv:hep-ph/0109036.
8. T. Gleisberg and S. Höche, “Comix, a new matrix element generator”, *JHEP* **12** (2008) 039, doi:10.1088/1126-6708/2008/12/039, arXiv:0808.3674.
9. A. Cafarella, C. G. Papadopoulos, and M. Worek, “Helac-Phegas: A Generator for all parton level processes”, *Comput. Phys. Commun.* **180** (2009) 1941, doi:10.1016/j.cpc.2009.04.023, arXiv:0710.2427.
10. J. Alwall et al., “MadGraph 5 : Going Beyond”, *JHEP* **06** (2011) 128, doi:10.1007/JHEP06(2011)128, arXiv:1106.0522.
11. W. Kilian, T. Ohl, and J. Reuter, “WHIZARD: Simulating Multi-Particle Processes at LHC and ILC”, *Eur. Phys. J. C* **71** (2011) 1742, doi:10.1140/epjc/s10052-011-1742-y, arXiv:0708.4233.
12. F. A. Berends and W. Giele, “Recursive Calculations for Processes with n Gluons”, *Nucl. Phys. B* **306** (1988) 759, doi:10.1016/0550-3213(88)90442-7.
13. C. Duhr, S. Höche, and F. Maltoni, “Color-dressed recursive relations for multi-parton amplitudes”, *JHEP* **08** (2006) 062, doi:10.1088/1126-6708/2006/08/062, arXiv:hep-ph/0607057.
14. M. Dinsdale, M. Ternick, and S. Weinzierl, “A Comparison of efficient methods for the computation of Born gluon amplitudes”, *JHEP* **03** (2006) 056, doi:10.1088/1126-6708/2006/03/056, arXiv:hep-ph/0602204.
15. S. Drell and T.-M. Yan, “Partons and their Applications at High-Energies”, *Annals Phys.* **66** (1971) 578, doi:10.1016/0003-4916(71)90071-6.
16. G. F. Sterman and S. Weinberg, “Jets from Quantum Chromodynamics”, *Phys. Rev. Lett.* **39** (December, 1977) 1436, doi:10.1103/PhysRevLett.39.1436.
17. J. E. Huth et al., “Towards a standardization of jet definitions”, in *Proceedings of the Snowmass Summer Study 1990: Research Directions for the Decade*, p. 134. Snowmass, USA, 1990.
18. G. C. Blazey et al., “Run II jet physics”, arXiv:hep-ex/0005012.
19. C. Buttar et al., “Standard Model Handles and Candles Working Group: Tools and Jets Summary Report”, arXiv:0803.0678.
20. JADE Collaboration, “Experimental Studies on Multi-Jet Production in $e^+ e^-$ Annihilation at PETRA Energies”, *Z. Phys. C* **33** (1986) 23, doi:10.1007/BF01410449.
21. G. P. Salam and G. Soyez, “A practical Seedless Infrared-Safe Cone jet algorithm”, *JHEP* **05** (2007) 086, arXiv:0704.0292.
22. M. Cacciari, G. P. Salam, and G. Soyez, “The anti- k_t jet clustering algorithm”, *JHEP* **04** (2008) 063, doi:10.1088/1126-6708/2008/04/063, arXiv:0802.1189.
23. M. Cacciari, G. P. Salam, and G. Soyez, “FastJet User Manual”, *Eur. Phys. J. C* **72** (2012) 1896, doi:10.1140/epjc/s10052-012-1896-2, arXiv:1111.6097.

24. G. P. Salam, “Towards Jetography”, *Eur. Phys. J. C* **67** (2010) 637, doi:10.1140/epjc/s10052-010-1314-6, arXiv:0906.1833.
25. UA1 Collaboration, “INCLUSIVE JET PRODUCTION AT $S^{*(1/2)} = 546\text{-GeV}$ ”, *Phys. Lett. B* **172** (1986) 461.
26. UA2 Collaboration, “Measurement of the $s^{*(1/2)}$ Dependence of Jet Production at the CERN anti-p p Collider”, *Phys. Lett. B* **160** (1985) 349, doi:10.1016/0370-2693(85)91341-3.
27. UA2 Collaboration, “Inclusive jet cross-section and a search for quark compositeness at the CERN $\bar{p}p$ collider”, *Phys. Lett. B* **257** (1991) 232, doi:10.1016/0370-2693(91)90887-V.
28. DØ Collaboration, “Measurement of the inclusive jet cross-section in $p\bar{p}$ collisions at $s^{(1/2)} = 1.96\text{-TeV}$ ”, *Phys. Rev. Lett.* **101** (2008) 062001, doi:10.1103/PhysRevLett.101.062001, arXiv:0802.2400.
29. CDF Collaboration, “Measurement of the Inclusive Jet Cross Section at the Fermilab Tevatron p anti-p Collider Using a Cone-Based Jet Algorithm”, *Phys. Rev. D* **78** (2008) 052006, doi:10.1103/PhysRevD.78.052006, 10.1103/PhysRevD.79.119902, arXiv:0807.2204.
30. ATLAS Collaboration, “Measurement of inclusive jet and dijet production in pp collisions at $\sqrt{s} = 7\text{ TeV}$ using the ATLAS detector”, *Phys. Rev. D* **86** (2012) 014022, doi:10.1103/PhysRevD.86.014022, arXiv:1112.6297.
31. CMS Collaboration, “Measurement of the Inclusive Jet Cross Section in pp Collisions at $\sqrt{s} = 7\text{ TeV}$ ”, *Phys. Rev. Lett.* **107** (2011) 132001, doi:10.1103/PhysRevLett.107.132001, arXiv:1106.0208.
32. CMS Collaboration, “Measurements of differential jet cross sections in proton-proton collisions at $\sqrt{s} = 7\text{ TeV}$ with the CMS detector”, *Phys. Rev. D* **87** (2013) 112002, doi:10.1103/PhysRevD.87.112002, arXiv:1212.6660.
33. ATLAS Collaboration, “Measurement of the inclusive jet cross-section in proton-proton collisions at $\sqrt{s} = 7\text{ TeV}$ using 4.5 fb^1 of data with the ATLAS detector”, *JHEP* **02** (2015) 153, doi:10.1007/JHEP02(2015)153, arXiv:1410.8857.
34. CMS Collaboration, “Measurement of the ratio of inclusive jet cross sections using the anti- k_T algorithm with radius parameters $R = 0.5$ and 0.7 in pp collisions at $\sqrt{s} = 7\text{ TeV}$ ”, *Phys. Rev. D* **90** (2014) 072006, doi:10.1103/PhysRevD.90.072006, arXiv:1406.0324.
35. ATLAS Collaboration, “Measurement of the inclusive jet cross section in pp collisions at $\sqrt{s}=2.76\text{ TeV}$ and comparison to the inclusive jet cross section at $\sqrt{s}=7\text{ TeV}$ using the ATLAS detector”, *Eur. Phys. J. C* **73** (2013) 2509, doi:10.1140/epjc/s10052-013-2509-4, arXiv:1304.4739.
36. V. Gribov and L. Lipatov, “Deep inelastic e p scattering in perturbation theory”, *Sov. J. Nucl. Phys.* **15** (1972) 438.
37. L. Lipatov, “The parton model and perturbation theory”, *Sov. J. Nucl. Phys.* **20** (1975) 94.
38. Y. L. Dokshitzer, “Calculation of the Structure Functions for Deep Inelastic Scattering and e+ e- Annihilation by Perturbation Theory in Quantum Chromodynamics.”, *Sov. Phys. JETP* **46** (1977) 641.
39. G. Altarelli and G. Parisi, “Asymptotic Freedom in Parton Language”, *Nucl. Phys. B* **126** (1977) 298, doi:10.1016/0550-3213(77)90384-4.
40. S. Moch, J. Vermaseren, and A. Vogt, “The Three loop splitting functions in QCD: The Nonsinglet case”, *Nucl. Phys. B* **688** (2004) 101, doi:10.1016/j.nuclphysb.2004.03.030, arXiv:hep-ph/0403192.
41. A. Vogt, S. Moch, and J. Vermaseren, “The Three-loop splitting functions in QCD: The Singlet case”, *Nucl. Phys. B* **691** (2004) 129, doi:10.1016/j.nuclphysb.2004.04.024, arXiv:hep-ph/0404111.
42. A. Buckley et al., “General-purpose event generators for LHC physics”, *Phys. Rept.* **504** (2011) 145, doi:10.1016/j.physrep.2011.03.005, arXiv:1101.2599.
43. G. Marchesini and B. Webber, “Simulation of QCD Coherence in Heavy Quark Production and Decay”, *Nucl. Phys. B* **330** (1990) 261, doi:10.1016/0550-3213(90)90310-A.
44. S. Gieseke, P. Stephens, and B. Webber, “New formalism for QCD parton showers”, *JHEP* **12** (2003) 045, doi:10.1088/1126-6708/2003/12/045, arXiv:hep-ph/0310083.
45. S. Schumann and F. Krauss, “A Parton shower algorithm based on Catani-Seymour dipole factorisation”, *JHEP* **03** (2008) 038, doi:10.1088/1126-6708/2008/03/038, arXiv:0709.1027.
46. M. Dinsdale, M. Ternick, and S. Weinzierl, “Parton showers from the dipole formalism”, *Phys. Rev. D* **76** (2007) 094003, doi:10.1103/PhysRevD.76.094003, arXiv:0709.1026.
47. S. Plätzer and S. Gieseke, “Coherent Parton Showers with Local Recoils”, *JHEP* **01** (2011) 024, doi:10.1007/JHEP01(2011)024, arXiv:0909.5593.

48. J.-C. Winter and F. Krauss, “Initial-state showering based on colour dipoles connected to incoming parton lines”, *JHEP* **07** (2008) 040, doi:10.1088/1126-6708/2008/07/040, arXiv:0712.3913.
49. M. Ritzmann, D. Kosower, and P. Skands, “Antenna Showers with Hadronic Initial States”, *Phys. Lett. B* **718** (2013) 1345, doi:10.1016/j.physletb.2012.12.003, arXiv:1210.6345.
50. CMS Collaboration, “Probing color coherence effects in pp collisions at $\sqrt{s} = 7$ TeV”, *Eur. Phys. J. C* **74** (2014) 2901, doi:10.1140/epjc/s10052-014-2901-8, arXiv:1311.5815.
51. T. Sjöstrand, S. Mrenna, and P. Z. Skands, “A Brief Introduction to PYTHIA 8.1”, *Comput. Phys. Commun.* **178** (2008) 852, doi:10.1016/j.cpc.2008.01.036, arXiv:0710.3820.
52. CMS Collaboration, “First Measurement of Hadronic Event Shapes in pp Collisions at $\sqrt{s} = 7$ TeV”, *Phys. Lett. B* **699** (2011) 48, doi:10.1016/j.physletb.2011.03.060, arXiv:1102.0068.
53. ATLAS Collaboration, “Measurement of event shapes at large momentum transfer with the ATLAS detector in pp collisions at $\sqrt{s} = 7$ TeV”, *Eur. Phys. J. C* **72** (2012) 2211, doi:10.1140/epjc/s10052-012-2211-y, arXiv:1206.2135.
54. CMS Collaboration, “Study of hadronic event-shape variables in multijet final states in pp collisions at $\sqrt{s} = 7$ TeV”, *JHEP* **10** (2014) 87, doi:10.1007/JHEP10(2014)087, arXiv:1407.2856.
55. ATLAS Collaboration, “ATLAS measurements of the properties of jets for boosted particle searches”, *Phys. Rev. D* **86** (2012) 072006, doi:10.1103/PhysRevD.86.072006, arXiv:1206.5369.
56. ATLAS Collaboration, “Jet mass and substructure of inclusive jets in $\sqrt{s} = 7$ TeV pp collisions with the ATLAS experiment”, *JHEP* **05** (2012) 128, doi:10.1007/JHEP05(2012)128, arXiv:1203.4606.
57. ATLAS Collaboration, “Measurement of k_T splitting scales in W - j lv events at $\sqrt{s} = 7$ TeV with the ATLAS detector”, *Eur. Phys. J. C* **73** (2013) 2432, doi:10.1140/epjc/s10052-013-2432-8, arXiv:1302.1415.
58. ATLAS Collaboration, “Measurement of the cross-section of high transverse momentum vector bosons reconstructed as single jets and studies of jet substructure in pp collisions at $\sqrt{s} = 7$ TeV with the ATLAS detector”, *New J. Phys.* **16** (2014) 113013, doi:10.1088/1367-2630/16/11/113013, arXiv:1407.0800.
59. ATLAS Collaboration, “Measurement of Dijet Azimuthal Decorrelations in pp Collisions at $\sqrt{s} = 7$ TeV”, *Phys. Rev. Lett.* **106** (2011) 172002, doi:10.1103/PhysRevLett.106.172002, arXiv:1102.2696.
60. CMS Collaboration, “Dijet Azimuthal Decorrelations in pp Collisions at $\sqrt{s} = 7$ TeV”, *Phys. Rev. Lett.* **106** (2011) 122003, doi:10.1103/PhysRevLett.106.122003, arXiv:1101.5029.
61. S. Höche, F. Krauss, S. Schumann, and F. Siegert, “QCD matrix elements and truncated showers”, *JHEP* **05** (2009) 053, doi:10.1088/1126-6708/2009/05/053, arXiv:0903.1219.
62. S. Catani and M. Seymour, “A General algorithm for calculating jet cross-sections in NLO QCD”, *Nucl. Phys. B* **485** (1997) 291, doi:10.1016/S0550-3213(96)00589-5, arXiv:hep-ph/9605323.
63. S. Frixione, Z. Kunszt, and A. Signer, “Three jet cross-sections to next-to-leading order”, *Nucl. Phys. B* **467** (1996) 399, doi:10.1016/0550-3213(96)00110-1, arXiv:hep-ph/9512328.
64. D. A. Kosower, “Antenna factorization of gauge theory amplitudes”, *Phys. Rev. D* **57** (1998) 5410, doi:10.1103/PhysRevD.57.5410, arXiv:hep-ph/9710213.
65. C. Chung, M. Kramer, and T. Robens, “An alternative subtraction scheme for next-to-leading order QCD calculations”, *JHEP* **06** (2011) 144, doi:10.1007/JHEP06(2011)144, arXiv:1012.4948.
66. G. Bevilacqua, M. Czakon, M. Kubocz, and M. Worek, “Complete Nagy-Soper subtraction for next-to-leading order calculations in QCD”, *JHEP* **10** (2013) 204, doi:10.1007/JHEP10(2013)204, arXiv:1308.5605.
67. A. Denner and S. Dittmaier, “Reduction schemes for one-loop tensor integrals”, *Nucl. Phys. B* **734** (2006) 62, doi:10.1016/j.nuclphysb.2005.11.007, arXiv:hep-ph/0509141.
68. G. Ossola, C. G. Papadopoulos, and R. Pittau, “Reducing full one-loop amplitudes to scalar integrals at the integrand level”, *Nucl. Phys. B* **763** (2007) 147, doi:10.1016/j.nuclphysb.2006.11.012, arXiv:hep-ph/0609007.
69. C. Anastasiou et al., “D-dimensional unitarity cut method”, *Phys. Lett. B* **645** (2007) 213, doi:10.1016/j.physletb.2006.12.022, arXiv:hep-ph/0609191.
70. R. K. Ellis, W. Giele, and Z. Kunszt, “A Numerical Unitarity Formalism for Evaluating One-Loop Amplitudes”, *JHEP* **03** (2008) 003, doi:10.1088/1126-6708/2008/03/003, arXiv:0708.2398.
71. W. T. Giele, Z. Kunszt, and K. Melnikov, “Full one-loop amplitudes from tree amplitudes”, *JHEP* **04** (2008) 049, doi:10.1088/1126-6708/2008/04/049, arXiv:0801.2237.

72. C. Berger et al., “An Automated Implementation of On-Shell Methods for One-Loop Amplitudes”, *Phys. Rev. D* **78** (2008) 036003, doi:10.1103/PhysRevD.78.036003, arXiv:0803.4180.
73. G. Bevilacqua et al., “HELAC-NLO”, *Comput. Phys. Commun.* **184** (2013) 986, doi:10.1016/j.cpc.2012.10.033, arXiv:1110.1499.
74. J. Alwall et al., “The automated computation of tree-level and next-to-leading order differential cross sections, and their matching to parton shower simulations”, *JHEP* **07** (2014) 079, doi:10.1007/JHEP07(2014)079, arXiv:1405.0301.
75. T. Gleisberg et al., “SHERPA 1. alpha: A Proof of concept version”, *JHEP* **02** (2004) 056, doi:10.1088/1126-6708/2004/02/056, arXiv:hep-ph/0311263.
76. T. Gleisberg et al., “Event generation with SHERPA 1.1”, *JHEP* **02** (2009) 007, doi:10.1088/1126-6708/2009/02/007, arXiv:0811.4622.
77. T. Gleisberg and F. Krauss, “Automating dipole subtraction for QCD NLO calculations”, *Eur. Phys. J. C* **53** (2008) 501, doi:10.1140/epjc/s10052-007-0495-0, arXiv:0709.2881.
78. M. Czakon, C. Papadopoulos, and M. Worek, “Polarizing the Dipoles”, *JHEP* **08** (2009) 085, doi:10.1088/1126-6708/2009/08/085, arXiv:0905.0883.
79. K. Hasegawa, S. Moch, and P. Uwer, “AutoDipole: Automated generation of dipole subtraction terms”, *Comput. Phys. Commun.* **181** (2010) 1802, doi:10.1016/j.cpc.2010.06.044, arXiv:0911.4371.
80. R. Frederix, T. Gehrmann, and N. Greiner, “Integrated dipoles with MadDipole in the MadGraph framework”, *JHEP* **06** (2010) 086, doi:10.1007/JHEP06(2010)086, arXiv:1004.2905.
81. R. Frederix, S. Frixione, F. Maltoni, and T. Stelzer, “Automation of next-to-leading order computations in QCD: The FKS subtraction”, *JHEP* **10** (2009) 003, doi:10.1088/1126-6708/2009/10/003, arXiv:0908.4272.
82. G. Cullen et al., “Automated One-Loop Calculations with GoSam”, *Eur. Phys. J. C* **72** (2012) 1889, doi:10.1140/epjc/s10052-012-1889-1, arXiv:1111.2034.
83. A. van Hameren, C. Papadopoulos, and R. Pittau, “Automated one-loop calculations: A Proof of concept”, *JHEP* **09** (2009) 106, doi:10.1088/1126-6708/2009/09/106, arXiv:0903.4665.
84. V. Hirschi et al., “Automation of one-loop QCD corrections”, *JHEP* **05** (2011) 044, doi:10.1007/JHEP05(2011)044, arXiv:1103.0621.
85. S. Badger, B. Biedermann, P. Uwer, and V. Yundin, “Numerical evaluation of virtual corrections to multi-jet production in massless QCD”, *Comput. Phys. Commun.* **184** (2013) 1981, doi:10.1016/j.cpc.2013.03.018, arXiv:1209.0100.
86. F. Cascioli, P. Maierhofer, and S. Pozzorini, “Scattering Amplitudes with Open Loops”, *Phys. Rev. Lett.* **108** (2012) 111601, doi:10.1103/PhysRevLett.108.111601, arXiv:1111.5206.
87. S. Actis et al., “Recursive generation of one-loop amplitudes in the Standard Model”, *JHEP* **04** (2013) 037, doi:10.1007/JHEP04(2013)037, arXiv:1211.6316.
88. T. Binoth et al., “A Proposal for a standard interface between Monte Carlo tools and one-loop programs”, *Comput. Phys. Commun.* **181** (2010) 1612, doi:10.1016/j.cpc.2010.05.016, arXiv:1001.1307.
89. S. Alioli et al., “Update of the Binoth Les Houches Accord for a standard interface between Monte Carlo tools and one-loop programs”, *Comput. Phys. Commun.* **185** (2014) 560, doi:10.1016/j.cpc.2013.10.020, arXiv:1308.3462.
90. C. Berger et al., “Precise Predictions for $W + 4$ Jet Production at the Large Hadron Collider”, *Phys. Rev. Lett.* **106** (2011) 092001, doi:10.1103/PhysRevLett.106.092001, arXiv:1009.2338.
91. Z. Bern et al., “Next-to-Leading Order $W + 5$ -Jet Production at the LHC”, *Phys. Rev. D* **88** (2013), no. 1, 014025, doi:10.1103/PhysRevD.88.014025, arXiv:1304.1253.
92. H. Ita et al., “Precise Predictions for $Z + 4$ Jets at Hadron Colliders”, *Phys. Rev. D* **85** (2012) 031501, doi:10.1103/PhysRevD.85.031501, arXiv:1108.2229.
93. Z. Bern et al., “Four-Jet Production at the Large Hadron Collider at Next-to-Leading Order in QCD”, *Phys. Rev. Lett.* **109** (2012) 042001, doi:10.1103/PhysRevLett.109.042001, arXiv:1112.3940.
94. S. Badger, B. Biedermann, P. Uwer, and V. Yundin, “NLO QCD corrections to multi-jet production at the LHC with a centre-of-mass energy of $\sqrt{s} = 8$ TeV”, *Phys. Lett. B* **718** (2013) 965, doi:10.1016/j.physletb.2012.11.029, arXiv:1209.0098.
95. S. Badger, B. Biedermann, P. Uwer, and V. Yundin, “Next-to-leading order QCD corrections to five jet production at the LHC”, *Phys. Rev. D* **89** (2014) 034019, doi:10.1103/PhysRevD.89.034019, arXiv:1309.6585.
96. G. Bevilacqua, M. Czakon, C. Papadopoulos, and M. Worek, “Dominant QCD Backgrounds in Higgs Boson Analyses at the LHC: A Study of $pp \rightarrow tt + 2$ jets at Next-To-Leading Order”, *Phys.*

- Rev. Lett.* **104** (2010) 162002, doi:10.1103/PhysRevLett.104.162002, arXiv:1002.4009.
97. S. Badger, A. Guffanti, and V. Yundin, “Next-to-leading order QCD corrections to di-photon production in association with up to three jets at the Large Hadron Collider”, *JHEP* **03** (2014) 122, doi:10.1007/JHEP03(2014)122, arXiv:1312.5927.
98. ATLAS Collaboration, “Measurement of dijet cross sections in pp collisions at 7 TeV centre-of-mass energy using the ATLAS detector”, *JHEP* **05** (2014) 059, doi:10.1007/JHEP05(2014)059, arXiv:1312.3524.
99. ATLAS Collaboration, “Measurement of three-jet production cross-sections in pp collisions at 7 TeV centre-of-mass energy using the ATLAS detector”, arXiv:1411.1855.
100. CMS Collaboration, “Measurement of the inclusive 3-jet production differential cross section in proton-proton collisions at 7 TeV and determination of the strong coupling constant in the TeV range”, arXiv:1412.1633.
101. S. Dittmaier, A. Huss, and C. Speckner, “Weak radiative corrections to dijet production at hadron colliders”, *JHEP* **11** (2012) 095, doi:10.1007/JHEP11(2012)095, arXiv:1210.0438.
102. S. Alekhin, J. Blümlein, and S. Moch, “Parton Distribution Functions and Benchmark Cross Sections at NNLO”, *Phys. Rev. D* **86** (2012) 054009, doi:10.1103/PhysRevD.86.054009, arXiv:1202.2281.
103. H.-L. Lai et al., “New parton distributions for collider physics”, *Phys. Rev. D* **82** (2010) 074024, doi:10.1103/PhysRevD.82.074024, arXiv:1007.2241.
104. M. Glück, P. Jimenez-Delgado, and E. Reya, “Dynamical parton distributions of the nucleon and very small-x physics”, *Eur. Phys. J. C* **53** (2008) 355, doi:10.1140/epjc/s10052-007-0462-9, arXiv:0709.0614.
105. H1 Collaboration and ZEUS Collaboration, “Combined Measurement and QCD Analysis of the Inclusive e+ p Scattering Cross Sections at HERA”, *JHEP* **01** (2010) 109, doi:10.1007/JHEP01(2010)109, arXiv:0911.0884.
106. A. Martin, W. Stirling, R. Thorne, and G. Watt, “Parton distributions for the LHC”, *Eur. Phys. J. C* **63** (2009) 189, doi:10.1140/epjc/s10052-009-1072-5, arXiv:0901.0002.
107. R. D. Ball et al., “Impact of Heavy Quark Masses on Parton Distributions and LHC Phenomenology”, *Nucl. Phys. B* **849** (2011) 296, doi:10.1016/j.nuclphysb.2011.03.021, arXiv:1101.1300.
108. NNPDF Collaboration, “Reweighting NNPDFs: the W lepton asymmetry”, *Nucl. Phys. B* **849** (2011) 112, doi:10.1016/j.nuclphysb.2011.03.017, 10.1016/j.nuclphysb.2011.10.024, 10.1016/j.nuclphysb.2011.09.011, arXiv:1012.0836.
109. NNPDF Collaboration, “A determination of parton distributions with faithful uncertainty estimation”, *Nucl. Phys. B* **809** (2009) 1, doi:10.1016/j.nuclphysb.2008.09.037, arXiv:0808.1231.
110. CMS Collaboration, “PDF constraints and extraction of the strong coupling constant from the inclusive jet cross section at 7 TeV”, arXiv:1410.6765.
111. D. Stump et al., “Uncertainties of predictions from parton distribution functions. 1. The Lagrange multiplier method”, *Phys. Rev. D* **65** (2001) 014012, doi:10.1103/PhysRevD.65.014012, arXiv:hep-ph/0101051.
112. G. Watt and R. Thorne, “Study of Monte Carlo approach to experimental uncertainty propagation with MSTW 2008 PDFs”, *JHEP* **08** (2012) 052, doi:10.1007/JHEP08(2012)052, arXiv:1205.4024.
113. H. Paukkunen and P. Zurita, “PDF reweighting in the Hessian matrix approach”, *JHEP* **12** (2014) 100, doi:10.1007/JHEP12(2014)100, arXiv:1402.6623.
114. S. Alekhin et al., “HERAFitter, Open Source QCD Fit Project”, arXiv:1410.4412.
115. H1 Collaboration, “A Precision Measurement of the Inclusive ep Scattering Cross Section at HERA”, *Eur. Phys. J. C* **64** (2009) 561, doi:10.1140/epjc/s10052-009-1169-x, arXiv:0904.3513.
116. R. Thorne and R. Roberts, “An Ordered analysis of heavy flavor production in deep inelastic scattering”, *Phys. Rev. D* **57** (1998) 6871, doi:10.1103/PhysRevD.57.6871, arXiv:hep-ph/9709442.
117. R. Thorne, “A Variable-flavor number scheme for NNLO”, *Phys. Rev. D* **73** (2006) 054019, doi:10.1103/PhysRevD.73.054019, arXiv:hep-ph/0601245.
118. NuTeV Collaboration, “Measurement of the Nucleon Strange-Antistrange Asymmetry at Next-to-Leading Order in QCD from NuTeV Dimuon Data”, *Phys. Rev. Lett.* **99** (2007) 192001, doi:10.1103/PhysRevLett.99.192001.

119. CMS Collaboration, “Measurement of the ratio of the inclusive 3-jet cross section to the inclusive 2-jet cross section in pp collisions at $\sqrt{s} = 7$ TeV and first determination of the strong coupling constant in the TeV range”, *Eur. Phys. J. C* **73** (2013) 2604, doi:10.1140/epjc/s10052-013-2604-6, arXiv:1304.7498.
120. C. Anastasiou, K. Melnikov, and F. Petriello, “A new method for real radiation at NNLO”, *Phys. Rev. D* **69** (2004) 076010, doi:10.1103/PhysRevD.69.076010, arXiv:hep-ph/0311311.
121. A. Gehrmann-De Ridder, T. Gehrmann, and E. N. Glover, “Antenna subtraction at NNLO”, *JHEP* **09** (2005) 056, doi:10.1088/1126-6708/2005/09/056, arXiv:hep-ph/0505111.
122. S. Catani and M. Grazzini, “An NNLO subtraction formalism in hadron collisions and its application to Higgs boson production at the LHC”, *Phys. Rev. Lett.* **98** (2007) 222002, doi:10.1103/PhysRevLett.98.222002, arXiv:hep-ph/0703012.
123. M. Czakon, “A novel subtraction scheme for double-real radiation at NNLO”, *Phys. Lett. B* **693** (2010) 259, doi:10.1016/j.physletb.2010.08.036, arXiv:1005.0274.
124. C. Anastasiou, L. J. Dixon, K. Melnikov, and F. Petriello, “Dilepton rapidity distribution in the Drell-Yan process at NNLO in QCD”, *Phys. Rev. Lett.* **91** (2003) 182002, doi:10.1103/PhysRevLett.91.182002, arXiv:hep-ph/0306192.
125. K. Melnikov and F. Petriello, “Electroweak gauge boson production at hadron colliders through $O(\alpha(s)^2)$ ”, *Phys. Rev. D* **74** (2006) 114017, doi:10.1103/PhysRevD.74.114017, arXiv:hep-ph/0609070.
126. S. Catani et al., “Vector boson production at hadron colliders: a fully exclusive QCD calculation at NNLO”, *Phys. Rev. Lett.* **103** (2009) 082001, doi:10.1103/PhysRevLett.103.082001, arXiv:0903.2120.
127. M. Grazzini, S. Kallweit, D. Rathlev, and A. Torre, “ $Z\gamma$ production at hadron colliders in NNLO QCD”, *Phys. Lett. B* **731** (2014) 204, doi:10.1016/j.physletb.2014.02.037, arXiv:1309.7000.
128. F. Cascioli et al., “ZZ production at hadron colliders in NNLO QCD”, *Phys. Lett. B* **735** (2014) 311, doi:10.1016/j.physletb.2014.06.056, arXiv:1405.2219.
129. T. Gehrmann et al., “ W^+W^- Production at Hadron Colliders in Next to Next to Leading Order QCD”, *Phys. Rev. Lett.* **113** (2014) 212001, doi:10.1103/PhysRevLett.113.212001, arXiv:1408.5243.
130. S. Catani et al., “Diphoton production at hadron colliders: a fully-differential QCD calculation at NNLO”, *Phys. Rev. Lett.* **108** (2012) 072001, doi:10.1103/PhysRevLett.108.072001, arXiv:1110.2375.
131. M. Czakon, P. Fiedler, and A. Mitov, “Total Top-Quark Pair-Production Cross Section at Hadron Colliders Through $O(\frac{4}{3})$ ”, *Phys. Rev. Lett.* **110** (2013), no. 25, 252004, doi:10.1103/PhysRevLett.110.252004, arXiv:1303.6254.
132. R. V. Harlander and W. B. Kilgore, “Next-to-next-to-leading order Higgs production at hadron colliders”, *Phys. Rev. Lett.* **88** (2002) 201801, doi:10.1103/PhysRevLett.88.201801, arXiv:hep-ph/0201206.
133. C. Anastasiou and K. Melnikov, “Higgs boson production at hadron colliders in NNLO QCD”, *Nucl. Phys. B* **646** (2002) 220, doi:10.1016/S0550-3213(02)00837-4, arXiv:hep-ph/0207004.
134. R. V. Harlander and W. B. Kilgore, “Higgs boson production in bottom quark fusion at next-to-next-to leading order”, *Phys. Rev. D* **68** (2003) 013001, doi:10.1103/PhysRevD.68.013001, arXiv:hep-ph/0304035.
135. O. Brein, A. Djouadi, and R. Harlander, “NNLO QCD corrections to the Higgs-strahlung processes at hadron colliders”, *Phys. Lett. B* **579** (2004) 149, doi:10.1016/j.physletb.2003.10.112, arXiv:hep-ph/0307206.
136. A. Pak, M. Rogal, and M. Steinhauser, “Finite top quark mass effects in NNLO Higgs boson production at LHC”, *JHEP* **02** (2010) 025, doi:10.1007/JHEP02(2010)025, arXiv:0911.4662.
137. R. V. Harlander, H. Mantler, S. Marzani, and K. J. Ozeren, “Higgs production in gluon fusion at next-to-next-to-leading order QCD for finite top mass”, *Eur. Phys. J. C* **66** (2010) 359, doi:10.1140/epjc/s10052-010-1258-x, arXiv:0912.2104.
138. P. Bolzoni, F. Maltoni, S. Moch, and M. Zaro, “Higgs production via vector-boson fusion at NNLO in QCD”, *Phys. Rev. Lett.* **105** (2010) 011801, doi:10.1103/PhysRevLett.105.011801, arXiv:1003.4451.
139. G. Ferrera, M. Grazzini, and F. Tramontano, “Associated WH production at hadron colliders: a fully exclusive QCD calculation at NNLO”, *Phys. Rev. Lett.* **107** (2011) 152003, doi:10.1103/PhysRevLett.107.152003, arXiv:1107.1164.

140. J. Currie, A. Gehrmann-De Ridder, E. Glover, and J. Pires, “NNLO QCD corrections to jet production at hadron colliders from gluon scattering”, *JHEP* **01** (2014) 110, doi:10.1007/JHEP01(2014)110, arXiv:1310.3993.
141. J. Currie et al., “Second order QCD corrections to gluonic jet production at hadron colliders”, arXiv:1407.5558.
142. S. Drell and T.-M. Yan, “Massive Lepton Pair Production in Hadron-Hadron Collisions at High-Energies”, *Phys. Rev. Lett.* **25** (1970) 316, doi:10.1103/PhysRevLett.25.316.
143. R. Gavin, Y. Li, F. Petriello, and S. Quackenbush, “FEWZ 2.0: A code for hadronic Z production at next-to-next-to-leading order”, *Comput. Phys. Commun.* **182** (2011) 2388, doi:10.1016/j.cpc.2011.06.008, arXiv:1011.3540.
144. Y. Li and F. Petriello, “Combining QCD and electroweak corrections to dilepton production in FEWZ”, *Phys. Rev. D* **86** (2012) 094034, doi:10.1103/PhysRevD.86.094034, arXiv:1208.5967.
145. U. Baur, S. Keller, and W. Sakumoto, “QED radiative corrections to Z boson production and the forward backward asymmetry at hadron colliders”, *Phys. Rev. D* **57** (1998) 199, doi:10.1103/PhysRevD.57.199, arXiv:hep-ph/9707301.
146. U. Baur et al., “Electroweak radiative corrections to neutral current Drell-Yan processes at hadron colliders”, *Phys. Rev. D* **65** (2002) 033007, doi:10.1103/PhysRevD.65.033007, arXiv:hep-ph/0108274.
147. S. Dittmaier and M. Kramer, “Electroweak radiative corrections to W boson production at hadron colliders”, *Phys. Rev. D* **65** (2002) 073007, doi:10.1103/PhysRevD.65.073007, arXiv:hep-ph/0109062.
148. C. Carloni Calame, G. Montagna, O. Nicrosini, and A. Vicini, “Precision electroweak calculation of the production of a high transverse-momentum lepton pair at hadron colliders”, *JHEP* **10** (2007) 109, doi:10.1088/1126-6708/2007/10/109, arXiv:0710.1722.
149. A. Arbuzov et al., “One-loop corrections to the Drell-Yan process in SANC. (II). The Neutral current case”, *Eur. Phys. J. C* **54** (2008) 451, doi:10.1140/epjc/s10052-008-0531-8, arXiv:0711.0625.
150. S. Dittmaier and M. Huber, “Radiative corrections to the neutral-current Drell-Yan process in the Standard Model and its minimal supersymmetric extension”, *JHEP* **01** (2010) 060, doi:10.1007/JHEP01(2010)060, arXiv:0911.2329.
151. ATLAS Collaboration, “Measurement of the inclusive W^\pm and Z/gamma cross sections in the electron and muon decay channels in pp collisions at $\sqrt{s} = 7$ TeV with the ATLAS detector”, *Phys. Rev. D* **85** (2012) 072004, doi:10.1103/PhysRevD.85.072004, arXiv:1109.5141.
152. CMS Collaboration, “Measurement of the Inclusive W and Z Production Cross Sections in pp Collisions at $\sqrt{s} = 7$ TeV”, *JHEP* **10** (2011) 132, doi:10.1007/JHEP10(2011)132, arXiv:1107.4789.
153. CMS Collaboration, “Measurement of inclusive W and Z boson production cross sections in pp collisions at $\sqrt{s} = 8$ TeV”, *Phys. Rev. Lett.* **112** (2014) 191802, doi:10.1103/PhysRevLett.112.191802, arXiv:1402.0923.
154. CMS Collaboration, “Measurement of the differential and double-differential Drell-Yan cross sections in proton-proton collisions at $\sqrt{s} = 7$ TeV”, *JHEP* **12** (2013) 030, doi:10.1007/JHEP12(2013)030, arXiv:1310.7291.
155. ATLAS Collaboration, “Measurement of the high-mass Drell-Yan differential cross-section in pp collisions at $\sqrt{s} = 7$ TeV with the ATLAS detector”, *Phys. Lett. B* **725** (2013) 223, doi:10.1016/j.physletb.2013.07.049, arXiv:1305.4192.
156. LHCb Collaboration, “Measurement of the forward W boson cross-section in pp collisions at $\sqrt{s} = 7$ TeV”, *JHEP* **12** (2014) 079, doi:10.1007/JHEP12(2014)079, arXiv:1408.4354.
157. M. Klasen and M. Brandt, “Parton densities from LHC vector boson production at small and large transverse momenta”, *Phys. Rev. D* **88** (2013) 054002, doi:10.1103/PhysRevD.88.054002, arXiv:1305.5677.
158. C. Balázs and C. Yuan, “Soft gluon effects on lepton pairs at hadron colliders”, *Phys. Rev. D* **56** (1997) 5558, doi:10.1103/PhysRevD.56.5558, arXiv:hep-ph/9704258.
159. M. Guzzi, P. M. Nadolsky, and B. Wang, “Nonperturbative contributions to a resummed leptonic angular distribution in inclusive neutral vector boson production”, *Phys. Rev. D* **90** (2014) 014030, doi:10.1103/PhysRevD.90.014030, arXiv:1309.1393.
160. S. Höche, Y. Li, and S. Prestel, “Drell-Yan lepton pair production at NNLO QCD with parton showers”, *Phys. Rev. D* **91** (2015) 074015, doi:10.1103/PhysRevD.91.074015, arXiv:1405.3607.

161. A. Karlberg, E. Re, and G. Zanderighi, “NNLOPS accurate Drell-Yan production”, *JHEP* **09** (2014) 134, doi:10.1007/JHEP09(2014)134, arXiv:1407.2940.
162. ATLAS Collaboration, “Measurement of the Z/γ^* boson transverse momentum distribution in pp collisions at $\sqrt{s} = 7$ TeV with the ATLAS detector”, *JHEP* **09** (2014) 145, doi:10.1007/JHEP09(2014)145, arXiv:1406.3660.
163. ATLAS Collaboration, “Measurement of the transverse momentum distribution of Z/γ^* bosons in proton-proton collisions at $\sqrt{s} = 7$ TeV with the ATLAS detector”, *Phys. Lett. B* **705** (2011) 415, doi:10.1016/j.physletb.2011.10.018, arXiv:1107.2381.
164. ATLAS Collaboration, “Measurement of the Transverse Momentum Distribution of W Bosons in pp Collisions at $\sqrt{s} = 7$ TeV with the ATLAS Detector”, *Phys. Rev. D* **85** (2012) 012005, doi:10.1103/PhysRevD.85.012005, arXiv:1108.6308.
165. CMS Collaboration, “Measurement of the Rapidity and Transverse Momentum Distributions of Z Bosons in pp Collisions at $\sqrt{s} = 7$ TeV”, *Phys. Rev. D* **85** (2012) 032002, doi:10.1103/PhysRevD.85.032002, arXiv:1110.4973.
166. J. Pumplin et al., “New generation of parton distributions with uncertainties from global QCD analysis”, *JHEP* **07** (2002) 012, doi:10.1088/1126-6708/2002/07/012, arXiv:hep-ph/0201195.
167. ATLAS Collaboration, “Measurement of the Muon Charge Asymmetry from W Bosons Produced in pp Collisions at $\sqrt{s} = 7$ TeV with the ATLAS detector”, *Phys. Lett. B* **701** (2011) 31, doi:10.1016/j.physletb.2011.05.024, arXiv:1103.2929.
168. CMS Collaboration, “Measurement of the lepton charge asymmetry in inclusive W production in pp collisions at $\sqrt{s} = 7$ TeV”, *JHEP* **04** (2011) 050, doi:10.1007/JHEP04(2011)050, arXiv:1103.3470.
169. ATLAS Collaboration, “Measurement of the $W \rightarrow \ell\nu$ and $Z/\gamma^* \rightarrow \ell\ell$ production cross sections in proton-proton collisions at $\sqrt{s} = 7$ TeV with the ATLAS detector”, *JHEP* **12** (2010) 060, doi:10.1007/JHEP12(2010)060, arXiv:1010.2130.
170. CMS Collaboration, “Measurements of Inclusive W and Z Cross Sections in pp Collisions at $\sqrt{s} = 7$ TeV”, *JHEP* **01** (2011) 080, doi:10.1007/JHEP01(2011)080, arXiv:1012.2466.
171. ATLAS Collaboration, “Measurement of the isolated di-photon cross-section in pp collisions at $\sqrt{s} = 7$ TeV with the ATLAS detector”, *Phys. Rev. D* **85** (2012) 012003, doi:10.1103/PhysRevD.85.012003, arXiv:1107.0581.
172. ATLAS Collaboration, “Measurement of isolated-photon pair production in pp collisions at $\sqrt{s} = 7$ TeV with the ATLAS detector”, *JHEP* **01** (2013) 086, doi:10.1007/JHEP01(2013)086, arXiv:1211.1913.
173. CMS Collaboration, “Measurement of the Production Cross Section for Pairs of Isolated Photons in pp collisions at $\sqrt{s} = 7$ TeV”, *JHEP* **01** (2012) 133, doi:10.1007/JHEP01(2012)133, arXiv:1110.6461.
174. CMS Collaboration, “Measurement of differential cross sections for the production of a pair of isolated photons in pp collisions at $\sqrt{s} = 7$ TeV”, *Eur. Phys. J. C* **74** (2014) 3129, doi:10.1140/epjc/s10052-014-3129-3, arXiv:1405.7225.
175. J. Butterworth et al., “Les Houches 2013: Physics at TeV Colliders: Standard Model Working Group Report”, arXiv:1405.1067.
176. T. Sjöstrand, S. Mrenna, and P. Z. Skands, “PYTHIA 6.4 Physics and Manual”, *JHEP* **05** (2006) 026, doi:10.1088/1126-6708/2006/05/026, arXiv:hep-ph/0603175.
177. S. Höche, S. Schumann, and F. Siegert, “Hard photon production and matrix-element parton-shower merging”, *Phys. Rev. D* **81** (2010) 034026, doi:10.1103/PhysRevD.81.034026, arXiv:0912.3501.
178. T. Binoth, J. Guillet, E. Pilon, and M. Werlen, “A full next-to-leading order study of direct photon pair production in hadronic collisions”, *Eur. Phys. J. C* **16** (2000) 311, doi:10.1007/s100520050024, arXiv:hep-ph/9911340.
179. C. Balázs, E. L. Berger, S. Mrenna, and C. Yuan, “Photon pair production with soft gluon resummation in hadronic interactions”, *Phys. Rev. D* **57** (1998) 6934, doi:10.1103/PhysRevD.57.6934, arXiv:hep-ph/9712471.
180. C. Balázs, E. L. Berger, P. M. Nadolsky, and C.-P. Yuan, “Calculation of prompt diphoton production cross-sections at Tevatron and LHC energies”, *Phys. Rev. D* **76** (2007) 013009, doi:10.1103/PhysRevD.76.013009, arXiv:0704.0001.
181. Z. Bern, L. J. Dixon, and C. Schmidt, “Isolating a light Higgs boson from the diphoton background at the CERN LHC”, *Phys. Rev. D* **66** (2002) 074018, doi:10.1103/PhysRevD.66.074018, arXiv:hep-ph/0206194.

182. J. C. Collins and D. E. Soper, “Angular Distribution of Dileptons in High-Energy Hadron Collisions”, *Phys. Rev. D* **16** (1977) 2219, doi:10.1103/PhysRevD.16.2219.
183. S. Catani, F. Krauss, R. Kuhn, and B. Webber, “QCD matrix elements + parton showers”, *JHEP* **11** (2001) 063, doi:10.1088/1126-6708/2001/11/063, arXiv:hep-ph/0109231.
184. L. Lönnblad, “Correcting the color dipole cascade model with fixed order matrix elements”, *JHEP* **05** (2002) 046, doi:10.1088/1126-6708/2002/05/046, arXiv:hep-ph/0112284.
185. F. Krauss, “Matrix elements and parton showers in hadronic interactions”, *JHEP* **08** (2002) 015, doi:10.1088/1126-6708/2002/08/015, arXiv:hep-ph/0205283.
186. M. L. Mangano, M. Moretti, F. Piccinini, and M. Treccani, “Matching matrix elements and shower evolution for top-quark production in hadronic collisions”, *JHEP* **01** (2007) 013, doi:10.1088/1126-6708/2007/01/013, arXiv:hep-ph/0611129.
187. J. Alwall et al., “Comparative study of various algorithms for the merging of parton showers and matrix elements in hadronic collisions”, *Eur. Phys. J. C* **53** (2008) 473, doi:10.1140/epjc/s10052-007-0490-5, arXiv:0706.2569.
188. L. Lönnblad and S. Prestel, “Matching Tree-Level Matrix Elements with Interleaved Showers”, *JHEP* **03** (2012) 019, doi:10.1007/JHEP03(2012)019, arXiv:1109.4829.
189. S. Plätzer, “Controlling inclusive cross sections in parton shower + matrix element merging”, *JHEP* **08** (2013) 114, doi:10.1007/JHEP08(2013)114, arXiv:1211.5467.
190. S. Frixione and B. R. Webber, “Matching NLO QCD computations and parton shower simulations”, *JHEP* **06** (2002) 029, doi:10.1088/1126-6708/2002/06/029, arXiv:hep-ph/0204244.
191. P. Nason, “A New method for combining NLO QCD with shower Monte Carlo algorithms”, *JHEP* **11** (2004) 040, doi:10.1088/1126-6708/2004/11/040, arXiv:hep-ph/0409146.
192. S. Frixione, P. Nason, and C. Oleari, “Matching NLO QCD computations with Parton Shower simulations: the POWHEG method”, *JHEP* **11** (2007) 070, doi:10.1088/1126-6708/2007/11/070, arXiv:0709.2092.
193. S. Alioli, P. Nason, C. Oleari, and E. Re, “A general framework for implementing NLO calculations in shower Monte Carlo programs: the POWHEG BOX”, *JHEP* **06** (2010) 043, doi:10.1007/JHEP06(2010)043, arXiv:1002.2581.
194. S. Plätzer and S. Gieseke, “Dipole Showers and Automated NLO Matching in Herwig++”, *Eur. Phys. J. C* **72** (2012) 2187, doi:10.1140/epjc/s10052-012-2187-7, arXiv:1109.6256.
195. S. Höche, F. Krauss, M. Schönherr, and F. Siegert, “A critical appraisal of NLO+PS matching methods”, *JHEP* **09** (2012) 049, doi:10.1007/JHEP09(2012)049, arXiv:1111.1220.
196. K. Hamilton and P. Nason, “Improving NLO-parton shower matched simulations with higher order matrix elements”, *JHEP* **06** (2010) 039, doi:10.1007/JHEP06(2010)039, arXiv:1004.1764.
197. S. Höche, F. Krauss, M. Schönherr, and F. Siegert, “NLO matrix elements and truncated showers”, *JHEP* **08** (2011) 123, doi:10.1007/JHEP08(2011)123, arXiv:1009.1127.
198. S. Höche, F. Krauss, M. Schönherr, and F. Siegert, “QCD matrix elements + parton showers: The NLO case”, *JHEP* **04** (2013) 027, doi:10.1007/JHEP04(2013)027, arXiv:1207.5030.
199. R. Frederix and S. Frixione, “Merging meets matching in MC@NLO”, *JHEP* **12** (2012) 061, doi:10.1007/JHEP12(2012)061, arXiv:1209.6215.
200. L. Lönnblad and S. Prestel, “Merging Multi-leg NLO Matrix Elements with Parton Showers”, *JHEP* **03** (2013) 166, doi:10.1007/JHEP03(2013)166, arXiv:1211.7278.
201. K. Hamilton, P. Nason, C. Oleari, and G. Zanderighi, “Merging H/W/Z + 0 and 1 jet at NLO with no merging scale: a path to parton shower + NNLO matching”, *JHEP* **05** (2013) 082, doi:10.1007/JHEP05(2013)082, arXiv:1212.4504.
202. S. Höche et al., “Next-to-leading order QCD predictions for top-quark pair production with up to two jets merged with a parton shower”, arXiv:1402.6293.
203. CMS Collaboration, “Differential cross section measurements for the production of a W boson in association with jets in protonproton collisions at $\sqrt{s} = 7$ TeV”, *Phys. Lett. B* **741** (2015) 12, doi:10.1016/j.physletb.2014.12.003, arXiv:1406.7533.
204. ATLAS Collaboration, “Study of jets produced in association with a W boson in pp collisions at $\sqrt{s} = 7$ TeV with the ATLAS detector”, *Phys. Rev. D* **85** (2012) 092002, doi:10.1103/PhysRevD.85.092002, arXiv:1201.1276.
205. J. M. Campbell, R. K. Ellis, and D. L. Rainwater, “Next-to-leading order QCD predictions for W + 2 jet and Z + 2 jet production at the CERN LHC”, *Phys. Rev. D* **68** (2003) 094021, doi:10.1103/PhysRevD.68.094021, arXiv:hep-ph/0308195.
206. C. Berger et al., “Vector Boson + Jets with BlackHat and Sherpa”, *Nucl. Phys. Proc. Suppl.* **205-206** (2010) 92, doi:10.1016/j.nuclphysbps.2010.08.025, arXiv:1005.3728.

207. ATLAS Collaboration, “Measurement of the production cross section of jets in association with a Z boson in pp collisions at $\sqrt{s} = 7$ TeV with the ATLAS detector”, *JHEP* **07** (2013) 032, doi:10.1007/JHEP07(2013)032, arXiv:1304.7098.
208. CMS Collaboration, “Jet Production Rates in Association with W and Z Bosons in pp Collisions at $\sqrt{s} = 7$ TeV”, *JHEP* **01** (2012) 010, doi:10.1007/JHEP01(2012)010, arXiv:1110.3226.
209. F. Berends et al., “Multi - Jet Production in W, Z Events at $p\bar{p}$ Colliders”, *Phys. Lett. B* **224** (1989) 237, doi:10.1016/0370-2693(89)91081-2.
210. E. Gerwick, T. Plehn, S. Schumann, and P. Schichtel, “Scaling Patterns for QCD Jets”, *JHEP* **10** (2012) 162, doi:10.1007/JHEP10(2012)162, arXiv:1208.3676.
211. I. W. Stewart and F. J. Tackmann, “Theory Uncertainties for Higgs and Other Searches Using Jet Bins”, *Phys. Rev. D* **85** (2012) 034011, doi:10.1103/PhysRevD.85.034011, arXiv:1107.2117.
212. BlackHat Collaboration, “Universality in W+Multijet Production”, arXiv:1407.6564.
213. ATLAS Collaboration, “Measurement of differential production cross-sections for a Z boson in association with b-jets in 7 TeV proton-proton collisions with the ATLAS detector”, *JHEP* **10** (2014) 141, doi:10.1007/JHEP10(2014)141, arXiv:1407.3643.
214. W. T. Giele, S. Keller, and E. Laenen, “QCD corrections to W boson plus heavy quark production at the Tevatron”, *Phys. Lett. B* **372** (1996) 141, doi:10.1016/0370-2693(96)00078-0, arXiv:hep-ph/9511449.
215. R. K. Ellis and S. Veseli, “Strong radiative corrections to W b anti-b production in p anti-p collisions”, *Phys. Rev. D* **60** (1999) 011501, doi:10.1103/PhysRevD.60.011501, arXiv:hep-ph/9810489.
216. J. M. Campbell and R. K. Ellis, “Radiative corrections to Z b anti-b production”, *Phys. Rev. D* **62** (2000) 114012, doi:10.1103/PhysRevD.62.114012, arXiv:hep-ph/0006304.
217. J. M. Campbell, R. K. Ellis, F. Maltoni, and S. Willenbrock, “Associated production of a Z Boson and a single heavy quark jet”, *Phys. Rev. D* **69** (2004) 074021, doi:10.1103/PhysRevD.69.074021, arXiv:hep-ph/0312024.
218. F. Maltoni, T. McElmurry, and S. Willenbrock, “Inclusive production of a Higgs or Z boson in association with heavy quarks”, *Phys. Rev. D* **72** (2005) 074024, doi:10.1103/PhysRevD.72.074024, arXiv:hep-ph/0505014.
219. J. M. Campbell, R. K. Ellis, F. Maltoni, and S. Willenbrock, “Production of a Z boson and two jets with one heavy-quark tag”, *Phys. Rev. D* **73** (2006) 054007, doi:10.1103/PhysRevD.77.019903, 10.1103/PhysRevD.73.054007, arXiv:hep-ph/0510362.
220. J. M. Campbell et al., “Associated Production of a W Boson and One b Jet”, *Phys. Rev. D* **79** (2009) 034023, doi:10.1103/PhysRevD.79.034023, arXiv:0809.3003.
221. F. Febres Cordero, L. Reina, and D. Wackerroth, “W- and Z-boson production with a massive bottom-quark pair at the Large Hadron Collider”, *Phys. Rev. D* **80** (2009) 034015, doi:10.1103/PhysRevD.80.034015, arXiv:0906.1923.
222. S. Badger, J. M. Campbell, and R. Ellis, “QCD corrections to the hadronic production of a heavy quark pair and a W-boson including decay correlations”, *JHEP* **03** (2011) 027, doi:10.1007/JHEP03(2011)027, arXiv:1011.6647.
223. C. Oleari and L. Reina, “W +- b \bar{b} production in POWHEG”, *JHEP* **08** (2011) 061, doi:10.1007/JHEP11(2011)040, 10.1007/JHEP08(2011)061, arXiv:1105.4488.
224. R. Frederix et al., “W and Z/ γ^* boson production in association with a bottom-antibottom pair”, *JHEP* **09** (2011) 061, doi:10.1007/JHEP09(2011)061, arXiv:1106.6019.
225. ATLAS Collaboration, “Measurement of the cross-section for b^- jets produced in association with a Z boson at $\sqrt{s} = 7$ TeV with the ATLAS detector”, *Phys. Lett. B* **706** (2012) 295, doi:10.1016/j.physletb.2011.11.059, arXiv:1109.1403.
226. CMS Collaboration, “Measurement of the production cross sections for a Z boson and one or more b jets in pp collisions at $\sqrt{s} = 7$ TeV”, *JHEP* **06** (2014) 120, doi:10.1007/JHEP06(2014)120, arXiv:1402.1521.
227. CMS Collaboration, “Measurement of the cross section and angular correlations for associated production of a Z boson with b hadrons in pp collisions at $\sqrt{s} = 7$ TeV”, *JHEP* **12** (2013) 039, doi:10.1007/JHEP12(2013)039, arXiv:1310.1349.
228. T. Becher, M. Neubert, and D. Wilhelm, “Electroweak Gauge-Boson Production at Small q_T : Infrared Safety from the Collinear Anomaly”, *JHEP* **02** (2012) 124, doi:10.1007/JHEP02(2012)124, arXiv:1109.6027.
229. A. Banfi, M. Dasgupta, S. Marzani, and L. Tomlinson, “Predictions for Drell-Yan ϕ^* and Q_T observables at the LHC”, *Phys. Lett. B* **715** (2012) 152, doi:10.1016/j.physletb.2012.07.035, arXiv:1205.4760.

230. A. Banfi, G. P. Salam, and G. Zanderighi, “Resummed event shapes at hadron - hadron colliders”, *JHEP* **08** (2004) 062, doi:10.1088/1126-6708/2004/08/062, arXiv:hep-ph/0407287.
231. A. Banfi, G. P. Salam, and G. Zanderighi, “Phenomenology of event shapes at hadron colliders”, *JHEP* **06** (2010) 038, doi:10.1007/JHEP06(2010)038, arXiv:1001.4082.
232. I. W. Stewart, F. J. Tackmann, and W. J. Waalewijn, “N-Jettiness: An Inclusive Event Shape to Veto Jets”, *Phys. Rev. Lett.* **105** (2010) 092002, doi:10.1103/PhysRevLett.105.092002, arXiv:1004.2489.
233. I. Feige, M. D. Schwartz, I. W. Stewart, and J. Thaler, “Precision Jet Substructure from Boosted Event Shapes”, *Phys. Rev. Lett.* **109** (2012) 092001, doi:10.1103/PhysRevLett.109.092001, arXiv:1204.3898.
234. E. Gerwick, S. Schumann, B. Gripaios, and B. Webber, “QCD Jet Rates with the Inclusive Generalized kt Algorithms”, *JHEP* **04** (2013) 089, doi:10.1007/JHEP04(2013)089, arXiv:1212.5235.
235. A. J. Larkoski, G. P. Salam, and J. Thaler, “Energy Correlation Functions for Jet Substructure”, *JHEP* **06** (2013) 108, doi:10.1007/JHEP06(2013)108, arXiv:1305.0007.
236. A. Idilbi and X. Ji, “Threshold resummation for Drell-Yan process in soft-collinear effective theory”, *Phys. Rev. D* **72** (2005) 054016, doi:10.1103/PhysRevD.72.054016, arXiv:hep-ph/0501006.
237. T. Becher, M. Neubert, and G. Xu, “Dynamical Threshold Enhancement and Resummation in Drell-Yan Production”, *JHEP* **07** (2008) 030, doi:10.1088/1126-6708/2008/07/030, arXiv:0710.0680.
238. M. Bonvini, S. Forte, and G. Ridolfi, “Soft gluon resummation of Drell-Yan rapidity distributions: Theory and phenomenology”, *Nucl. Phys. B* **847** (2011) 93, doi:10.1016/j.nuclphysb.2011.01.023, arXiv:1009.5691.
239. M. Cacciari et al., “Top-pair production at hadron colliders with next-to-next-to-leading logarithmic soft-gluon resummation”, *Phys. Lett. B* **710** (2012) 612, doi:10.1016/j.physletb.2012.03.013, arXiv:1111.5869.
240. J. Forshaw, J. Keates, and S. Marzani, “Jet vetoing at the LHC”, *JHEP* **07** (2009) 023, doi:10.1088/1126-6708/2009/07/023, arXiv:0905.1350.
241. R. M. Duran Delgado, J. R. Forshaw, S. Marzani, and M. H. Seymour, “The dijet cross section with a jet veto”, *JHEP* **08** (2011) 157, doi:10.1007/JHEP08(2011)157, arXiv:1107.2084.
242. A. Banfi, G. P. Salam, and G. Zanderighi, “NLL+NNLO predictions for jet-veto efficiencies in Higgs-boson and Drell-Yan production”, *JHEP* **06** (2012) 159, doi:10.1007/JHEP06(2012)159, arXiv:1203.5773.
243. A. Banfi, P. F. Monni, G. P. Salam, and G. Zanderighi, “Higgs and Z-boson production with a jet veto”, *Phys. Rev. Lett.* **109** (2012) 202001, doi:10.1103/PhysRevLett.109.202001, arXiv:1206.4998.
244. F. J. Tackmann, J. R. Walsh, and S. Zuberi, “Resummation Properties of Jet Vetoes at the LHC”, *Phys. Rev. D* **86** (2012) 053011, doi:10.1103/PhysRevD.86.053011, arXiv:1206.4312.
245. E. Kuraev, L. Lipatov, and V. S. Fadin, “The Pomernanchuk Singularity in Nonabelian Gauge Theories”, *Sov. Phys. JETP* **45** (1977) 199.
246. I. Balitsky and L. Lipatov, “The Pomernanchuk Singularity in Quantum Chromodynamics”, *Sov. J. Nucl. Phys.* **28** (1978) 822.
247. J. R. Forshaw, A. Kyrieleis, and M. Seymour, “Gaps between jets in the high energy limit”, *JHEP* **06** (2005) 034, doi:10.1088/1126-6708/2005/06/034, arXiv:hep-ph/0502086.
248. J. R. Andersen and J. M. Smillie, “Constructing All-Order Corrections to Multi-Jet Rates”, *JHEP* **01** (2010) 039, doi:10.1007/JHEP01(2010)039, arXiv:0908.2786.
249. ATLAS Collaboration, “Measurement of dijet production with a veto on additional central jet activity in pp collisions at $\sqrt{s} = 7$ TeV using the ATLAS detector”, *JHEP* **09** (2011) 053, doi:10.1007/JHEP09(2011)053, arXiv:1107.1641.
250. ATLAS Collaboration, “Measurements of jet vetoes and azimuthal decorrelations in dijet events produced in pp collisions at $\sqrt{s} = 7$ TeV using the ATLAS detector”, *Eur. Phys. J. C* **74** (2014) 3117, doi:10.1140/epjc/s10052-014-3117-7, arXiv:1407.5756.
251. S. Alioli et al., “Jet pair production in POWHEG”, *JHEP* **04** (2011) 081, doi:10.1007/JHEP04(2011)081, arXiv:1012.3380.
252. J. R. Andersen and J. M. Smillie, “Multiple Jets at the LHC with High Energy Jets”, *JHEP* **06** (2011) 010, doi:10.1007/JHEP06(2011)010, arXiv:1101.5394.
253. J. R. Andersen, L. Lönnblad, and J. M. Smillie, “A Parton Shower for High Energy Jets”, *JHEP* **07** (2011) 110, doi:10.1007/JHEP07(2011)110, arXiv:1104.1316.

254. M. Deak, F. Hautmann, H. Jung, and K. Kutak, “Forward Jets and Energy Flow in Hadronic Collisions”, *Eur. Phys. J. C* **72** (2012) 1982, doi:10.1140/epjc/s10052-012-1982-5, arXiv:1112.6354.
255. S. Alioli et al., “Probing higher-order corrections in dijet production at the LHC”, *Phys. Rev. D* **85** (2012) 114034, doi:10.1103/PhysRevD.85.114034, arXiv:1202.1475.
256. S. Höche and M. Schönherr, “Uncertainties in next-to-leading order plus parton shower matched simulations of inclusive jet and dijet production”, *Phys. Rev. D* **86** (2012) 094042, doi:10.1103/PhysRevD.86.094042, arXiv:1208.2815.
257. Y. Hatta et al., “A QCD description of the ATLAS jet veto measurement”, *Phys. Rev. D* **87** (2013), no. 5, 054016, doi:10.1103/PhysRevD.87.054016, arXiv:1301.1910.
258. A. Abdesselam et al., “Boosted objects: A Probe of beyond the Standard Model physics”, *Eur. Phys. J. C* **71** (2011) 1661, doi:10.1140/epjc/s10052-011-1661-y, arXiv:1012.5412.
259. A. Altheimer et al., “Jet Substructure at the Tevatron and LHC: New results, new tools, new benchmarks”, *J. Phys. G* **39** (2012) 063001, doi:10.1088/0954-3899/39/6/063001, arXiv:1201.0008.
260. A. Altheimer et al., “Boosted objects and jet substructure at the LHC. Report of BOOST2012, held at IFIC Valencia, 23rd-27th of July 2012”, *Eur. Phys. J. C* **74** (2014) 2792, doi:10.1140/epjc/s10052-014-2792-8, arXiv:1311.2708.
261. S. D. Ellis, C. K. Vermilion, and J. R. Walsh, “Recombination Algorithms and Jet Substructure: Pruning as a Tool for Heavy Particle Searches”, *Phys. Rev. D* **81** (2010) 094023, doi:10.1103/PhysRevD.81.094023, arXiv:0912.0033.
262. CMS Collaboration, “Studies of jet mass in dijet and W/Z + jet events”, *JHEP* **05** (2013) 090, doi:10.1007/JHEP05(2013)090, arXiv:1303.4811.
263. CMS Collaboration, “Search for Anomalous $t\bar{t}$ Production in the Highly-Boosted All-Hadronic Final State”, *JHEP* **09** (2012) 029, doi:10.1007/JHEP09(2012)029, arXiv:1204.2488.
264. CMS Collaboration, “Search for massive resonances in dijet systems containing jets tagged as W or Z boson decays in pp collisions at $\sqrt{s} = 8$ TeV”, *JHEP* **08** (2014) 173, doi:10.1007/JHEP08(2014)173, arXiv:1405.1994.
265. CMS Collaboration, “Search for massive resonances decaying into pairs of boosted bosons in semi-leptonic final states at $\sqrt{s} = 8$ TeV”, *JHEP* **08** (2014) 174, doi:10.1007/JHEP08(2014)174, arXiv:1405.3447.
266. D. Krohn, J. Thaler, and L.-T. Wang, “Jet Trimming”, *JHEP* **02** (2010) 084, doi:10.1007/JHEP02(2010)084, arXiv:0912.1342.
267. J. M. Butterworth, A. R. Davison, M. Rubin, and G. P. Salam, “Jet substructure as a new Higgs search channel at the LHC”, *Phys. Rev. Lett.* **100** (2008) 242001, doi:10.1103/PhysRevLett.100.242001, arXiv:0802.2470.
268. T. Plehn, G. P. Salam, and M. Spannowsky, “Fat Jets for a Light Higgs”, *Phys. Rev. Lett.* **104** (2010) 111801, doi:10.1103/PhysRevLett.104.111801, arXiv:0910.5472.
269. A. J. Larkoski, S. Marzani, G. Soyez, and J. Thaler, “Soft Drop”, *JHEP* **05** (2014) 146, doi:10.1007/JHEP05(2014)146, arXiv:1402.2657.
270. H.-N. Li, Z. Li, and C.-P. Yuan, “QCD resummation for jet substructures”, *Phys. Rev. Lett.* **107** (2011) 152001, doi:10.1103/PhysRevLett.107.152001, arXiv:1107.4535.
271. H.-N. Li, Z. Li, and C.-P. Yuan, “QCD resummation for light-particle jets”, *Phys. Rev. D* **87** (2013) 074025, doi:10.1103/PhysRevD.87.074025, arXiv:1206.1344.
272. M. Dasgupta, K. Khelifa-Kerfa, S. Marzani, and M. Spannowsky, “On jet mass distributions in Z+jet and dijet processes at the LHC”, *JHEP* **10** (2012) 126, doi:10.1007/JHEP10(2012)126, arXiv:1207.1640.
273. T. T. Jouttenus et al., “Jet mass spectra in Higgs boson plus one jet at next-to-next-to-leading logarithmic order”, *Phys. Rev. D* **88** (2013), no. 5, 054031, doi:10.1103/PhysRevD.88.054031, arXiv:1302.0846.
274. M. Dasgupta, A. Fregoso, S. Marzani, and G. P. Salam, “Towards an understanding of jet substructure”, *JHEP* **09** (2013) 029, doi:10.1007/JHEP09(2013)029, arXiv:1307.0007.
275. M. Dasgupta, A. Fregoso, S. Marzani, and A. Powling, “Jet substructure with analytical methods”, *Eur. Phys. J. C* **73** (2013), no. 11, 2623, doi:10.1140/epjc/s10052-013-2623-3, arXiv:1307.0013.
276. Y. L. Dokshitzer, G. Leder, S. Moretti, and B. Webber, “Better jet clustering algorithms”, *JHEP* **08** (1997) 001, doi:10.1088/1126-6708/1997/08/001, arXiv:hep-ph/9707323.
277. M. Wobisch and T. Wengler, “Hadronization corrections to jet cross-sections in deep inelastic scattering”, arXiv:hep-ph/9907280.

278. M. Wobisch, "Measurement and QCD analysis of jet cross-sections in deep inelastic positron proton collisions at $s^{*}(1/2) = 300\text{-GeV}$ ". PhD thesis, RWTH Aachen, 2000. DESY-THESIS-2000-049.
279. M. Dasgupta, L. Magnea, and G. P. Salam, "Non-perturbative QCD effects in jets at hadron colliders", *JHEP* **02** (2008) 055, doi:10.1088/1126-6708/2008/02/055, arXiv:0712.3014.
280. S. D. Ellis, Z. Kunszt, and D. E. Soper, "Jets at hadron colliders at order $\alpha - s^3$: A Look inside", *Phys. Rev. Lett.* **69** (1992) 3615, doi:10.1103/PhysRevLett.69.3615, arXiv:hep-ph/9208249.
281. CDF Collaboration, "A Measurement of jet shapes in $p\bar{p}$ collisions at $\sqrt{s} = 1.8\text{ TeV}$ ", *Phys. Rev. Lett.* **70** (1993) 713, doi:10.1103/PhysRevLett.70.713.
282. CDF Collaboration, "Study of jet shapes in inclusive jet production in $p\bar{p}$ collisions at $\sqrt{s} = 1.96\text{ TeV}$ ", *Phys. Rev. D* **71** (2005) 112002, doi:10.1103/PhysRevD.71.112002, arXiv:hep-ex/0505013.
283. R. K. Ellis, W. J. Stirling, and B. R. Webber, "QCD and Collider Physics". Cambridge University Press, Cambridge, United Kingdom, 1996.
284. ATLAS Collaboration, "Study of Jet Shapes in Inclusive Jet Production in pp Collisions at $\sqrt{s} = 7\text{ TeV}$ using the ATLAS Detector", *Phys. Rev. D* **83** (2011) 052003, doi:10.1103/PhysRevD.83.052003, arXiv:1101.0070.
285. CMS Collaboration, "Shape, Transverse Size, and Charged Hadron Multiplicity of Jets in pp Collisions at 7 TeV ", *JHEP* **06** (2012) 160, doi:10.1007/JHEP06(2012)160, arXiv:1204.3170.
286. M. Cacciari, J. Rojo, G. P. Salam, and G. Soyez, "Quantifying the performance of jet definitions for kinematic reconstruction at the LHC", *JHEP* **12** (2008) 032, doi:10.1088/1126-6708/2008/12/032, arXiv:0810.1304.
287. G. Soyez, "A Simple description of jet cross-section ratios", *Phys. Lett. B* **698** (2011) 59, doi:10.1016/j.physletb.2011.02.061, arXiv:1101.2665.
288. Z. Nagy, "Three jet cross-sections in hadron hadron collisions at next-to-leading order", *Phys. Rev. Lett.* **88** (2002) 122003, doi:10.1103/PhysRevLett.88.122003, arXiv:hep-ph/0110315.
289. Z. Nagy, "Next-to-leading order calculation of three-jet observables in hadron hadron collisions", *Phys. Rev. D* **68** (2003) 094002, doi:10.1103/PhysRevD.68.094002, arXiv:hep-ph/0307268.
290. ZEUS Collaboration, "Inclusive-jet cross sections in NC DIS at HERA and a comparison of the kT, anti-kT and SIScone jet algorithms", *Phys. Lett. B* **691** (2010) 127, doi:10.1016/j.physletb.2010.06.015, arXiv:1003.2923.
291. ALICE Collaboration, "Measurement of the inclusive differential jet cross section in pp collisions at $\sqrt{s} = 2.76\text{ TeV}$ ", *Phys. Lett. B* **722** (2013) 262, doi:10.1016/j.physletb.2013.04.026, arXiv:1301.3475.
292. H. G. Dosch, P. Gauron, and B. Nicolescu, "Heisenberg's universal $\ln^{*2} s$ increase of total cross-sections", *Phys. Rev. D* **67** (2003) 077501, doi:10.1103/PhysRevD.67.077501, arXiv:hep-ph/0206214.
293. M. Froissart, "Asymptotic behavior and subtractions in the Mandelstam representation", *Phys. Rev. D* **123** (1961) 1053, doi:10.1103/PhysRev.123.1053.
294. ATLAS Collaboration, "Measurement of the total cross section from elastic scattering in pp collisions at $\sqrt{s} = 7\text{TeV}$ with the ATLAS detector", *Nucl. Phys. B* **889** (2014) 486, doi:10.1016/j.nuclphysb.2014.10.019, arXiv:1408.5778.
295. H. Yukawa, "On the interaction of elementary particles", *Proc. Phys. Math. Soc. Jap.* **17** (1935) 48.
296. A. Kaidalov, "Regge poles in QCD", arXiv:hep-ph/0103011.
297. P. Collins, "An Introduction to Regge Theory and High-Energy Physics". Cambridge University Press, Cambridge, United Kingdom, 1977.
298. G. F. Chew, S. C. Frautschi, and S. Mandelstam, "Regge poles in $\pi\pi$ scattering", *Phys. Rev. D* **126** (1961) 1202, doi:10.1103/PhysRev.126.1202.
299. A. Donnachie and P. Landshoff, "Total cross-sections", *Phys. Lett. B* **296** (1992) 227, doi:10.1016/0370-2693(92)90832-0, arXiv:hep-ph/9209205.
300. ATLAS Collaboration, "Measurement of the Inelastic Proton-Proton Cross-Section at $\sqrt{s} = 7\text{ TeV}$ with the ATLAS Detector", *Nature Commun.* **2** (2011) 463, doi:10.1038/ncomms1472, arXiv:1104.0326.
301. CMS Collaboration, "Measurement of the inelastic proton-proton cross section at $\sqrt{s} = 7\text{ TeV}$ ", *Phys. Lett. B* **722** (2013) 5, doi:10.1016/j.physletb.2013.03.024, arXiv:1210.6718.
302. TOTEM Collaboration, "Measurement of proton-proton elastic scattering and total cross-section at $S^{*}(1/2) = 7\text{-TeV}$ ", *Europhys. Lett.* **101** (2013) 21002, doi:10.1209/0295-5075/101/21002.

303. TOTEM Collaboration, “Luminosity-Independent Measurement of the Proton-Proton Total Cross Section at $\sqrt{s} = 8\text{TeV}$ ”, *Phys. Rev. Lett.* **111** (2013), no. 1, 012001, doi:10.1103/PhysRevLett.111.012001.
304. ARGO-YBJ Collaboration, “Proton-air cross section measurement with the ARGO-YBJ cosmic ray experiment”, *Phys. Rev. D* **80** (2009) 092004, doi:10.1103/PhysRevD.80.092004, arXiv:0904.4198.
305. M. Honda et al., “Inelastic cross-section for p-air collisions from air shower experiment and total cross-section for p p collisions at SSC energy”, *Phys. Rev. Lett.* **70** (1993) 525, doi:10.1103/PhysRevLett.70.525.
306. R. Baltrusaitis et al., “Total Proton Proton Cross-Section at $s^{*(1/2)} = 30\text{-TeV}$ ”, *Phys. Rev. Lett.* **52** (1984) 1380, doi:10.1103/PhysRevLett.52.1380.
307. J. Cudell et al., “Benchmarks for the forward observables at RHIC, the Tevatron Run II and the LHC”, *Phys. Rev. Lett.* **89** (2002) 201801, doi:10.1103/PhysRevLett.89.201801, arXiv:hep-ph/0206172.
308. A. Donnachie and P. Landshoff, “ pp and $\bar{p}p$ total cross sections and elastic scattering”, *Phys. Lett. B* **727** (2013) 500, doi:10.1016/j.physletb.2013.10.068, arXiv:1309.1292.
309. T. Sjöstrand and M. van Zijl, “A Multiple Interaction Model for the Event Structure in Hadron Collisions”, *Phys. Rev. D* **36** (1987) 2019, doi:10.1103/PhysRevD.36.2019.
310. T. Sjöstrand and P. Z. Skands, “Multiple interactions and the structure of beam remnants”, *JHEP* **03** (2004) 053, doi:10.1088/1126-6708/2004/03/053, arXiv:hep-ph/0402078.
311. T. Sjöstrand and P. Z. Skands, “Transverse-momentum-ordered showers and interleaved multiple interactions”, *Eur. Phys. J. C* **39** (2005) 129, doi:10.1140/epjc/s2004-02084-y, arXiv:hep-ph/0408302.
312. M. Bähr, S. Gieseke, and M. H. Seymour, “Simulation of multiple partonic interactions in Herwig++”, *JHEP* **07** (2008) 076, doi:10.1088/1126-6708/2008/07/076, arXiv:0803.3633.
313. ATLAS Collaboration, “Measurement of distributions sensitive to the underlying event in inclusive Z-boson production in pp collisions at $\sqrt{s} = 7\text{ TeV}$ with the ATLAS detector”, *Eur. Phys. J. C* **74** (2014) 3195, doi:10.1140/epjc/s10052-014-3195-6, arXiv:1409.3433.
314. CMS Collaboration, “Measurement of the underlying event in the Drell-Yan process in proton-proton collisions at $\sqrt{s} = 7\text{ TeV}$ ”, *Eur. Phys. J. C* **72** (2012) 2080, doi:10.1140/epjc/s10052-012-2080-4, arXiv:1204.1411.
315. CDF Collaboration, “Study of four jet events and evidence for double parton interactions in $p\bar{p}$ collisions at $\sqrt{s} = 1.8\text{ TeV}$ ”, *Phys. Rev. D* **47** (1993) 4857, doi:10.1103/PhysRevD.47.4857.
316. CMS Collaboration, “Measurement of four-jet production in proton-proton collisions at $\sqrt{s} = 7\text{ TeV}$ ”, *Phys. Rev. D* **89** (2014) 092010, doi:10.1103/PhysRevD.89.092010, arXiv:1312.6440.
317. CDF Collaboration, “Double parton scattering in $p\bar{p}$ collisions at $\sqrt{s} = 1.8\text{TeV}$ ”, *Phys. Rev. D* **56** (1997) 3811, doi:10.1103/PhysRevD.56.3811.
318. DØ Collaboration, “Double parton interactions in photon+3 jet events in pp^- bar collisions $\sqrt{s} = 1.96\text{ TeV}$ ”, *Phys. Rev. D* **81** (2010) 052012, doi:10.1103/PhysRevD.81.052012, arXiv:0912.5104.
319. DØ Collaboration, “Double parton interactions in photon + 3 jet and photon + b/c jet + 2 jet events in $ppbar$ collisions at $\sqrt{s}=1.96\text{ TeV}$ ”, *Phys. Rev. D* **89** (2014) 072006, doi:10.1103/PhysRevD.89.072006, arXiv:1402.1550.
320. ATLAS Collaboration, “Measurement of hard double-parton interactions in $W(\rightarrow l\nu)+2\text{ jet}$ events at $\sqrt{s}=7\text{ TeV}$ with the ATLAS detector”, *New J. Phys.* **15** (2013) 033038, doi:10.1088/1367-2630/15/3/033038, arXiv:1301.6872.
321. CMS Collaboration, “Study of double parton scattering using $W+2\text{-jet}$ events in proton-proton collisions at $\sqrt{s} = 7\text{ TeV}$ ”, *JHEP* **03** (2014) 032, doi:10.1007/JHEP03(2014)032, arXiv:1312.5729.
322. D. Treleani, “Double parton scattering, diffraction and effective cross section”, *Phys. Rev. D* **76** (2007) 076006, doi:10.1103/PhysRevD.76.076006, arXiv:0708.2603.
323. M. Bähr, M. Myska, M. H. Seymour, and A. Siodmok, “Extracting $\sigma_{\text{effective}}$ from the CDF $\gamma+3\text{jets}$ measurement”, *JHEP* **03** (2013) 129, doi:10.1007/JHEP03(2013)129, arXiv:1302.4325.
324. M. Diehl, D. Ostermeier, and A. Schäfer, “Elements of a theory for multiparton interactions in QCD”, *JHEP* **03** (2012) 089, doi:10.1007/JHEP03(2012)089, arXiv:1111.0910.